Experimental Determination of Rock Hydrological Properties using Elastic Parameters

By

Michael Du Preez

THESIS

Submitted in the fulfilment of the requirements for the degree of Doctor of Philosophy in the Faculty of Natural and Agricultural Sciences, Institute for Groundwater Studies, University of the Free State, Bloemfontein

Promoter: Prof GJ van Tonder

November 2007

I do not think there is any thrill that can go through the human heart like that felt by the inventor as he sees some creation of the brain unfolding to success....Such emotions make a man forget food, sleep, friends, love, everything.

-- Nikola Tesla

Acknowledgements

Contents

List of Tables

List of Figures

List of Parameters

L	- Sample Length	-m
m	- Sample Dry Mass	-Kg
r	- Sample Radius	-m
La	- Aquifer Thickness	-m
β	- Compressibility of Water	-1/Pa
g	- Gravitational Acceleration	$-m/s^2$
S	- Sample Rate	-Hz
Ts	- Shear Wave Travel Time	-s
Tp	- Compressional Wave travel Time	-s
Vs	- Shear Wave Velocity	-m/s
Vp	- Compressional Wave Velocity	-m/s
V	- Sample Volume	$-m^3$
p	- Sample Density	$-Kg/m^3$
Sv	- Specific Volume	$-m^3/Kg$
G	- Shear Modulus	-Pa
K	- Bulk Modulus	-Pa
α_p	- Pore Space Compressibility	-1/Pa
λ	- Lame Constant	-Pa
U	- Lame Constant	-Pa
V	- Poisson Ratio	
E	- Young's Modulus	-Pa
Z	- Acoustic Impedance	$-Pa\ s/m^3$
f	- First Torsional Resonance Frequency	-Hz
Ss	- Specific Storage	-1/m
S	- Storativity	
D	- Hydraulic Diffusivity	$-m^2/s$
K	- Hydraulic Conductivity	-m/s
k	- Intrinsic Permeability	$-m^2$
T	- Transmissivity	$-m^2/s$
n	- Sample Porosity	-%

Chapter 1- Introduction

1.1 Background

As groundwater becomes increasingly vital as a viable source of fresh water in arid or remote areas, where surface water supplies are insufficient to sustain life, agriculture and industry, it has become important to accurately estimate, manage and monitor this valuable resource. Much has been done to improve the management of this precious resource by the development of numerical models that give a realistic estimate on how groundwater reserves will react to changing circumstances in groundwater conditions. The accuracy of these predictions is limited to the effective accuracy of the predictive model, which in turn relies on accurate data for all the variables which will affect the flow of groundwater.

There are a number of hydrological parameters which affect how water reserves would react in an aquifer. These include hydraulic conductivity, storativity, porosity, permeability and diffusivity to name a few. The traditional way of determining these parameters is by the use of pump tests on boreholes drilled into the aquifer of interest. These tests give a very good global estimation of the aquifer hydraulic parameters at the point of testing. However, there are a few of these parameters that cannot be estimated by traditional pump tests. These parameters include; vertical hydraulic conductivity, specific storage and effective porosity. These parameters need to be determined by extensive laboratory testing on samples or by estimation by numerical means. Laboratory testing can be restrictively expensive and time consuming which can make it impractical to use. Numerical estimation with models requires a large amount of data to make a realistic estimation of these parameters. This can also be restrictive as it is not always possible to obtain data on large scale.

What is needed is an effective method of determining these parameters in a manner that is both accurate and cost effective, within a realistic time frame. This can be achieved by the determination of the elastic parameters of the aquifer. These elastic parameters can then be used to determine the required hydrological information about the aquifer. This study aims to describe a novel method to achieve these goals.

1.2 Objectives

This thesis presents a method to determine hydrological parameters of core rock samples by measuring its elastic parameters by using non-destructive ultrasound methods. These parameters include, rock elastic parameters: bulk, shear and Young's modulus as well as the Poisson's ratio and compressibility, as well as the hydrological parameters: specific storage, hydraulic diffusivity and hydraulic conductivity.

1.3 Methodology

The hydrological parameters of an aquifer are determined by experimentally measuring the elastic parameters of a rock sample, in this case a core sample. These measurements are done in two ways: The first is to measure the compressive and shear wave velocities of the rock by inducing an ultrasonic pulse into one side of the core sample and measuring the time it takes the pulse to travel through the sample. The travel times are then converted into compressive and shear velocities which in turn are used to determine the bulk modulus and shear modulus of the sample. The second method uses resonant ultrasound spectrography which measures the natural resonance frequencies of a rock sample induced by an ultrasonic frequency sweep. These resonance frequencies are then analytically verified against the bulk modulus and shear modulus of the rock sample determined by the time of flight method. If a correlation exists, the measured modulus of elasticity is considered to be correct. Both of these methods use apparatus which clamp a cylindrical rock core sample between two sets of ultrasonic transducers. One set of transducers produce compressive ultrasonic waves, and the other produce shear ultrasonic waves. An analogue to digital converter is used to read the changing voltage levels in the transducers, induced by the ultrasonic pulse travelling through the sample or the resonant vibrations of the sample induced by an ultrasonic frequency sweep. Once the rock samples elastic parameters are known, they are applied to equations which relate hydrological parameters to the samples elastic parameters. The resultant hydrological parameter values can then be determined. Similar work has been done by the Centre for rock physics and the Polish Institute for Agriphysics, who use acoustic determinations of elastic parameters of rock samples. The ASTM D2815-05 standard outlines a standard procedure for ultrasonic testing.

1.4 Document structure

This document aims to explain the research done in this study by addressing the individual aspects of the project. These aspects are discussed as follows.

- The second chapter will explain the theory of sound and its application to the research done in this study. This includes how sound travels in a rock and how it is induced and recorded in the rock sample.
- The third chapter will discuss the elastic parameters of a rock sample and explain how a rock sample deforms with relation to the stresses and strains it is placed under.
- The fourth chapter will discuss the hydrological parameters measured and calculated in this study.
- The fifth chapter will explain the time of flight method of determining elastic parameters of a rock sample.
- The sixth chapter will discuss the resonant ultrasound spectrography technique and how it is used to determine the rock elastic parameters.
- The seventh chapter discusses the experimental apparatus and methods used to measure the elastic parameters of the rock samples under test.
- The eighth chapter discusses the results of the experimental study

Chapter 2- Theory of sound

2.1 Introduction

The methods used in this study employ sound to measure rock elastic parameters. Before elastic parameters of a medium can be discussed, a proper understanding of acoustics and how sound travels must be derived. This section will discuss the basics of acoustics and wave travel in elastic media.

2.2 History

The history of the study of sound dates back to 600 BC, when Pythagoras of Samos observed that a string on a musical instrument being plucked vibrated. He also observed that the width of the blurred area of the string related to its loudness and when the vibrations stopped, the sound disappeared. He noticed that a shorter string produced vibrations that made a higher pitched sound. (Cartage, 2007)

Two hundred years later Archytus of Tarentum, while attending the Pythagorean school, postulated that sound could be produced by slamming two rocks together. The faster and harder the two rocks were slammed together, the higher the pitch of the sound.

Fifty years later in 350BC, Aristotle continued the study of sound by observing that a vibrating string was in fact striking the air many times at a very high rate. He concluded that sound needed a medium to be transmitted and would not be transmitted in the absence of a medium i.e. a vacuum.

Working from Aristotle's theories Marcus Vituruvius Pollio, a roman engineer, realized that the vibrations of a string caused the air to vibrate as well. He postulated that these air vibrations were perceived as sound (Cartage, 2007).

It was not until 600 years later in 500 AD that the connection between sound and wave motion was made by a roman philosopher, Anicius Manilius Severinus Boethius. He compared the movement of sound to that of a wave moving in water by dropping a pebble in water and observing the movement of the wave away from the

source. Although the analogy is not completely correct, the connection between sound and waves was a great step forward. Marin Mersenne (1588-1648), considered by many as the father of modern acoustics, furthered this sound wave relation in his works "*Mathematical Discourses Concerning Two New Sciences*" . He was the first to determine the absolute frequency of a vibrating string and demonstrated that the absolute frequency ratio between two vibrating strings making a tone and its octave is 1:2. (Wave Express, 2007)

The sound and wave connection was further strengthened by Robert Boyle's (1640) classic experiment, where a ticking watch was placed in a partially evacuated container. In the partially evacuated chamber the ticking was less audible. This provided the necessary evidence that a medium is needed to conduct sound.

It was Isaac Newton that fathered the mathematical theory of sound with the publication of his work "*Principia*" in which he described sound as a pressure wave transmitted through adjacent particles. His work made use of a number of assumptions and approximations and took his successors a while to understand. However, it is considered to be the first step toward modern acoustic study.

Since then, there have been a number of people who have contributed to the study of sound. A few of these include Euler (1707-1783), Lagrange (1736-1813), and d'Alembert (1717-1783). Modern theory on sound is based largely on the work done by these men (Wave Express, 2007).

2.3 Sound

Sound can be described as a longitudinal or a traverse deformation induced in and moving through a compressible medium. In essence, any impulsive or oscillating force can deform a compressible medium, such as air or rock, to produce longitudinal or transverse deformation to travel away from the source through the medium.

An example of this is a speaker, which, by pulsating or oscillating a cone shaped diaphragm back and forth, produces sound waves that travel in air away from the speaker. This is accomplished, by the speaker through the compression of the air in front of the diaphragm by moving it forward, then extending the air by moving it

backward. These compressions and expansions of the air molecules are then interpreted by the ear as vibrations of the ear drum and sound is heard.

| Compression of air molecules | Expansion of air molecules | Ear hears the vibrations |
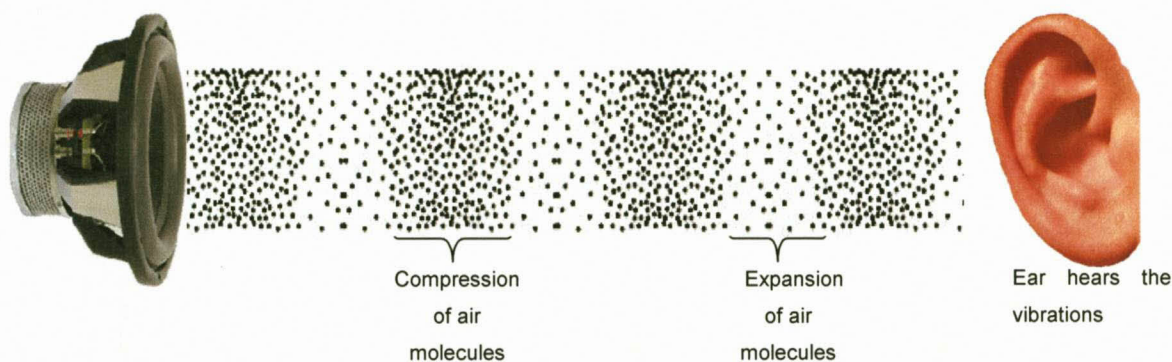
Figure 1 - Wave Travel

Sound waves are classified by their frequency; a sound wave with a frequency below 10Hz is called infrasound. Infrasound travels well through solids such as rock and has found application in seismic surveys and medicine. Sound with a frequency between 10 Hz and 20 kHz is usually audible to the human ear and is thus called audible sound.

Sound generated above the human hearing range (typically 20 kHz) is called ultrasound. However, the frequency range normally employed in sonic time of flight testing and hydrological determinations is 1 KHz to 1MHz. Although ultrasound behaves in a similar manner to audible sound, it has a much shorter wavelength. This means, it can be reflected of very small surfaces such as defects inside materials. It is this property that makes ultrasound useful for non-destructive testing of materials. The acoustic spectrum in Figure 2 breaks down sound into 3 ranges of frequencies (Wayne, Hykes, & Hedrick, 2005).
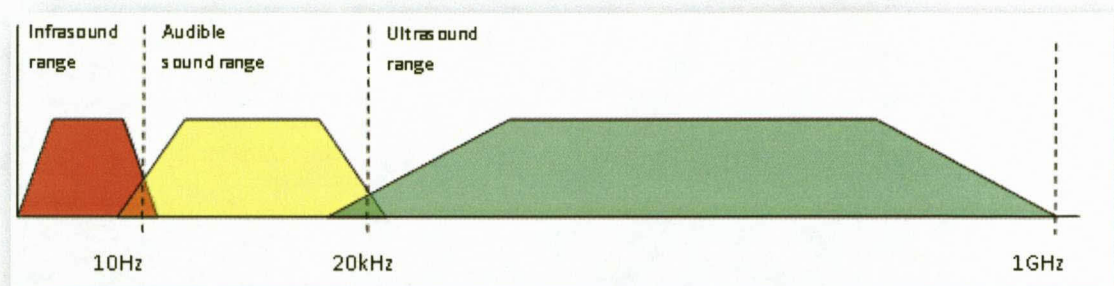
Figure 2 - Acoustic frequency spectrum (Wayne, Hykes, & Hedrick, 2005)

2.4 Wave propagation and particle motion

The most common methods of sonic examination utilize either longitudinal waves or shear waves. Other forms of sound propagation exist; these include surface waves and Lamb waves. The longitudinal wave is a compression wave in which the particle motion is in the same direction as the propagation of the wave (Bueche, 1986).
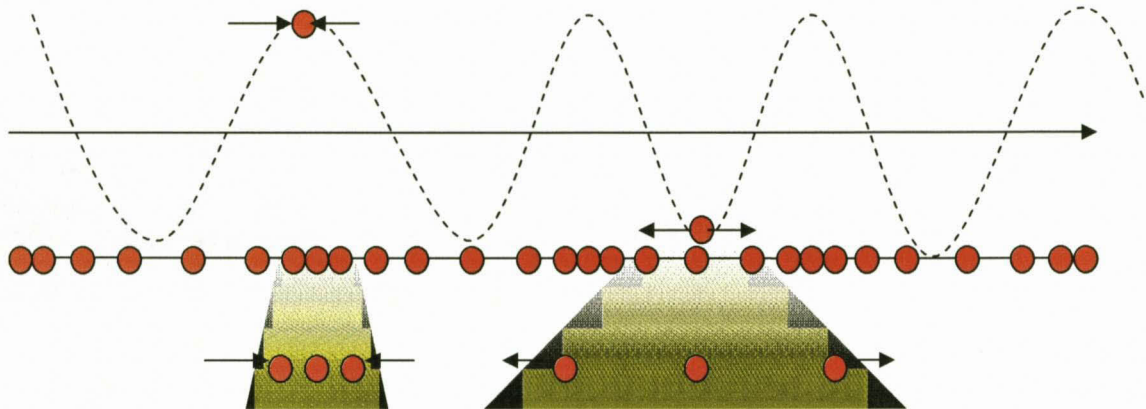
Figure 3 - Compression wave travel
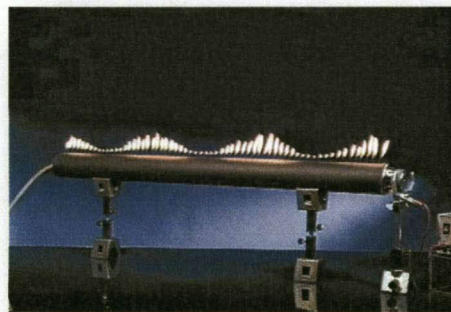
Figure 4 - Flame wave illustration (Physics Curriculum and Instruction, 2007)

Figure 3 illustrates a longitudinal wave. Although the wave is moving in one direction the particles in the medium are not. The particles are illustrated in Figure 3 as a group of red dots on a string. As a longitudinal wave moves through the string the particles on the string either move forward or backwards. This produces the effect of compression of the dots at some points on the string and expansions at other points. The sound moves through the string as a series of compression fronts. Another example of these compressions and expansions is shown in Figure 4. Here longitudinal pressure waves are sent down a pipe filled with gas blowing out of holes drilled through the top of the pipe. The compressions caused by the sound wave as it moves through the pipe forces more gas out of the tube while the expansions draw air in. This creates the effect of a wave pattern on the flame height.

The shear wave is a wave motion in which the particle motion is perpendicular to the direction of the propagation.

Figure 5 illustrates a string with red dots attached to it. The wave moves in one direction but the red dots move perpendicularly up and down along the string.
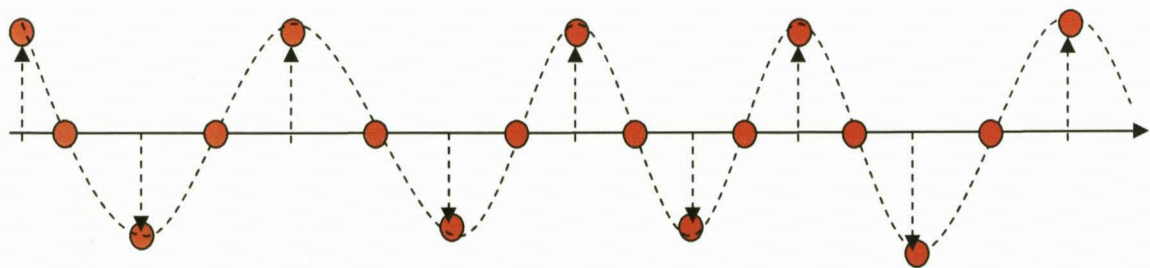
Figure 5 - Shear wave travel

The degree of movement up or down is a function of the amplitude of the wave moving through the medium. This is different from longitudinal wave travel in that it is a perpendicular deformation of the medium instead of a longitudinal compression. In this study both compression and shear waves are used to realize the elastic properties of a rock sample, namely its bulk and shear modulus. These will be discussed in the next section. It is possible for these wave types to move simultaneously through the same medium, and often they do (Kane & Sternheim, 1983).
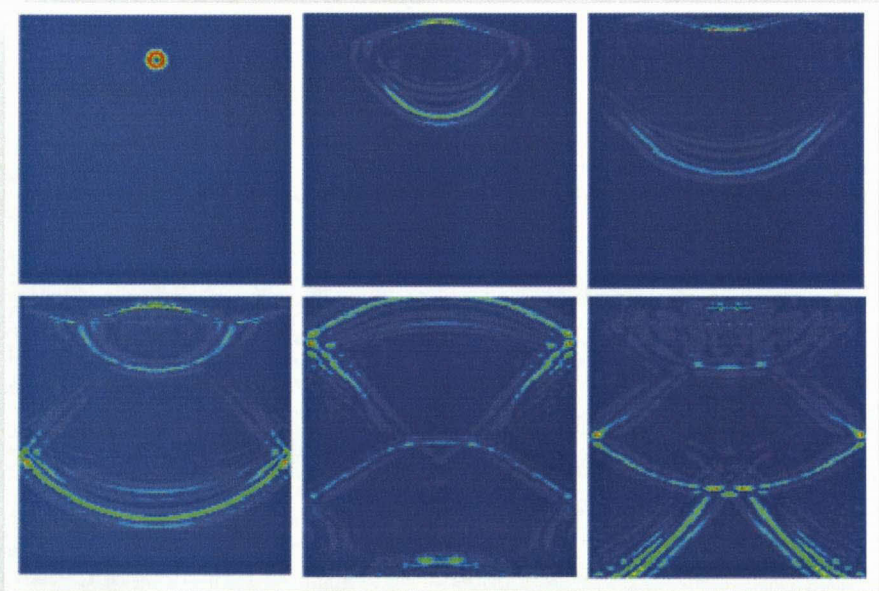
Figure 6 - 2D wave travel in a cylinder (Texas University, 2007)

Figure 6 Shows the movement of a pressure wave as it passes through a two dimensional rectangle. The wave moves spherically away from the source until it hits a reflective interface, in this case a side wall. It is then reflected in a different direction as a spherical wave moving away from the point of reflection and interferes with the surrounding waves. This illustrates that a sound wave moves in a homogeneous medium as a uniform spherical wave away from the point of origin whether that be the source point or from the reflected surface.

2.5 Absorption and scattering
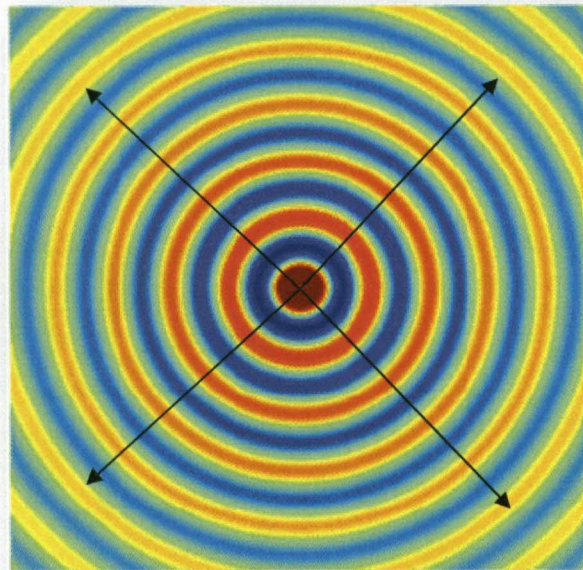
Figure 7 - Absorption and scattering effects (ISVR, 2007)

Figure 7 shows the pressure wave front emanating from a source in the middle of the picture. The wave fronts move away from the source in a uniform spherical pattern. As the wave move further from the source, the amplitude of the waves decreases. This is due to loss of energy through absorption of energy by the medium or scattering of the pressure wave through diffraction (Bueche, 1986).

Equation 1 defines absorption attenuation of a porous medium (Xin, 2000).

$$z = \sqrt{\rho K}\sqrt{\frac{n}{\gamma}}\sqrt{1 + j\tan(\delta_p)}\sqrt{1 + j\tan(\delta_B)}\coth\left\{\frac{j\omega D}{c}\sqrt{n\gamma\frac{1 - j\tan(\delta_p)}{1 - j\tan(\delta_B)}}\right\}$$

Equation 1

Where; ρ = Effective density

K = Bulk modulus

ω = Angular frequency

n = Structure factor

γ = Thermal attenuation

D = Thickness of sample

δ_p = Angular attenuation

δ_B = Angular attenuation

Equation 1 shows that the frequency of the pressure wave travelling in a medium affects it's attenuation due to absorption. The higher the frequency the higher the absorption of the energy will be in the medium. The thermal attenuation, structure factor and angular attenuation also vary greatly in practical situations and are difficult to determine. This makes the accurate measurement of attenuation due to absorption very difficult in practical situations

2.6 Frequency and period

Like light waves, sound can be expressed in terms of its oscillatory nature. Every oscillation has a defined wave length, period and frequency. Figure 8 shows an example of a vibrating sound wave.
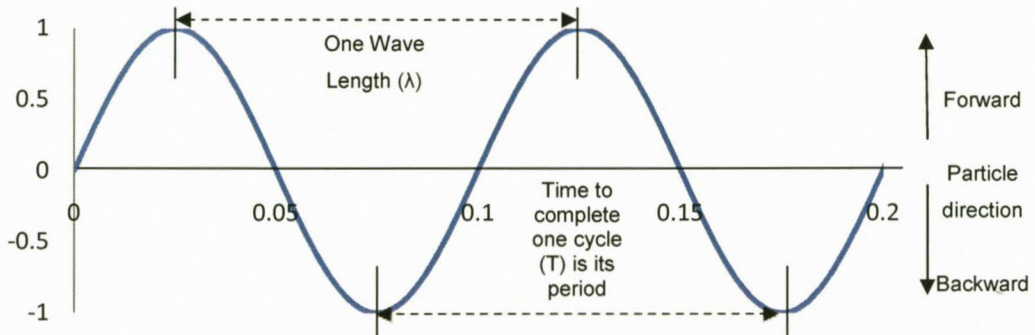
Figure 8 - Frequency and period

The wave length is defined as the length in meters between two similar points on the wave form. The wave length is dependent on the speed at which the sound moves in a given medium as well as its frequency. The time it takes for one wave length to pass a given point in the medium is its period measured in seconds (Bueche, 1986).

The number of cycles completed in one second is called frequency (f) and is measured in Hertz (Hz). The relation between frequency and period in a wave is given in equation 2.

$$f = \frac{1}{T}$$

Equation 2

2.7 Velocity of sound and wavelength

The velocity of sound (c) in a perfectly elastic material at a given temperature and pressure, is constant. The relation between c, f, λ and T is given by Equations 3 and 4: (Wayne, Hykes, & Hedrick, 2005)

$$\lambda = \frac{c}{f}$$

Equation 3

$$\lambda = cT$$

Equation 4

Where;   λ   = Wavelength

c   = Material Sound Velocity

f   = Frequency

T   = Period of time
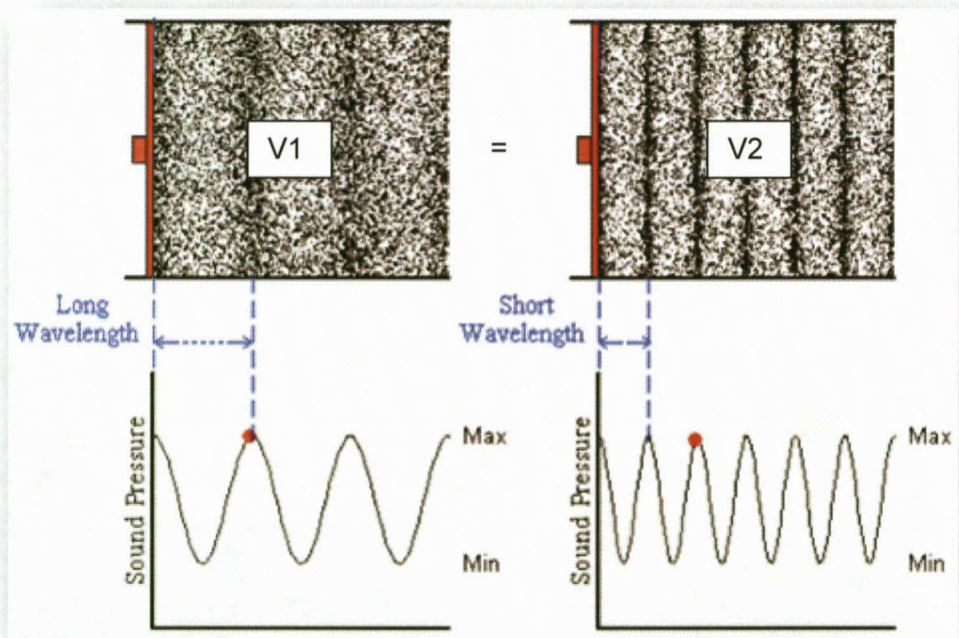
Figure 9 - Constant velocity versus wave length (ISVR, 2007)

This relation is shown in Figure 9. If the acoustic velocity in a medium remains constant, then as the frequency increases, the wavelength and period decreases.
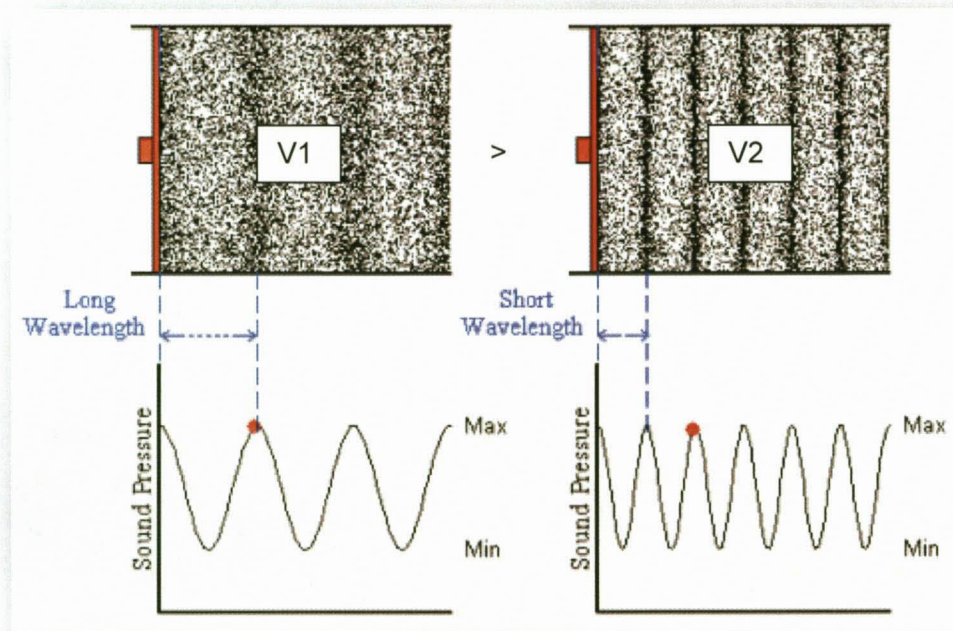
Figure 10 - Changing velocity versus constant wavelength (ISVR, 2007)

However, as illustrated in Figure 10, if the acoustic velocity in the medium increases then a wave with constant frequency increases in wave length.

2.8 Interference
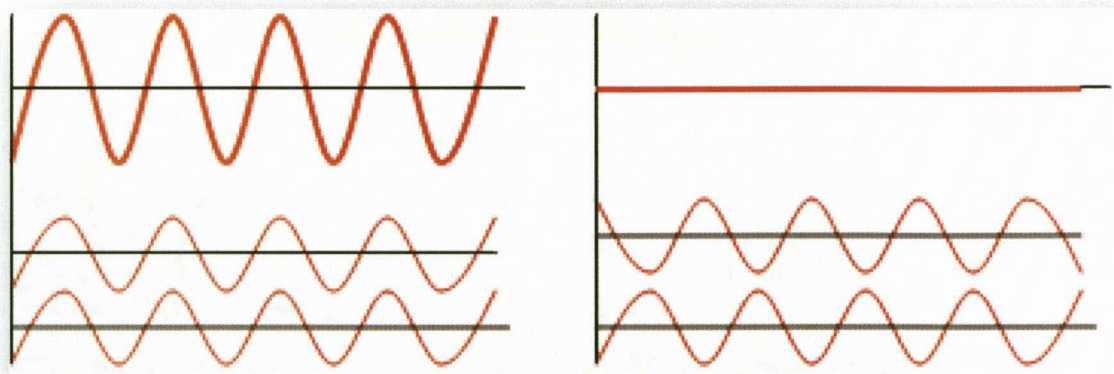
Figure 11 – Interference (Kane & Sternheim, 1983)

Interference is the superposition of two or more waves into a new wave pattern. There are two types of interference, namely constructive and destructive interference. Figure 11 illustrates these types of interference. The figure on the left

shows the superposition, or adding, of two wave forms of identical phase, amplitude and frequency to form a new wave. This wave will have the same phase and frequency as the added waves but twice the amplitude. This is called constructive interference. The diagram on the right shows the same two waves, however the two waves are 180 degrees out of phase. When they are added up they cancel each other out. This is called destructive interference.

$$f_4 = 5 f_0$$

$$+$$

$$f_3 = 4 f_0$$

$$+$$

$$f_2 = 3 f_0$$

$$+$$

$$f_1 = 2 f_0$$

$$+$$

$$f_0$$

Resultant
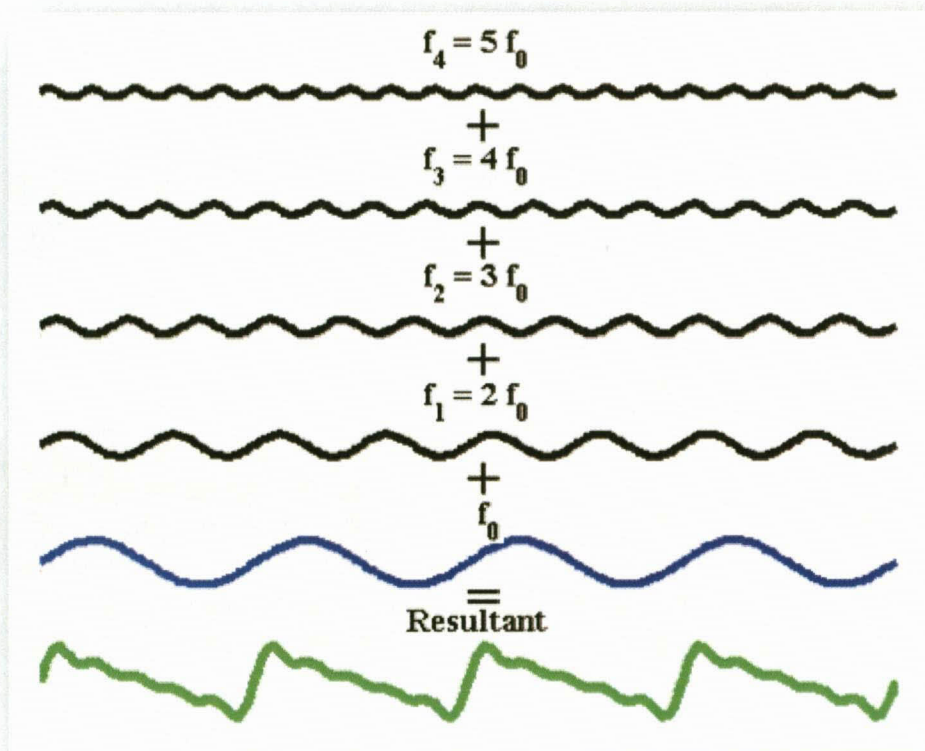
Figure 12 - Complex wave forms (ISVR, 2007)

A good example of how interference works is shown in Figure 12. The summation of a number of sine waves with varying amplitudes phases and frequencies combine to form a complex triangular wave form. This is important to this study as frequency transmission through a core sample is complex. This is especially true for shear wave transmission as it travels through the medium in a number of different modes of vibration.

2.9 Resonance
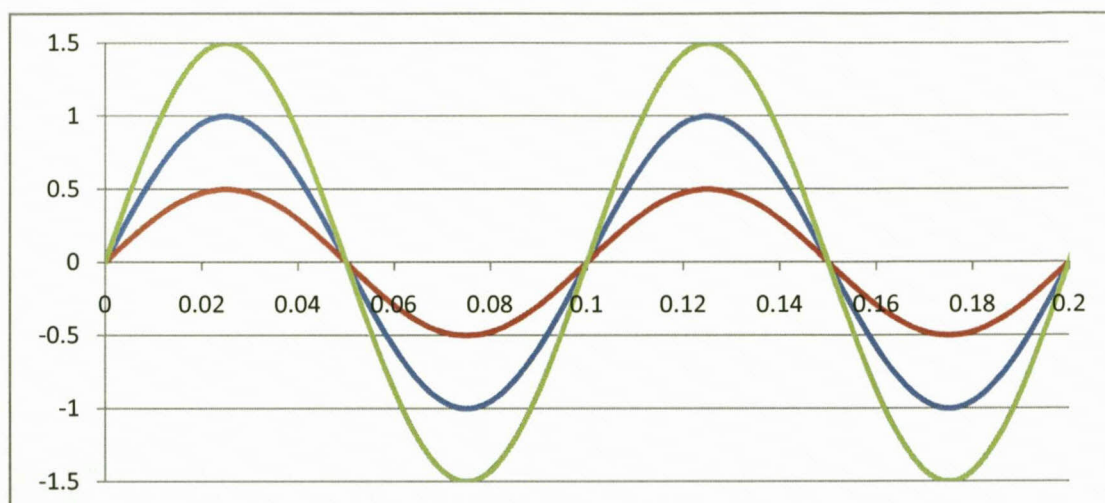
Figure 13 – Resonance

Sound waves travelling in a medium of finite length can be caused to resonate. Resonation of sound is a function of its wave length and the length of the sample medium. If sound travels down a solid pipe, e.g. a core rock sample, a part of the wave will be reflected back up the pipe when it strikes the opposite end of the core. This reflected wave will then travel back up the core and interfere with the wave traveling down the core. If the two waves are out of phase, destructive interference will occur and the sum of the two waves at every point will be less than that of the largest wave's amplitude. If the waves are in phase, the sum of the waves amplitude will be greater than that of the largest wave amplitude. Every time the in phase waves are reflected off either of the ends of the core, they contribute more energy to the resonating wave form, producing a far more powerful wave at the resonant frequency than would have been possible if no resonance occurred. Resonance can also be problematic in the building industry, as all physical structure can resonate. In the event of an earthquake, the resonance of a poorly designed building can cause it to collapse. (Komodromos, 2007) This forces engineers to design buildings and bridges to resonate at frequencies outside of an earthquake's frequency range. Figure 13 illustrates constructive interference. The blue and red traces are those of the transmitted wave and the reflected wave respectively. The green trace shows the constructive effect of the two in phase wave forms.

Resonance frequencies in a core sample of known dimensions can be predicted by the following formula: (Seymour & Mortell, 2006)

$$f_{res} = N \frac{v}{4L}$$

<div align="right">**Equation 5**</div>

Where; f_{res} = resonant frequency

N   = the fundamental or harmonic number

v   = the velocity of the sound in the medium

L   = the length of the core sample
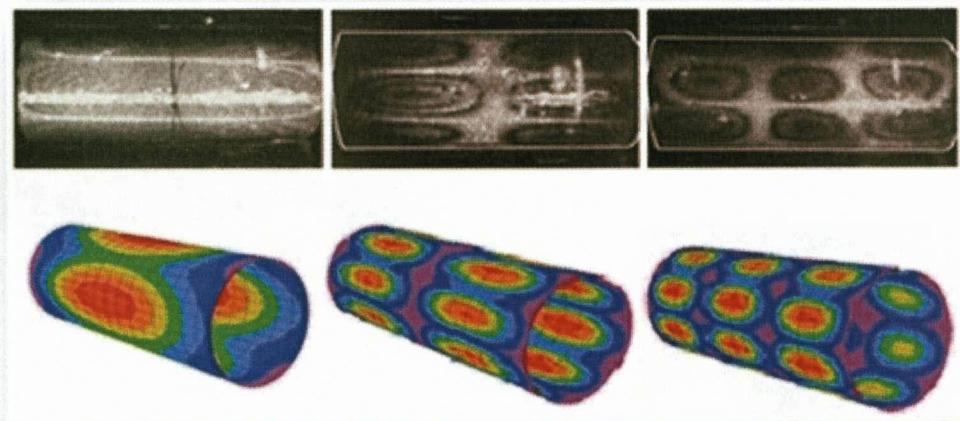
Figure 14 - Resonance modes in a cylinder (University of Oxford, 2007)

Figure 14 shows the resonance patterns inside a closed or solid pipe. The red areas show the points of constructive interference at the resonant frequencies. The resonance frequencies occur in frequency steps known as resonance modes. Each resonant mode is a multiple of the fundamental resonant frequency, which is defined by the lowest resonant frequency of the tube. These frequencies are defined by N in equation 5 where N equals 1 is the fundamental and N equals 2 is the second harmonic, ect.

2.10 Refraction

Refraction of a sound wave occurs when it crosses a boundary between two materials with different elastic properties. When a wave travels from a medium of high velocity to a medium of low velocity it is refracted toward the normal as shown in Figure 15. If the wave travels from a medium of low velocity to one of higher velocity, the opposite occurs and the wave is refracted away from the normal. Figure 15 shows the process of refraction of a wave travelling from a medium of high to low velocity. As shown the angle of incidence θ_1 is larger than the angle of refraction θ_2.
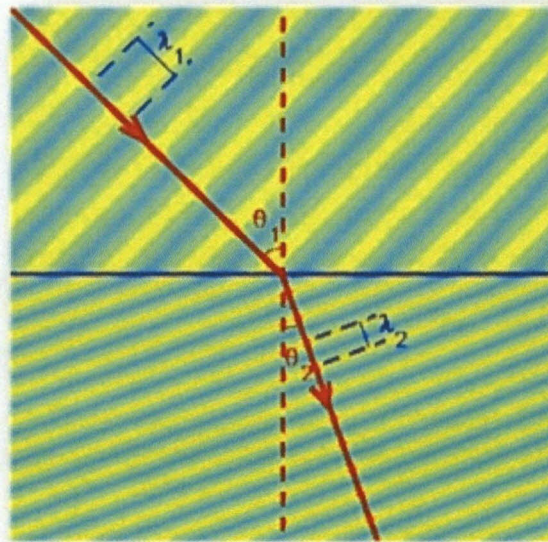
Figure 15 – Refraction (ISVR, 2007)

The angle of refraction is defined by Snell's law of refraction which is described by the following equation: (Kane & Sternheim, 1983)

$$\frac{V_1}{V_2} = \frac{\sin(\theta_1)}{\sin(\theta_2)}$$

Equation 6

Where; V_1 = Velocity of the first layer

V_2 = Velocity of the second layer

θ_1 = Angle of incidence

θ_2 = Angle of refraction

17

This effect can also be described as a function of the wave length of the sound in each medium, derived from equation 3. The following equation defines this relation.

$$\frac{\lambda_1}{\lambda_2} = \frac{\sin(\theta_1)}{\sin(\theta_2)}$$

<div align="right">**Equation 7**</div>

Where; λ_1 = Wavelength of sound in the first layer

λ_2 = Wavelength of sound in the second layer

Θ_1 = Angle of incidence

Θ_2 = Angle of refraction

2.11 Diffraction

Diffraction is described as the spreading of a wave as it passes by the end of an obstacle or passes through a gap between obstacles. Figure 16 illustrates this process. A linear sound wave passes a barrier that reflects a part of the wave and diffracts the sound wave as it passes the barrier. The diffracted wave is shown behind the barrier as a bending or spreading of the wave with a lower intensity than the original wave form. The reflected waves interfere with the incoming source waves to cause the high intensity waves in front of the barrier. (Argatov & Sabina, 2008)
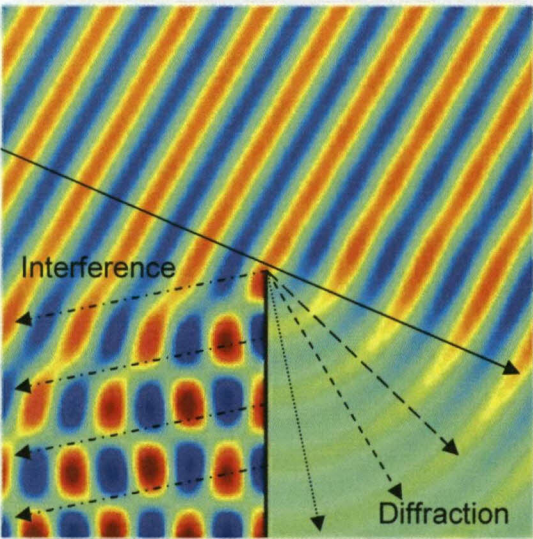
Figure 16 - Diffraction (ISVR, 2007)

2.12 Doppler effect

The Doppler effect was discovered by Christian Doppler when he realized that the perceived frequency between a moving wave source and/or moving receiver is determined by the speed at which the source and/or receiver is moving away or toward each other (Bueche, 1986). Most people have experienced the Doppler effect at a train station. As the train approaches it transmits sound at a certain pitch, however as it passes the station it transmits sound at a lower pitch. This difference in pitch is caused by the Doppler effect. Figure 17 illustrates the Doppler effect. The particle in the center of the diagram is moving at speed from right to left. As it moves it transmits a sound of a fixed frequency. The sound moves away from the particle at a given speed. The Doppler effect causes the waves in the direction of the source to have a higher frequency than the transmitted frequency. The waves moving opposite to the movement of the particle are at a lower frequency than that of the transmitted frequency. This frequency shift from the normal can be calculated and is known as the Doppler shift frequency (Bueche, 1986).
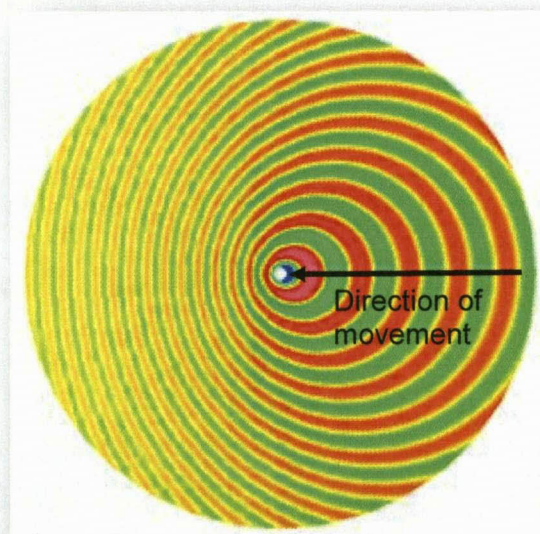
Figure 17 - The Doppler effect (Elmer, 2007)

The Doppler effect can play a role in elastic measurements if the sample under test is not sufficiently anchored to the test equipment. However, the effect is usually very small and can be ignored.

The equation for the Doppler shift is: (DuBose & Baker, 2007)

$$Fd = Fs\left(\frac{V}{C}\right)$$

Where;   Fd   = Doppler shift frequency.

         Fs   = frequency of the sound.

         V   = particle velocity

         C   = speed of sound.

2.13 Acoustic impedance, reflectivity, and attenuation

The acoustic impedance of a material is the resistance to displacement of its particles by sound and occurs in many equations. Acoustic impedance is calculated as follows:

$$Z = \rho V_p$$

Where;

Z   = Acoustic Impedance

V_p = Material Sound Velocity

ρ   = Material Density

The boundary between two materials of different acoustic impedances is called an acoustic interface. When sound strikes an acoustic interface at normal incidence, a part of the sound energy is reflected and a part is transmitted across the boundary (Wayne, Hykes, & Hedrick, 2005). The dB loss of energy, which is a logarithmic unit of measurement that expresses the magnitude of measurement relative to a referenced level of magnitude, on transmitting a signal from medium 1 into medium 2 is given by:

$$dB = 10\log_{10}(\frac{4Z1Z2}{2(Z1+Z2)})$$

Where;   Z1   = Acoustic Impedance of First Material

          Z2   = Acoustic Impedance of Second Material

The dB loss of energy of the echo signal in medium 1 reflecting from an interface boundary with medium 2 is given by (Wayne, Hykes, & Hedrick, 2005):

$$dB = 10 \log_{10} (\frac{2(Z2 - Z1)}{2(Z1 + Z2)})$$

Equation 11

2.14 Applying ultrasound

Ultrasonic non-destructive testing introduces high frequency sound waves into a test object to obtain information about the object without altering or damaging it in any way. Two basic quantities are measured in ultrasonic testing; time of flight or the amount of time for the sound to travel through the sample and amplitude of received signal. Based on velocity and round trip time of flight through the material, the material thickness can be calculated as follows: (Jennings & Flint, 1995)

$$T = \frac{cts}{2}$$

Equation 12

Where; T = Half travel distance

          c   = Material sound velocity

          ts   = Time of flight

Measurements of the relative change in signal amplitude can be used in determining the resonance frequencies of a material. The relative change in signal amplitude is commonly measured in decibels. Decibel values are the logarithmic value of the ratio of two signal amplitudes.

This can be calculated using the following equation. (Jennings & Flint, 1995)

$$dB = 20\log 10(\frac{A1}{A2})$$

Equation 13

Where;   dB   = Decibels

A1   = Amplitude of signal 1

A2   = Amplitude of signal 2

Chapter 3- Rock elastic parameters

3.1 Introduction

In nature all materials are deformable and hence are considered to be either elastic or inelastic. Inelastic materials do not return to their original shape after a force, in the form of a pressure applied to its surface, deforms the material. A good example of this is moist putty that children mold into different shapes. If putty was not inelastic in nature this would not be possible as the putty would simply return to its previous state. Elastic materials are able to do just that, and return to their original state after an external force has acted on them to deform them. A good example of an elastic material is an elastic band. These bands can be stretched and deformed to lengths many time their natural length and still be able to return to their original state once the applied force is removed. All materials in nature are elastic to a certain extent, that is, they can be deformed and return to their original state as long as they are not deformed past their linear elastic properties. The elastic band is stretch with applied force but if the force is too great it will break and will not be able to return to its original shape. This means with sufficient force an elastic band can be forced to be inelastic (Kane & Sternheim, 1983).

Understanding the linear elastic parameters of a material, such as porous rock in the case of this study, yields an understanding of how the material will react when a force is applied to it. The relation between a rock's elastic parameters and its hydrological parameters is of particular interest in this study as it allows for the determination of these properties by simple means.

To gain an understanding of how these properties relate to each other, the relationship of the force applied to a material and how it deforms must be understood. The concepts of stress and strain will be discussed in this section as well as how these two properties determine the elastic parameters of a material.

3.2 Stress

External forces are applied to all naturally occurring materials at all times. These forces come in a number of forms, be it gravitational forces, force in the form of pressure, either tensile or compressional and many other naturally occurring phenomenon. In most cases the internal and external forces acting on a material are in equalibrium or vary too slowly to be visibly apparent to an observer. Atomic theory of matter dictates that an object can only be deformed by changing the distance between the atoms that it is comprised of. This can only be achieved by applying an external force to the object in such a way as to unbalance the internal forces acting on the object until a new balance between the internal forces and external deforming forces are met. (Felberbaum, Laporte, & Mortense, 2008) In the case of this study, the external force is applied in the form of acoustic pressure transmitted from a piezo electric transducer. Stress is defined as the ratio of internal forces acting within an object to the area the force is acting on. Equation 14 defines this ratio. (Botha & Cloot, 2004)

$$\vec{r} = \frac{\vec{P}}{A}$$

Equation 14

Where; $\vec{r}$ = Stress

$\vec{P}$ = Applied force

A   = Area

Stress as defined in Equation 14 has the same dimensions as pressure. However the difference is that stress is a vector force and pressure is a scalar. The stress vector must be applied in a given direction in order to be interpreted correctly. One method of describing stress is by using the Cartesian coordinate system. This will allow the stress direction to be described as a vector directed from its normal direction. *Figure 18* illustrates the Cartesian coordinate system. The three dimensional plains are indicated by X, Y and Z that can be rotated arbitrarily. However, using this system the stress vector is still independent of a fixed measurement direction. This means that the vector is essentially useless until it is attached to a fixed measurement coordinate system. If a more generalised tensor system is used then the measurements of the vector are dependent on direction, amplitude and measurement direction. The tensor system is notated by (x,y,z) and the measured vector is donated by (Xx,Yy,Zz). An example of a sensor on a fixed coordinate system is illustrated on Figure 19.
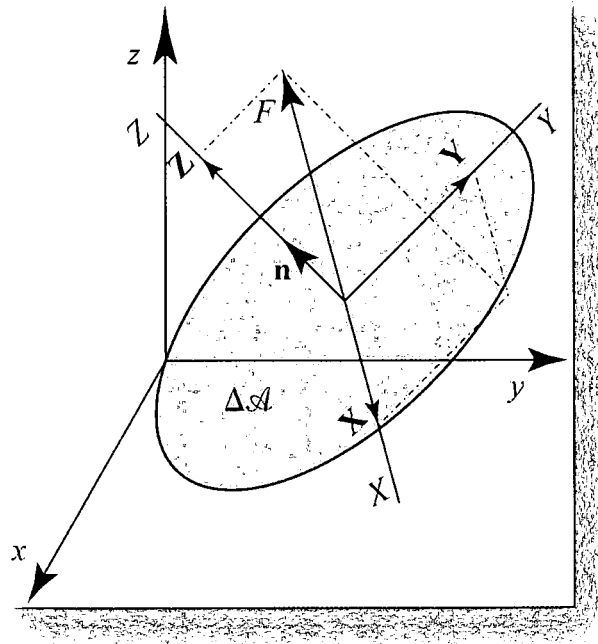
Figure 18 - Cartesian coordinate system (Botha & Cloot, 2004)
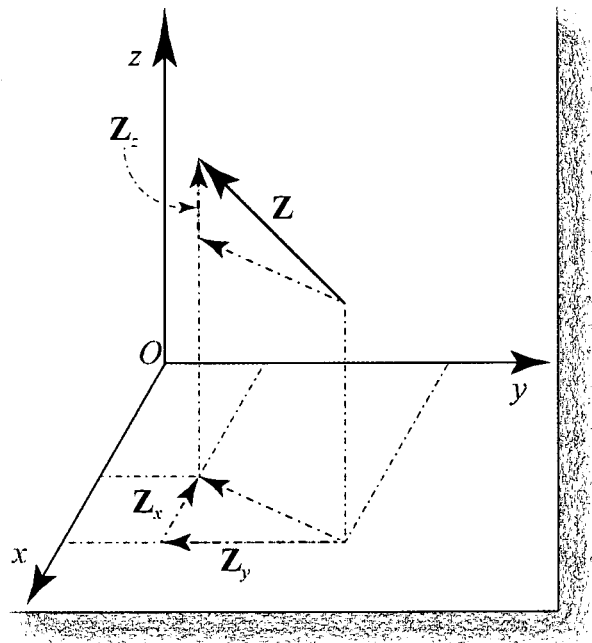
Figure 19 - Tensor System (Botha & Cloot, 2004)

Figure 19 illustrates the Z component of the vector in relation to the fixed coordinate system. The full descriptions of individual elements are given by the convention in Equation 15. Alternatively, the stress vector can be described by the symbol $\sigma_{\alpha\beta}$ where $\alpha\beta$ is the coordinates (x,y,z). (Botha & Cloot, 2004)

$$\left(X_x, X_y, X_z\right), \left(Y_x, Y_y, Y_z\right), \left(Z_x, Z_y, Z_z\right)$$

3.3 Strain

Strain is the measure of the change in dimensions in a material that has stress applied to it. In its most elementary form, strain can be defined as the deformation of an object along one axis. Equation 16 defines this: (Botha & Cloot, 2004)

$$\varepsilon = \frac{\Delta L}{L}$$

Equation 16

Where; ε = Strain

              ΔL = Change in length

              L   = Original length

When a material is stretched, it elongates and its change in length and strain are positive. Alternatively, if it is compressed its change in length and strain is negative. This is defined as normal strains, the stresses applied do not change the object's mechanical shape but do change its dimensions. Illustrations of normal strains produced by tensile and compressive stress are shown on Figure 20 and Figure 21.
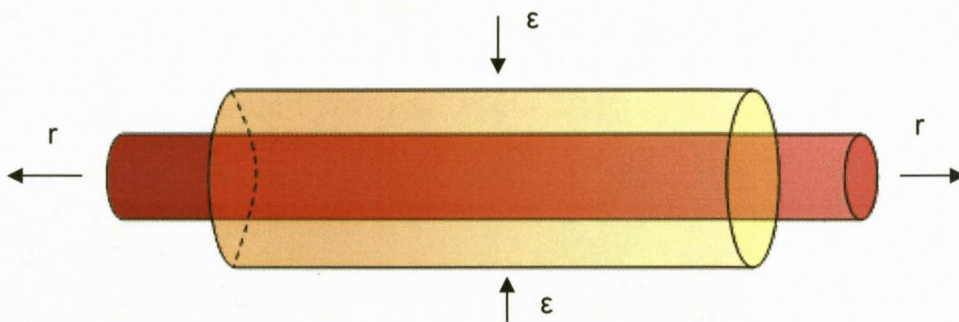
Figure 20 - Cylinder under tensile stress

Figure 20 shows a cylinder which has been put under tensile stress by pulling the ends of the cylinder apart. The cylinder still stays cylindrical in shape but becomes longer and thinner.
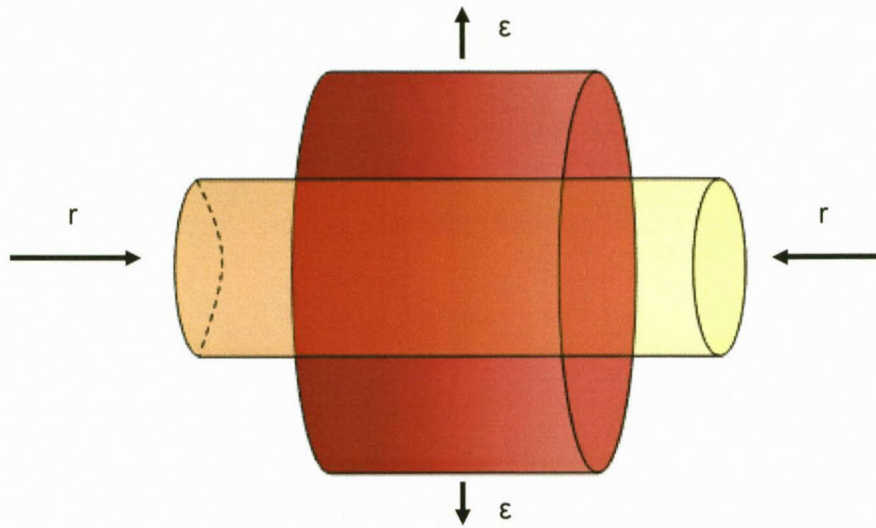
Figure 21 - Cylinder under compressive stress

Figure 21 shows the same cylinder under compressive stress. It is still cylindrical in shape, but is shorter and thicker.

The second type of strain is called shear strain. When shear stress is applied to an object it does not change the dimensions of the object but it does change its angles or its shape. Figure 22 shows a rectangular block that has been put under shear stress. The dimensions of the block do not change but its shape does.
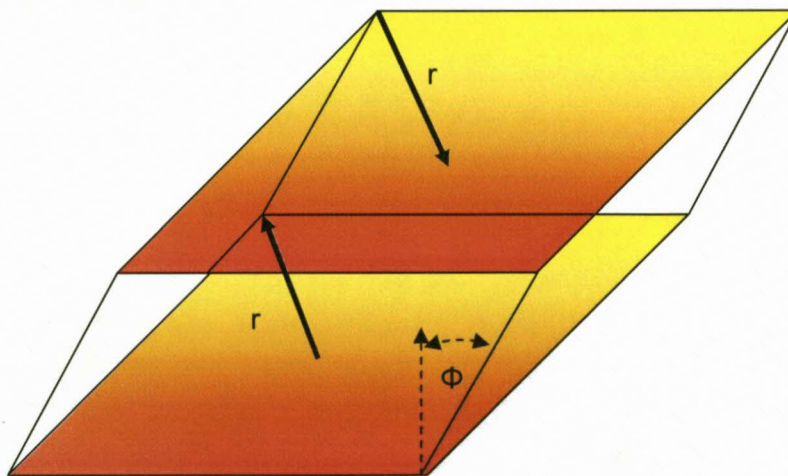
Figure 22 - Cube under shear stress

The shear strain is defined by the change in the angle Φ over each of the axes of the block. Strains can also be described as displacements, that is, how far a point in an object moved. These displacements are usually notated by (u,v,w). Normal strains are then defined in Equation 17 (Botha & Cloot, 2004):

$$\varepsilon_{XX} = \frac{\partial u}{\partial x}$$

$$\varepsilon_{yy} = \frac{\partial v}{\partial y}$$

$$\varepsilon_{zz} = \frac{\partial w}{\partial z}$$

<div align="right">**Equation 17**</div>

When a stress acts on a compressible object it changes its volume. This is another way of describing strains, i.e., by describing it in terms of total volume change. Volumetric strain is defined in Equation 18 (Botha & Cloot, 2004).

$$\mathbf{e} = \frac{V - V_0}{V_0}$$

<div align="right">**Equation 18**</div>

Where; $\mathbf{e}$ = Volumetric strain

                V   = Volume under stress

                V_0 = Original volume
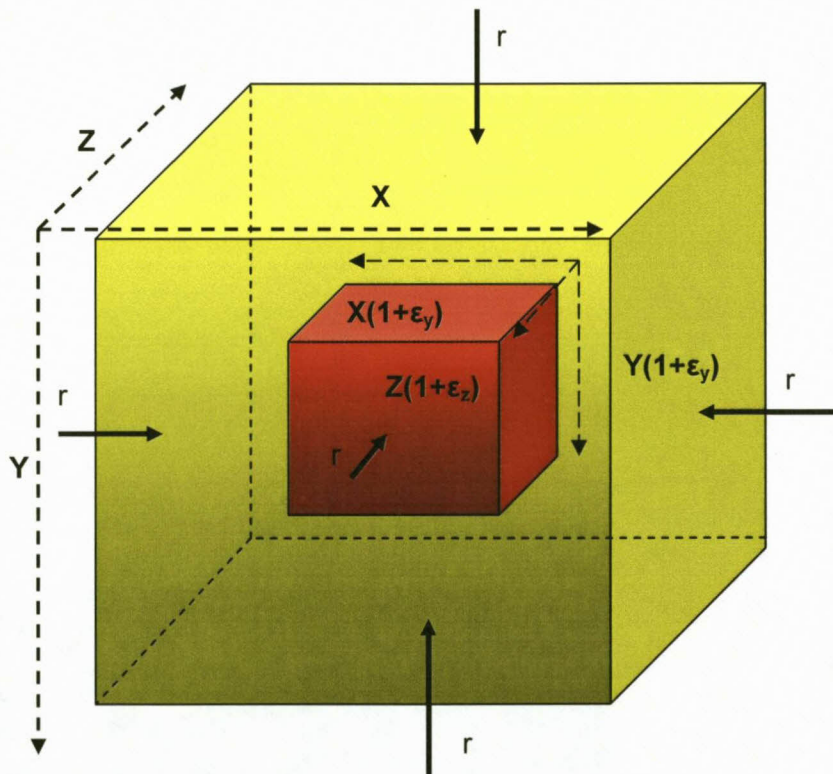
Figure 23 - Volumetric strain

Volumetric strain can be described in terms of normal strains, this is shown in Equation 19 (Botha & Cloot, 2004).

$$V = X(1 + \varepsilon_x)Y(1 + \varepsilon_y)Z(1 + \varepsilon_z)$$

<div align="right">**Equation 19**</div>

Strains produced by the stress induced by the piezo transducers used in this study, the higher order terms used in Equation 19 can be discarded. This means that Equation 19 can be re-written as Equation 20

$$V \approx XYZ(1 + \varepsilon_x + \varepsilon_y + \varepsilon_z)$$

<div align="right">**Equation 20**</div>

Since XYZ describes the original volume of the object, Equation 20 can be re-written as:

$$V = V_0(1 + \varepsilon_x + \varepsilon_y + \varepsilon_z)$$

<div align="right">**Equation 21**</div>

If we apply this to the equation for volumetric strain described in Equation 18, volumetric strain can be defined in terms of normal strains. Equation 22 shows this relation. (University of Bradford, 2002)

$$e = \varepsilon_x + \varepsilon_y + \varepsilon_z$$

<div align="right">**Equation 22**</div>

3.4 Hooke's law

In 1676, a British physicist, Robert Hooke stated a law which described the relation between stresses placed on an object and the deformations or strains they affected upon the object. Equation 23 describes Hooke's law. (Ugural & Fenster, 2003)

$$\vec{F} = -k\vec{x}$$

<div align="right">**Equation 23**</div>

Where;   F   = Force exerted on the object

              k   = force constant

              x   = Displacement of the object

The law states that the force exerted on an object is proportional to the displacement it affects on the object. This proportionality relation is called the force constant or the

spring constant. Materials that obey Hooke's law are known as linear elastic materials (Ugural & Fenster, 2003).
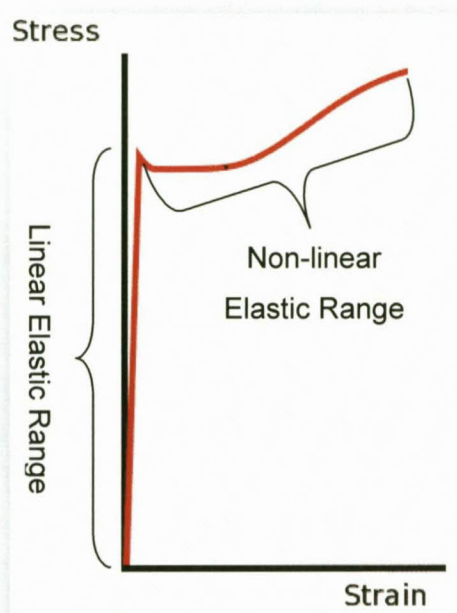
Figure 24 - Stress strain curve

This stress strain relation is unique to all materials. Figure 24 shows the stress strain relation curve for low carbon steel. As seen the material is only linear for the first part of the curve where Hooke's law applies. Beyond this linear region the relation becomes non-linear and cannot be predicted by Hooke's law. However, for the purposes of this study, the stresses used to measure the elastic parameters of a sample are very small. This means all measurements made, are done in the linear elastic part of the curve for all the samples tested. (Champion & Champion, 2007) The assumption that all the samples under test obey Hooke's law applies to this study. This assumption is made due to the fact that the equipment used in the experimental measurements are non-destructive in nature, that is, it does not have the ability to apply pressure to a sample beyond its linear elastic limits.

3.5 Young's modulus

Young's modulus describes the stiffness of a material and is known as the modulus of elasticity, elastic modulus or tensile modulus. It is the ratio of the rate of change between the stress applied, to the strain affected. (Hristopulos & Demertzi, 2008)

Equation 24 defines Young's Modulus (Botha & Cloot, 2004):

$$E = \frac{\sigma}{\varepsilon}$$

Equation 24

Where;   E   = Young's Modulus

σ   = Tensile Stress

ε   = Tensile Strain

Young's modulus can also be used to determine the force exerted over a given area with a certain strain produced.

$$F = \frac{E A_0 \Delta L}{L_0}$$

Equation 25

Where;   F   = Force exerted

E   = Young's Modulus

A_0 = Area

ΔL   = Displacement

L_0 = Original length

3.6 Bulk modulus

Bulk modulus is a materials resistance to uniform compressional force. It is defined as the amount of pressure increase needed to affect a volume change on an object. Equation 26 defines bulk modulus (Aster, 2006).

$$K = -V \frac{\Delta p}{\Delta V}$$

Equation 26

Where;   K   = Bulk modulus

V   = original volume

Δp = Change in pressure

ΔV = Change in volume

Bulk modulus can be categorised as either dry bulk modulus or wet bulk modulus. The dry bulk modulus is the modulus calculated for a sample that has no fluids present in its pore spaces between the grains of minerals that constitute the matrix. The wet bulk modulus is the modulus calculated for a sample where the pore spaces between the grains of minerals are saturated with fluids. The dry bulk modulus is donated by K_d, and the wet bulk modulus is notated by K_w. (Phani & Sanyal, 2008)

3.7 Compressibility

Compressibility is the inverse of bulk modulus and is defined as the measure of volume change to applied pressure. It is defined by Equation 27 (Fine & Millero, 1973).

$$\alpha = -\frac{1}{K}$$

Equation 27

Where;   K   = Bulk modulus

There are a number of compressibility's in a rock sample. These include:

- **Bulk compressibility**

  Bulk compressibility is defined as the total sample compressibility which includes the compressibility of the grains, fluids and gasses that the sample consists of. In order to define the individual states of the bulk compressibility of a sample it must be described by one of the following;

- o *Dry compressibility*

  The compressibility of the sample when there is no pore fluids present. This is denoted by α_d.

- o *Wet compressibility*

  The compressibility of the sample, when its pore spaces are completely saturated by fluid. It is donated by α_w.

- o *Partially saturated compressibility*

  The compressibility of the sample, when the pore spaces are partially saturated with fluid. It is donated by α_p.

- **Fluid compressibility**

  The fluid compressibility is notated by α_f. The fluid used in this study is pure water which has a compressibility of 0.46 GPa^{-1}.

- **Grain compressibility**

  The grain compressibility is the compressibility of the individual grains that make up the sample, in other words the compressibility of the solid mass of the sample. This is notated by α_g.

- **Pore compressibility**

  The pore compressibility is the compressibility of the pore space between the grains. In this study the assumption is made that the grains that make up the sample are incompressible. This is done because the grain compressibility is very small in relation to bulk compressibility. If this assumption is made, then the dry bulk modulus of a sample is equivalent to the pore compressibility. (Horseman, Harrington, & Noy, 2006)

3.8 Shear modulus

The shear modulus, also known as the modulus of rigidity, is defined as the ratio of shear stress applied to a material to the shear strain affected within it. Shear modulus is mathematically defined in Equation 28 (Crandall & Dahl, 1959).

$$G = \frac{\frac{F}{A}}{\frac{\Delta x}{h}}$$

Where; F/A = shear stress

$\Delta x / h$ = shear strain

3.9 Lame's constants

The Lame constants λ and μ can be calculated in a number of ways using a number of different elastic and physical rock properties. The Lame's constants are material properties that are related to the elastic modulus and Poisson ratio. They define the stress to strain relations of a rock sample. The second Lame's constant (u) is identical to the shear modulus (G). (Akiyoshi, Sun, & Fuchida, 1998)The equations below show these equations. (Weisstein, 2007)

$$\lambda = \rho(v_p^2 - 2v_s^2)$$

$$\mu = \rho v_s^2$$

Where; E = Young's modulus

v   = the Poisson ratio

G = the shear modulus, K is the bulk modulus

p   = the density

Vp   = *Compressional* wave speed

Vs   = Shear wave speed

3.10 Poisson's ratio

When an object is put under tensile stress, i.e. if it is stretched, it becomes longer and thinner. Poisson's ratio is a measure of this as it measures the ratio of contractional strain to extensional strain. (Nieves, Gascon, & Bayon, 2007) The Poisson ratio can be described in terms of the Lamé constants λ and u as well as elastic parameters K and G and velocity values V_s and V_p. (Weisstein, 2007)

$$v = \frac{\lambda}{2(\lambda + \mu)}$$

$$v = \frac{\lambda}{2K - \lambda}$$

$$v = \frac{3K - 2\mu}{2(3K + \mu)}$$

$$v = \frac{1}{2} \frac{(\frac{V_p}{V_s})^2 - 2}{(\frac{V_p}{V_s})^2 - 1}$$

Equation 30

Where; λ = Lame constant

u   = lame constant

K   = is the bulk modulus

U   = is the rigidity

Vp   = is the *P*-wave speed

Vs   = is the *S*-wave speed

3.11 Shear velocity
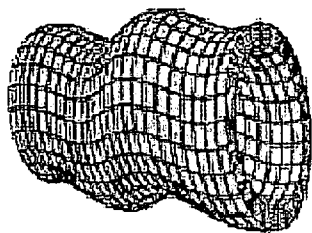
Figure 25 - Shear wave (Leisure & Willis, 1997)

Shear velocity is a vector for rate of change of position. It is a measure of displacement over time in a given direction. If a shear force is applied to an object, in this case, the end of solid cylinder, the shear strains induced in the cylinder will travel down the cylinder away from the source. This shear displacement will move at a speed dictated by the elastic parameters of the cylinder. Figure 25 illustrates how a shear impulse displacement will deform a cylinder while moving from one end of the cylinder to the other. To calculate the shear displacement velocity Equation 31 can be applied. (Song & Suh, 2004)

$$V_s = \frac{\Delta x}{\Delta t}$$

Equation 31

Where; V_s = the shear velocity

Δx = Distance traveled

Δt = Time passed to travel distance

The shear velocity of a material can be determined by its shear modulus and density. Equation 32 defines this relation. (Song & Suh, 2004)

$$V_s = \sqrt{\frac{G}{p}}$$

Equation 32

Where; G = Shear modulus

V_s = Shear velocity

p = Density of the rock sample

36

3.12 Compressional velocity
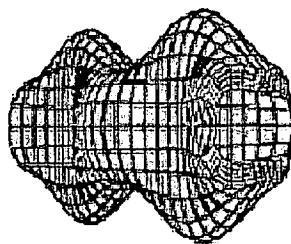
Figure 26 - Compression wave (Leisure & Willis, 1997)

Compressional velocity is a vector for rate of change of position. It is a measure of displacement over time in a given direction. If a longitudinal force is applied to an object, in this case, the end of solid cylinder, the longitudinal strains induced in the cylinder will travel down the cylinder away from the source. This Longitudinal displacement will move at a speed dictated by the elastic parameters of the cylinder. Figure 26 illustrates how a longitudinal impulse displacement will deform a cylinder while moving from one end of the cylinder to the other. To calculate the longitudinal displacement velocity Equation 33 can be applied. (Song & Suh, 2004)

$$V_c = \frac{\Delta x}{\Delta t}$$

Equation 33

Where; V_c = The compressional velocity

Δx = Distance traveled

Δt = Time passed to travel distance

The longitudinal velocity of a material can be determined by its bulk modulus, shear modulus and density. Equation 34 defines this relation. (Song & Suh, 2004)

$$V_p = \sqrt{\frac{1}{p}(K + \frac{4G}{3})}$$

Equation 34

Where; K =   Bulk modulus

V_p =   Compressional wave velocity

G =   Shear modulus

p =   Density of the rock sample

Chapter 4 – Hydrological parameters

4.1 Introduction

The objective of this study is to determine rock core samples hydrological parameters from its elastic parameters. The previous section dealt with the rock elastic parameters. In this section, the rock hydrological parameters to be determined are discussed.

4.2 Porosity

Porosity is a measure of how much space or voids a porous material is made up of as a percentage or fraction of the material's total volume. It is expressed as a fraction between 1 and 0 or 0% and 100% (Ramos da Silva, Schroeder, & Verbrugge, 2008). Porosity can be mathematically expressed as shown in Equation 35.

$$n = \frac{V_{Voids}}{V_{Total}}$$

Equation 35

Where;   n   = Porosity

V_{Voids} = Volume of voids

V_{Total} = Total volume of material

There are a number of porosity types used to describe the porosity of an aquifer as a whole. This study assumes that the samples under test are very small in proportion to the dimensions of the aquifer they were extracted from. As such, they are assumed to be as homogeneous as possible. Hence only a few of the porosity terms apply to this study. These are (Spitz & Moreno, 1996):

- **Inter-granular Porosity** – This is the porosity between granules in a rock matrix. Figure 27 shows an illustration of inter-granular porosity. This type of porosity constitutes the largest contribution to porosity in porous rock.
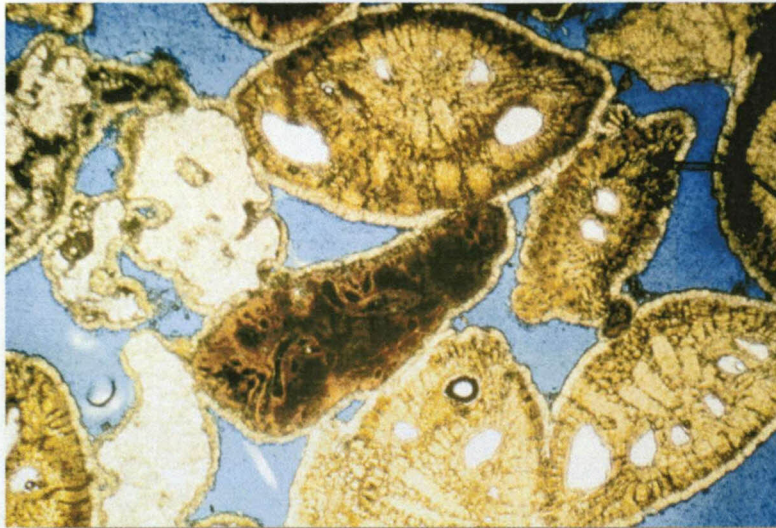
Figure 27 - Inter-granular porosity (GCRP, 2007)

- **Inter particle porosity** – This is the porosity within the individual grains that make up the rock matrix. An illustration of this is shown in Figure 28 .
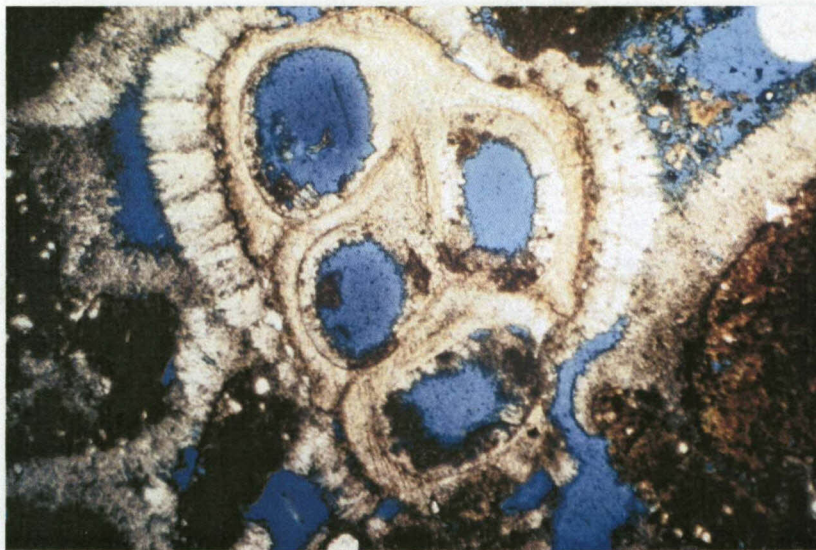
Figure 28 - Inter-particle porosity (GCRP, 2007)

- **Residual Porosity** – Under natural conditions, a part of the voids that make up a sample are isolated from the rest of the voids in the sample. This means they are connected to other voids only through inter-particle porosity. Figure 29 illustrates this.
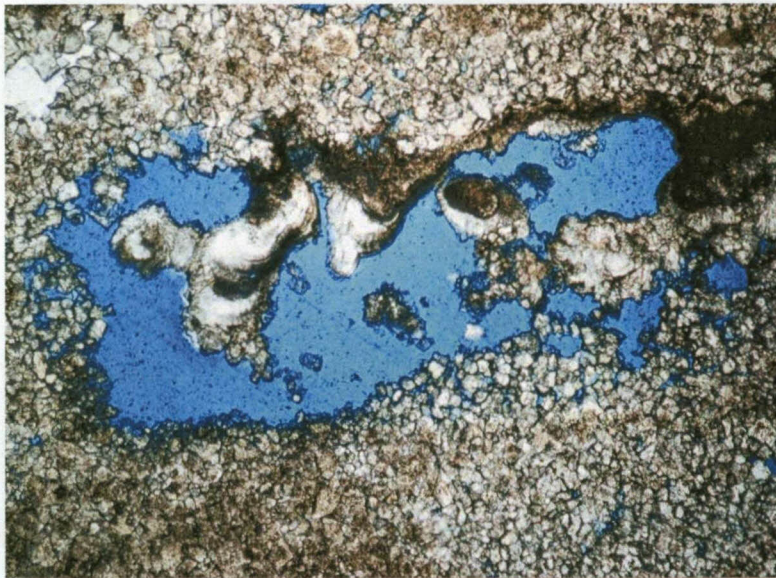
Figure 29 - Isolated pore space (GCRP, 2007)

- **Fracture Porosity** - The porosity contribution by fractures or micro fractures in the sample. Figure 30 illustrates fracture porosity.
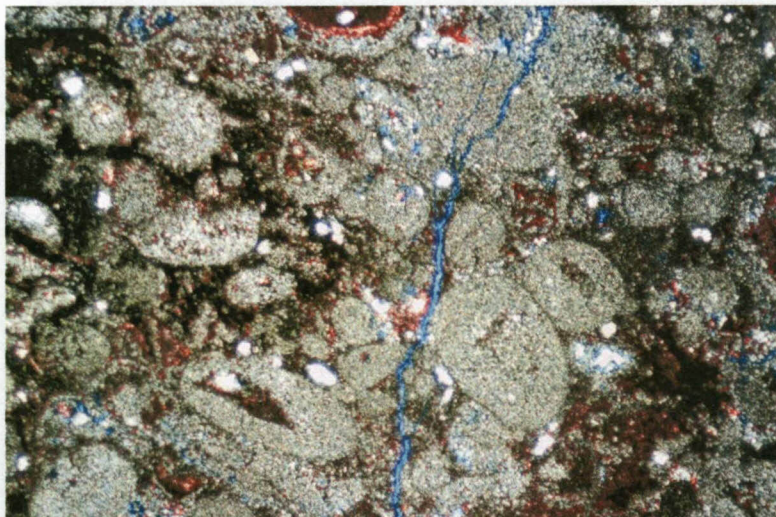
Figure 30 - Fracture porosity (GCRP, 2007)

- **Dual Porosity** – In dual porosity systems the main form of porosity comes from the inter-granular porosity. The main transport systems are fractures between these voids. Figure 31 illustrates a dual porosity system.
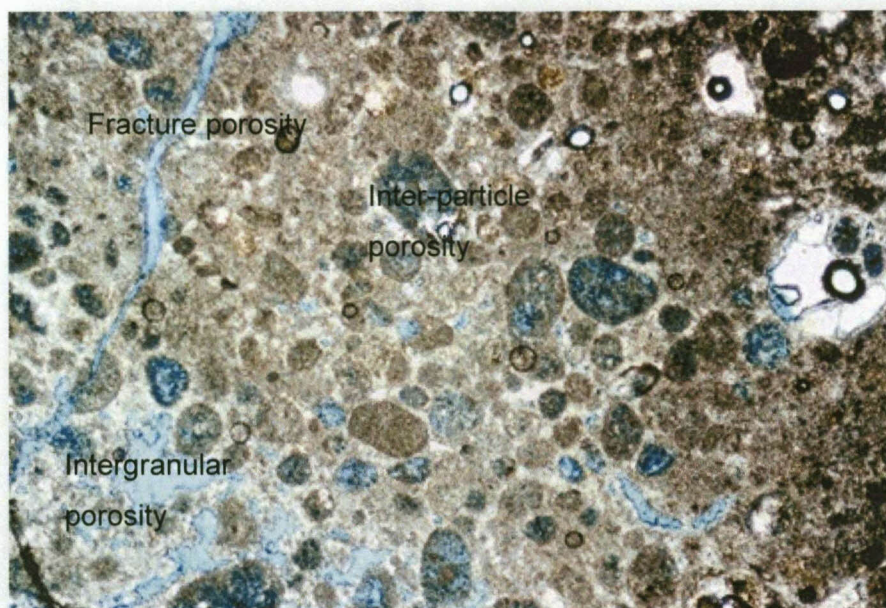
Figure 31 - Dual porosity (GCRP, 2007)

Inter-particle porosity contributes only a very small part of a porous rock total porosity, means that the majority of the voids in the matrix are inter-granular in nature. However, no rock matrix has perfect pore space interconnectivity. As such, there are a number of pore spaces that are isolated from the rest of the pore space. This isolated pore space is known as residual porosity. Thus the total porosity of a rock matrix is the sum of its connected and isolated pore spaces. As mentioned previously, the isolated pores contribute to the residual porosity and the connected pores contribute to the connected porosity. Equation 35 should then be modified to include the residual porosity effects. Equation 36 shows the residual porosity equation. (Spitz & Moreno, 1996)

$$n = \frac{V_C + V_I}{V_s + V_V} = n_c + n_r$$

Equation 36

Where; V_c = Volume of connected pores

V_i = Volume of isolated pores

V_s = Volume of solid particles

V_v = Volume of voids

n_c = Connected porosity

n_r = Residual porosity

In this study, connected porosity is used to calculate the hydrological parameters. It is determined by measuring the mass of a rock sample that has been heated until all the connected pore space within it has been evacuated of water or moisture. The same sample is then submerged in boiling water until all the connected pore space has been filled with water. This done by periodical weighing the samples and comparing the weight to previous measurements. Once the weight measurements have stabilized, the sample is taken to be saturated by water. The difference is the mass of the water in the pores which represents the volume of pore space in the material. The volume of water to the total volume of the sample is its connected porosity.

Porosity varies with applied stress. An example of this is given by Gang and Maurice (2002) where the porosity measured at atmospheric pressure is different to that at geological pressures. This is due to the volumetric stress placed on a sample of porous rock at depth by the geological pressure of the formations above it. Equation 37 describes this relation. (Gang & Maurice, 2002)

$$\Delta\emptyset = \Delta\left(\frac{V_p}{V_b}\right) = \frac{\Delta V_p}{V_b} - \emptyset\frac{\Delta V_b}{V_b}$$

Equation 37

Where; $\emptyset$ = Porosity

V_p = Pore volume

V_b = Bulk volume

Equation 37 relates the change in porosity to the relative change between pore volume and bulk volume in the sample. However, this does not define porosity change with applied volumetric stress. Equation 38 relates the change in porosity to the effective stress on the sample. (Gang & Maurice, 2002)

$$\Delta\emptyset = -\alpha_b(1 - \emptyset)\Delta\sigma_e$$

Equation 38

Where; $\emptyset$ = Porosity

α_b = Bulk compressibility

σ_e = Effective volumetric stress

The effective stress placed on a sample is defined in Equation 39. (Gang & Maurice, 2002)

$$\sigma_e = \sigma_t - P_p$$

<div align="right">**Equation 39**</div>

Where; σ_t = Total stress

P_p = Pore fluid pressure

4.3 Density

The density of a material is described as its mass per unit volume. Highly dense materials such as rock weigh more than less dense materials of similar volume such as gas or liquids. The mathematical description for density is shown in Equation 40.

$$\rho = \frac{m}{V_s}$$

<div align="right">**Equation 40**</div>

Where; ρ = Density

m   = Mass of volume

V_s = Total volume of solid mass

The density of a rock sample can be determined by measuring the dry mass of a sample material. This dry mass is attained by drying out the sample in an oven. The mass is then divided by the sample volume to obtain its density. A more accurate measure of the density of a porous consolidated rock is to measure its bulk density. The bulk density of a porous rock takes the average density of the grains of solid particles and the voids that make up the volume of the sample. Since sedimentary rock is formed by the consolidation of loose granules, the total volume consists of the void space between the consolidated granules as well as the volume of the solid granules themselves. Equation 41 describes this. (Spitz & Moreno, 1996)

$$\rho_B = \frac{m}{V_s + V_v}$$

<div align="right">**Equation 41**</div>

Where; V_s = Volume of the solids

V_v = Volume of the voids
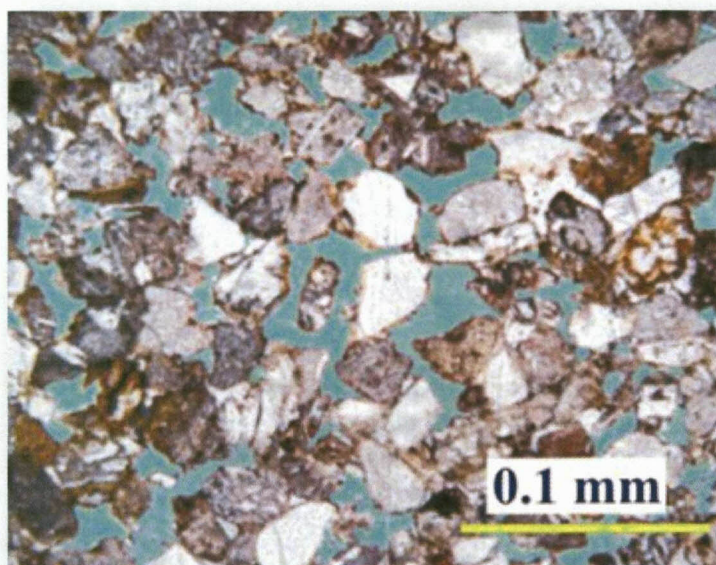
Figure 32 - Low bulk density formation (Petrophysical Studies, 2007)

Figure 33 - High bulk density formation (Petrophysical Studies, 2007)

The bulk density of a porous substance will increase if the particles that make up the matrix are packed closely together minimising the pore space volume. Figure 32 shows a lower density granular formation. There are large voids in this granular matrix and the bulk density is lower than the tightly packed crystalline formation illustrated in Figure 33, which has less voids and a higher bulk density.

4.4 Volume

The volume of a sample is indicative of the three dimensional space it takes up. Volume can be analytically calculated for regular shaped objects. A few examples are shown in Table 1. (Bueche, 1986)
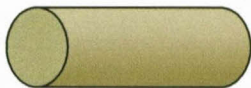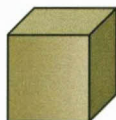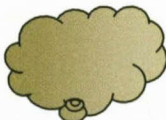
Object	Object Name	Object Volume
	Cylinder	
	Cube	
	Rectangle	
	Half Cylinder	
	Irregular	Water volume displacement

Table 1 - Volume calculations (Bueche, 1986)

There are many more analytical calculations for other shapes, however the shapes listed in Table 1 show the commonly used shape in this study. The volume calculations are used in calculating the bulk density of the object under study. For irregular shapes there are no analytical solutions and the volume must be measured by the water volume displacement method. This method entails the emersion of the irregular object into a known volume of water. The volume of water that is displaced

once the object is emerged is equal to the total volume of the object. This method assumes that the object is minimally porous such that very little water is absorbed by the object. Figure 34 illustrates the measurement technique.

Figure 34 - Irregular shape volume measurement (dkimages, 2007)

4.5 Specific volume

Specific volume is defined as the volume occupied by a specific mass of material. It is therefore the inverse of density. Equation 42 shows this (Bueche, 1986).

$$\frac{1}{\rho} = \frac{V_s}{m}$$

Equation 42

Where; ρ = Density

m   = Mass of volume

V_s = Total volume of solid mass

4.6 Specific storage

The specific storativity, also known as specific storage, is the amount of water which a given volume of aquifer will produce, provided a unit change in hydraulic head is applied to it (while it still remains fully saturated); it has units of inverse length, $[L^{-1}]$. It is the primary mechanism for storage in confined aquifers It is defined by Equation 43 (Hermance, 2003):

$$S_s = \frac{Vw}{\frac{dH}{Va}}$$

Equation 43

Where; S_s = Specific storativity

Vw   = Volume of water in the aquifer

dH   = Change in head in the aquifer

Va   = Volume of the aquifer

In terms of measurable physical properties, specific storativity can be expressed as (Burbey, 2001)

$$S_s = \rho g(\alpha + \eta \beta)$$

Equation 44

Where;   p   = density of water

g   = gravitational constant

α = compressibility of the rock

β = compressibility of the water

η = porosity of the rock

Figure 35 shows the conceptual diagram of how specific storativity is defined in a confined aquifer. It is important to note that this applies only to confined aquifers that are fully saturated.. (Hermance, 2003)
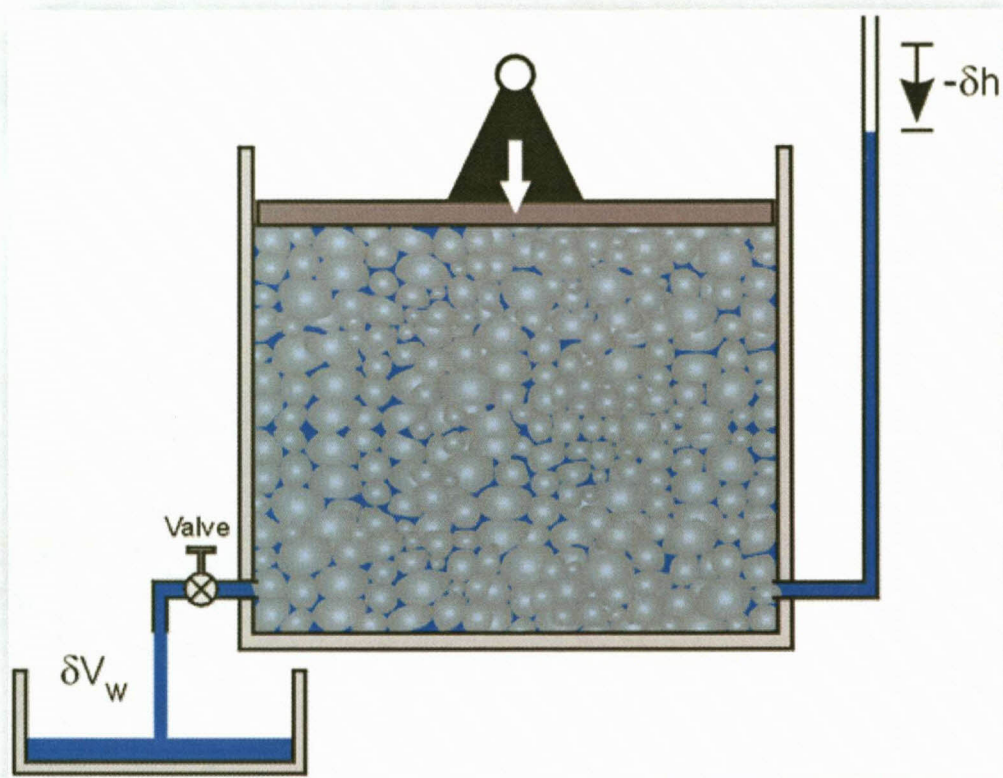
Figure 35 - Specific storativity (Hermance, 2003)

4.7 Storativity

Storativity is the vertically averaged specific storativity value for an aquifer or aquitard. For a homogeneous aquifer or aquitard they are simply related by

$$S = Ss \times b$$

Equation 45

Where b is the thickness of aquifer. Storativity is a dimensionless quantity and can be expressed as the volume of water release from storage per unit decline in hydraulic head in the aquifer, per unit surface area of the aquifer. (Hermance, 2003)

This is defined by Equation 46.

$$S = \frac{dVw}{dH \times A}$$

Equation 46

Where;   dVw   = change in volume of water

dH   = change in head

A   = area
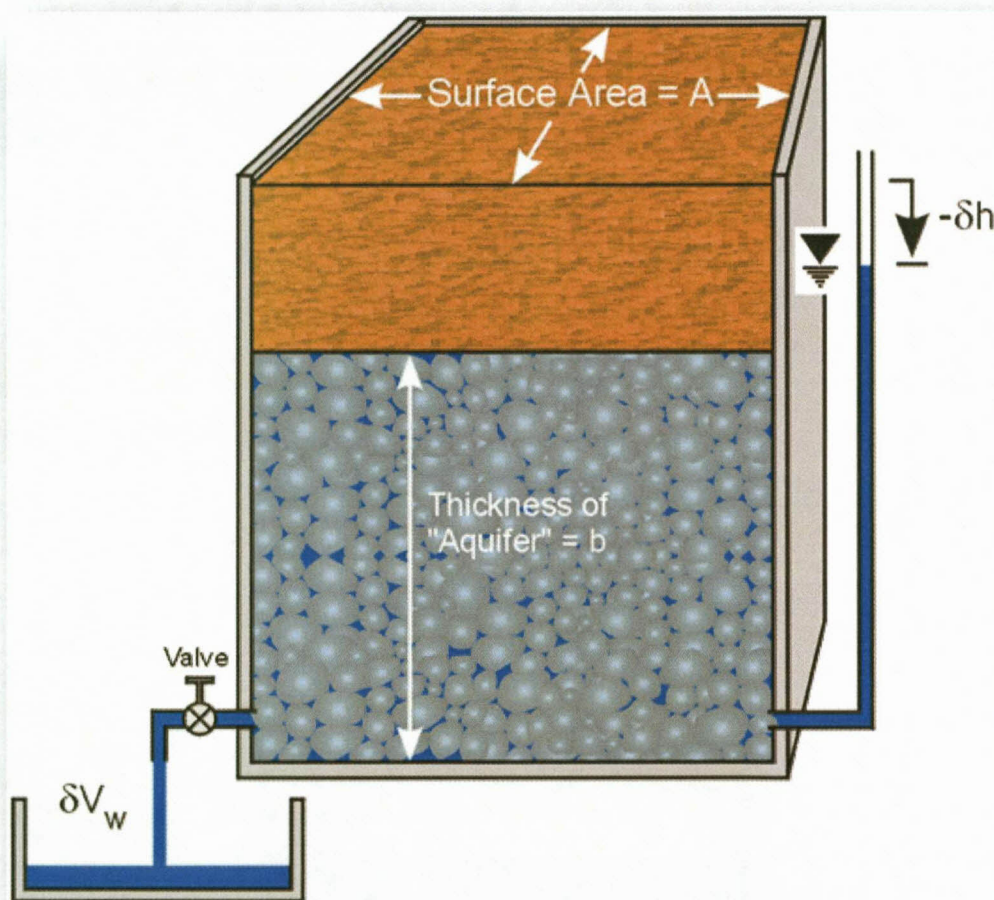
Figure 36 - Storativity (Hermance, 2003)

Figure 36 shows the storativity concept diagram. Storativity is related to specific storativity by the thickness of the aquifer b. The thicker the aquifer, the larger the value of storativity will be.

4.8 Hydraulic diffusivity

Diffusivity is defined as the ratio of transmissivity to storativity in a confined aquifer. If a sample is compressed by a stress, it is the time it takes for the sample to stabilize at its new length. In essence it is the samples deformation impulse response. (Knudby & Carrera, 2006) It can also be defined as the ratio of hydraulic conductivity to specific storativity in a confined aquifer. Equation 47 define these relations (Spitz & Moreno, 1996)

$$D = \frac{K}{S_s} = \frac{T}{S}$$

Equation 47

Where;   D   = Hydraulic diffusivity

K   = Hydraulic Conductivity

S_s = Specific storativity

S   = Storativity

T   = Transmissivity

However, diffusivity can also be described in terms of compressibility under certain assumptions. Hart and Hammon (2002), describe a method to determine the hydraulic conductivity and specific storativity of marine sediments by using a Manheim squeezer. The method measures the compressibility of a sample of marine by compressing the sample and measuring the axial displacement over time. The compressibility is then computed using Equation 48.

$$c_m = \frac{\frac{\Delta w}{w_0}}{\Delta \sigma_z}$$

Equation 48

Where; Δw = displacement (m)

W_0 = Original sample length (m)

$\Delta \sigma_z$ = Axial stress (Mpa)

If the compressibility is known, Equation 48 can be modified to calculate the axial displacement.

This is shown in Equation 49.

$$\Delta w = c_m w_0 \Delta \sigma_z$$

Equation 49

Where; c_m = compressibility

Δw = displacement (m)

W_0 = Original sample length (m)

$\Delta \sigma_z$ = Axial stress (Mpa)

If an axial stress is chosen, then the displacement can be calculated for the sample under that stress.

Hart and Hammond (2002) then used a square root of time method to relate the diffusivity to the axial displacement and compressibility of the sample. This is done using Equation 50.

$$\Delta w(t) = 2 c_m \gamma \sigma_z \sqrt{\frac{Dt}{\pi}}$$

Equation 50

Where; Δw = displacement (m)

σ_z = Axial stress (Mpa)

c_m = compressibility

t   = time (s)

γ = Loading efficiency

D   = Hydraulic diffusivity

The loading efficiency is calculated using Equation 51.

$$\gamma = \frac{\Delta P_{pore}}{\Delta \sigma_z}$$

Equation 51

Where; γ = Loading efficiency

$\Delta \sigma_z$ = Axial stress (Mpa)

ΔP_{pore} = Pore fluid pressure
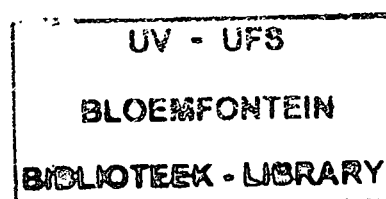
If it is assumed that the pore fluid and grains that constitute the sediment in the sample are incompressible. This leads to a loading efficiency of 1. If the assumption that the loading efficiency of one is used, then the diffusivity can be calculated using Equation 50. This is shown in Equation 52.

$$D = \frac{\Delta w^2 \pi}{4c_m^2 \Delta \sigma_z^2 t}$$

Equation 52

Where; Δw = displacement (m)

c_m = compressibility

γ = Loading efficiency

D = Hydraulic diffusivity

t = Time

σ_z = Axial stress (Mpa)

If Equation 52 is further simplified, it can be shown that hydraulic diffusivity is independent of the stress applied. If Equation 49 is substituted into Equation 52 the result is shown in Equation 54b.

$$D = \frac{w_0^2 \pi}{4t}$$

Equation 54b

Where; W_0 = Original sample length (m)

D = Hydraulic diffusivity

t = Time

To determine the time that should be substituted into Equation 54b, a simulation is run that calculates the hydraulic diffusivity for a set of sample lengths over a time period of 100 seconds. The results are shown in Figure 37. The time data used is taken at 95% of the total compression of the sample. This is calculated by comparing the hydraulic conductivity values measured for each sample to the hydraulic conductivities calculated using the time elapsed at 95% of compression. If the values correlate well over the range of samples used then that time elapsed period is used, otherwise the process must be recalculated using another compression percentage. In this study, the stabilization time that fits best with all the samples used is 10 seconds. Therefore it is taken that for all the sample lengths used in this study, a stabilization point is reached after 10 seconds. This is the elapsed time where the majority of the axial displacement on the sample has taken place and

is used as the value t in Equation 54b. The logarithmic plot of Figure 37 is shown on Figure 38.
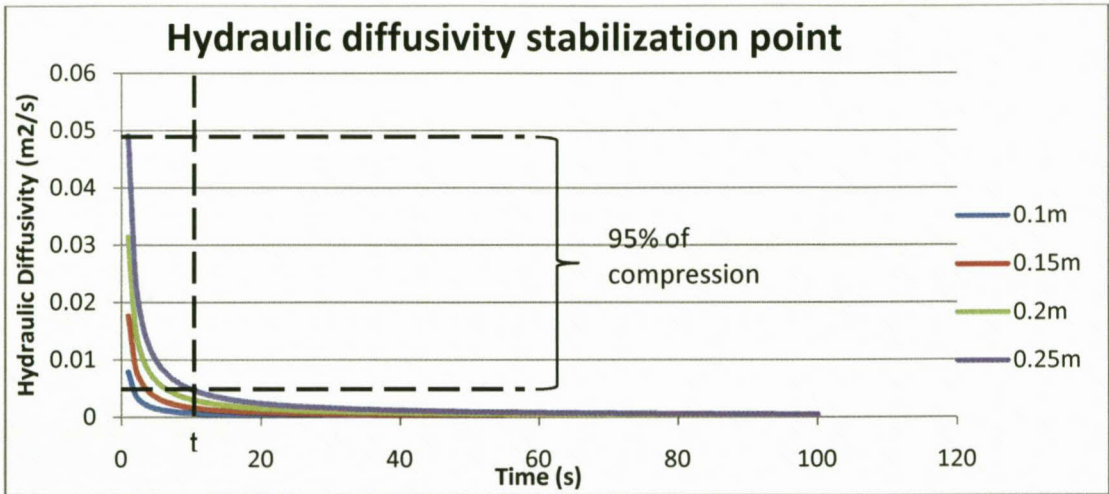
Figure 37 - Hydraulic diffusivity equalization point
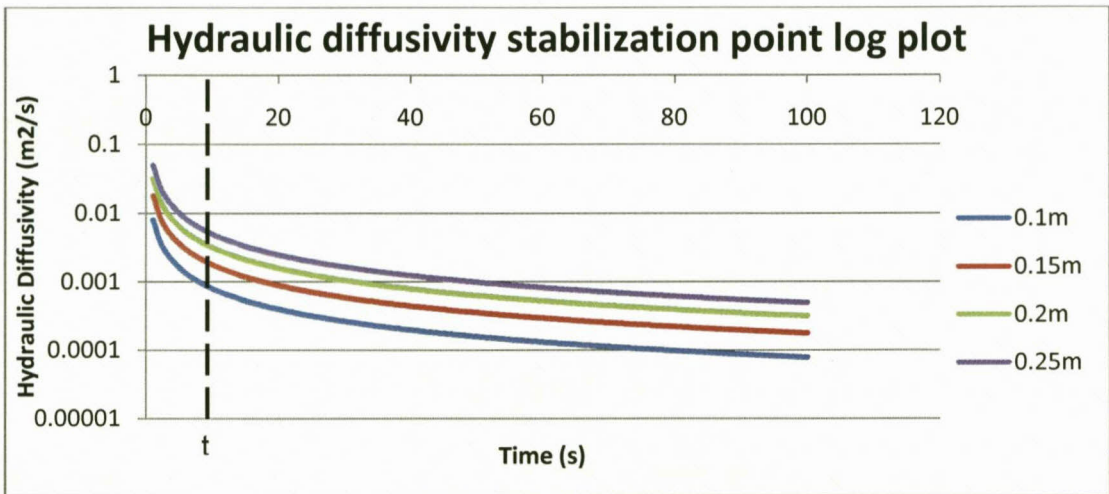
Figure 38 - Hydraulic diffusivity log plot

4.9 Hydraulic conductivity

Hydraulic conductivity as defined by Darcy's law is the amount of water that flows through a cross sectional area of an aquifer under a hydraulic pressure gradient. Equation 53 defines this relation: (Spitz & Moreno, 1996)

$$K = \frac{Q}{iA}$$

Equation 53

Where;   K   = Hydraulic conductivity

i   = Hydraulic pressure gradient

A   = Area

Q   = Flow rate

4.10 Transmissivity

Transmissivity is defined as the volume of water flowing through the cross sectional area of the whole aquifer. It is in essence the hydraulic conductivity over the entire thickness of the aquifer. It is defined in Equation 54. (Spitz & Moreno, 1996)

$$T = Kb$$

Equation 54

Where;   T   = Transmissivity

K   = Hydraulic conductivity

b   = Thickness of the aquifer

4.11 Intrinsic permeability

Intrinsic permeability is a measure of how a porous material transmits water. This is in part due to the shape, orientation and configuration and types of flow paths in the medium. It is the relation between the physical rock properties, the fluid properties and the flow rate under a pressure gradient.

Equation 55 defines this relation. (Spitz & Moreno, 1996)

$$k = Cd^2$$

<div align="right">**Equation 55**</div>

Where; k = Intrinsic permeability

     C = Configuration of flow paths

     D = Effective pore diameter

Permeability can also be related to hydraulic conductivity and fluid viscosity as shown in Equation 56. (Botha & Cloot, 2004)

$$k = \frac{Ku}{pg}$$

<div align="right">**Equation 56**</div>

Where; k = Intrinsic permeability

     K = Hydraulic conductivity

     P = Fluid density

     g = Gravitational acceleration

     u = Fluid viscosity

4.12 Micro fracturing

Micro fractures are small cracks that appear in rock grains due to stress conditions. Micro fracturing occurs within rock grains for a number of reasons. The most common of these are sudden change in stress applied to a sample and mechanical stress placed on a sample volume by drilling extraction equipment such as core drills. (Sayers, 2007)

Figure 39 - Micro fracturing (University of Texas, 2007)

Figure 39 shows micro fractures in rock grains. Micro fracturing affects acoustic pulse velocities in a rock sample in that it effectively slows the pulse down. When pressure is applied to a sample, these micro fractures are compressed closed and the acoustic velocity increases. As this pressure increases, the acoustic velocity increases until it becomes a linear increase of velocity. (Sayers, 2007) Figure 40 illustrates this principle. In the event that there is no micro fracturing, the compressional wave velocity is V_o. As pressure placed on the sample increases, so does the P-Wave velocity. This velocity increase is linear as long as the sample obeys Hooke's law and stays within its linear elastic range. If micro fracturing is present the sample P-wave velocity will be lower by V_{dif}. As the pressure on the sample increases so does the p-wave velocity. This velocity increase is non-linear until the point is reached at P_{100} where the micro factures are closed. The velocity increase is then linear from that point onwards. These velocity changes are typically very small. This study assumes that the velocity difference is smaller than the velocity error produced by the sampling rate and is thus ignored. These errors are discussed in chapter 5.
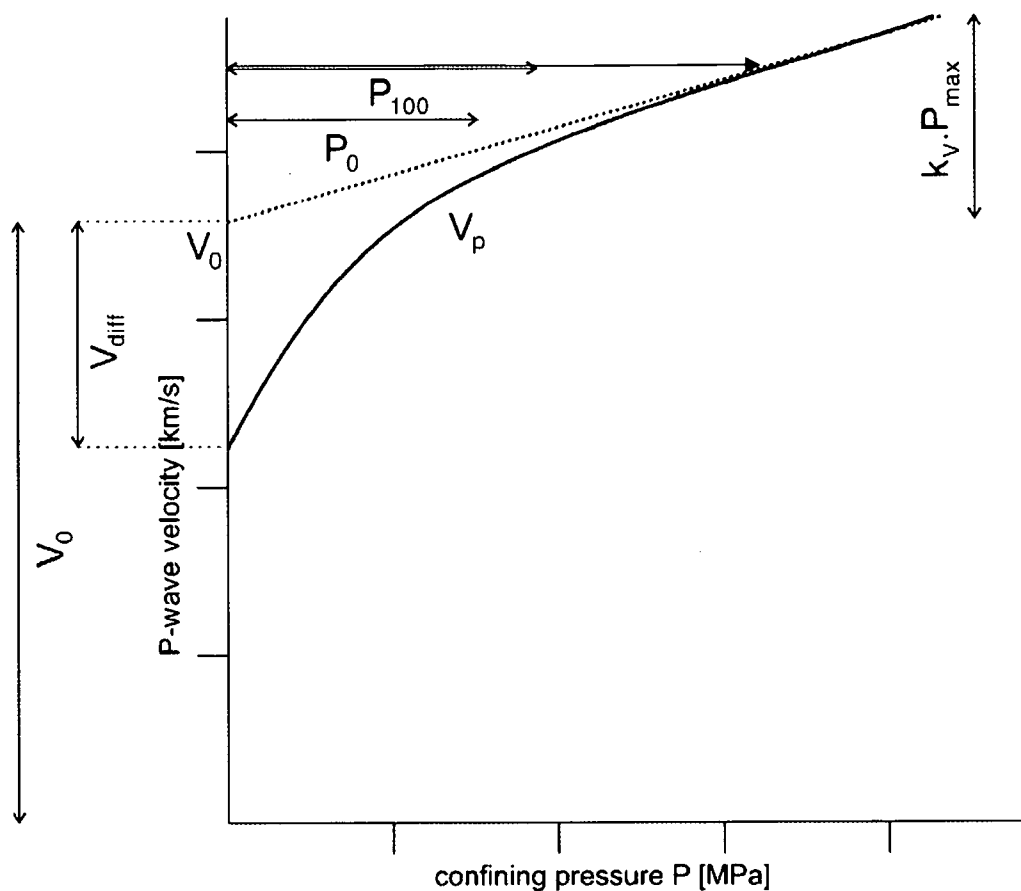
Figure 40 - Micro fracturing induced velocity difference (Přikryl, Lokajíček, Pros, & Klíma, 2007)

Equation 57 relates the variables on Figure 40 to each other. (Přikryl, Lokajíček, Pros, & Klíma, 2007)

$$V_p = V_o + k_v * P - V_{dif} * 10^{\left(-\frac{P}{P_o}\right)}$$

Equation 57

Where; V_p = Compressional wave velocity

V_0 = Velocity if no micro fracturing present

K_v = Velocity coefficient

P = Applied pressure

V_{dif} = Difference in ideal and real velocity at atmospheric pressure

P_o = Pressure at ideal velocities

It is important to note that all velocity tests done in this study are done at atmospheric pressure. As the absolute pressure of the formation and pore fluid pressure at depth is not practically available for this study, it has been omitted as unknowns.

57

Chapter 5 – Theory of time of flight

5.1 Introduction

In this section time of flight methods, as a way to determine a material's elastic properties, will be discussed. There are a number of time of flight methods in current use. These include:

- **Passive listening**
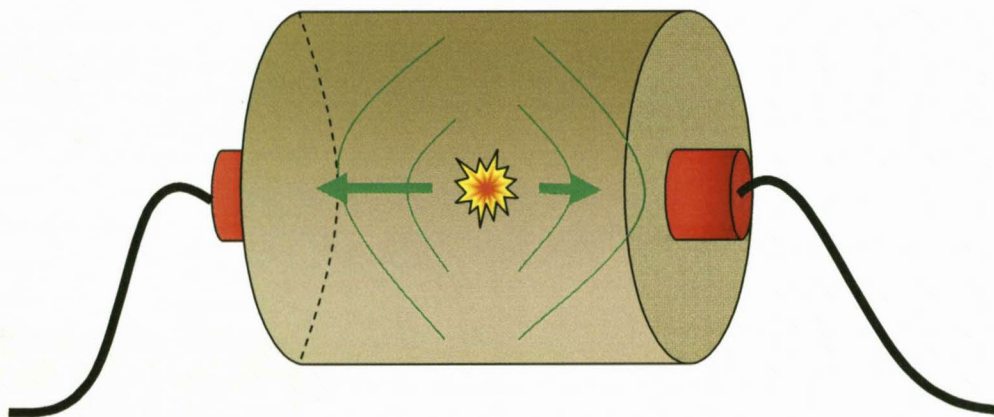
Figure 41 - Passive time of flight method

Passive time of flight techniques make use of only passive or listening receivers. They are set at known geometric locations such as the red sensors at the ends of the sample cylinder shown on Figure 41. When a mechanical event occurs within the sample or on the sample surface such as an explosion or hammer blow, time taken for the produced sound to reach both sensors is measured and the acoustic velocity is calculated from these measurements. If the material's acoustic velocity is already known, then the dimensions of the sample can be calculated using the time difference between acoustic pulse arrivals at the sensors. If the velocity is known, the exact location of the mechanical event can also be calculated by the pulse time arrival differences. This is very similar to acoustic sonar used in submarines. Since this study is interested in non destructive testing of materials, passive techniques will not be employed as a test method. (Song & Suh, 2004)

- **Pulse echo**
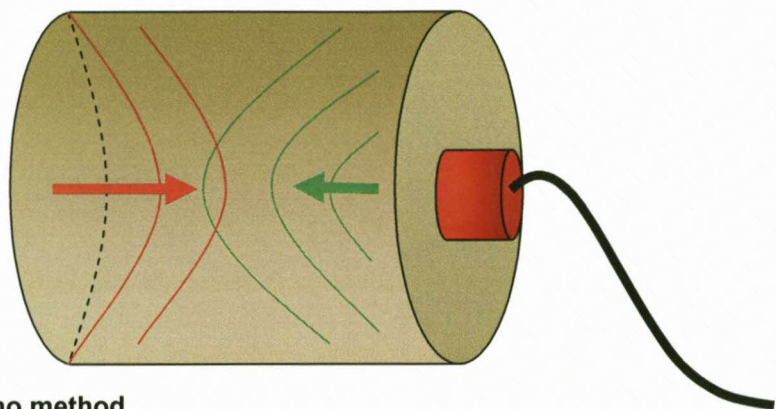
Figure 42 - Pulse-echo method

Pulse-echo techniques are mostly used in the building industry. The reason for this is that they are used primarily to test for structural integrity of building surfaces such as walls, foundations and support beams. The technique works on the principle of reflection. A transducer placed against the object to be tested, sends a high frequency acoustic pulse through the sample. This pulse travels to the end of the sample where it is reflected by the opposite surface. It then travels back to the receiving transducer. The time it took to travel the distance to the end of the sample and back is measured and used to calculate the acoustic velocity of the material, which in turn is used to calculate the materials elastic parameters (MCEN, 2001).
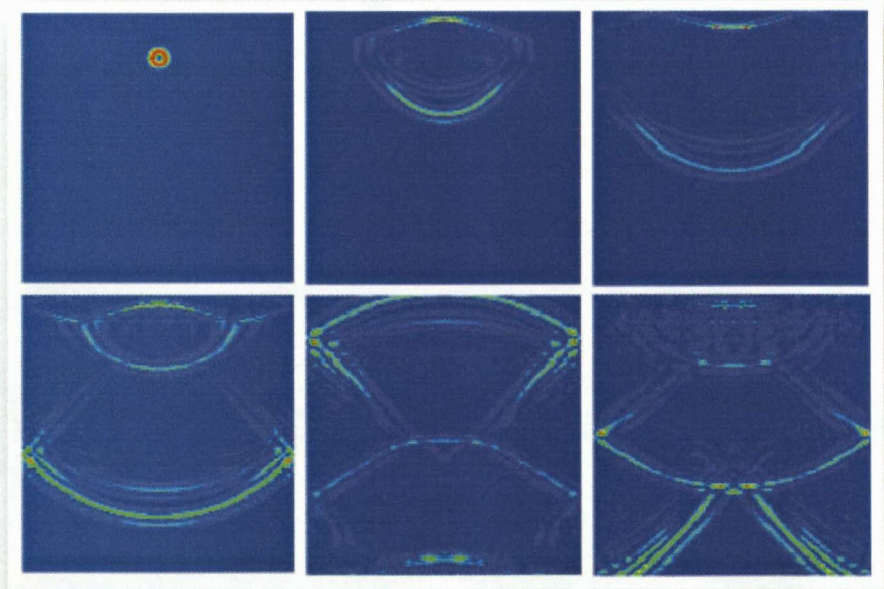
Figure 43 - Diffraction effects (Texas University, 2007)

The pulse-echo technique requires that the pulse frequency used has a wave length much smaller than the dimensions of the object being tested. This is done to avoid the effects of refraction of the acoustic wave from interfering with the measurement of the acoustic velocities. Figure 43 shows a simulated wave moving through a cylinder. The effects of the diffraction can clearly be seen as the primary wave front hits the side wall and reflects back to the source. This in effect will give a false, earlier time of arrival reading at the receiving sensor that interprets the velocity to be higher than it is. If the pulse frequency is higher, then the curvature of the main wave front will be flatter and much less energy will be reflected back to the source. These low energy reflections can then be filtered out or ignored by system.

High frequency transducers used in pulse-echo systems are very expensive and require special acoustic coupling gels to make good contact with the sample under test. For this reason, this study did not employ this technique in measuring acoustic velocities of core samples.

- **Pitch Catch**
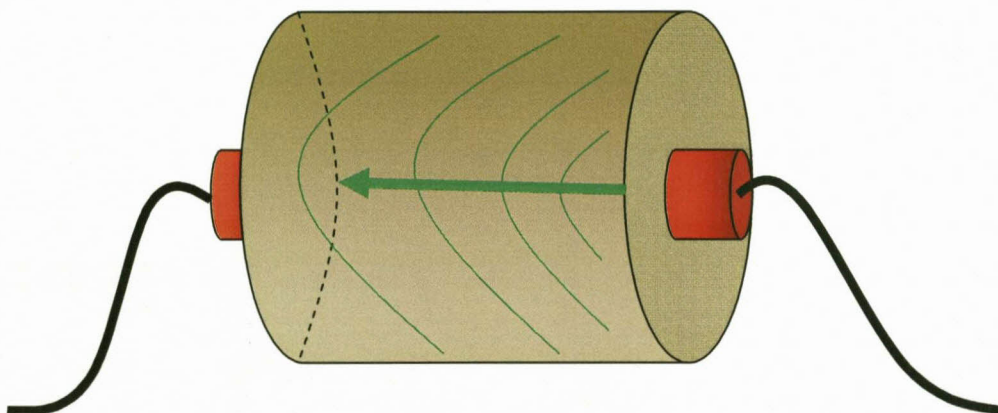
Figure 44 - Pitch-catch method

The last time of flight technique is the pitch-catch method. As the name implies the system transmits a pulse or continuous sound wave from a transmitter located at one end of the sample which travels down the sample to the opposite end where it is received by another transducer. This is shown in Figure 44 The time taken for the primary acoustic front wave to travel down the sample is measured and used to calculate its acoustic velocity. This method is geometrically more complex to implement than the pulse-echo

technique, which requires only one transducer. However, it has the advantage that it does not require the use of expensive high frequency transducers. This is due to the fact that this method does not have to deal with reflection noise caused by diffraction of low frequency acoustic waves. Figure 43 shows that the primary wave will always be the first to arrive at the receiving transducer. This makes the calculation of time of arrival far simpler and more precise than pulse- echo techniques (Du Preez, Dennis, & van Tonder, 2007).

The use of pitch-catch methods to calculate material acoustic velocities in this study not only simplifies the experimental methods and equipment, but also saves costs. As low frequency transmitted acoustics waves can be used, only inexpensive coupling liquids such as glycerin can be used. (MCEN, 2001)

5.2 Methods

The pitch-catch method measures the time it takes a sound pulse of a given frequency to travel through a substance, in this case a cylindrical core rock sample, from a transmitting ultrasound transducer to a receiving ultrasound transducer at the opposite end of the sample. This is achieved by clamping piezo-electric transducers to either end of the cylinder rock sample and inducing a pulse of ultrasound at one transducer. The receiving ultrasound transducer records simultaneously by means of analog to digital converters at a rate of one million samples per second. The time it takes for the ultrasound pulse to travel across the sample is measured by looking at the recorded data and delineating a sudden rise in voltage at the frequency of the traveling ultrasonic pulse. The time is then recorded at this point and is divided by the length of the sample. This gives a value for the velocity of the wave for that specific sample.

The samples used in determination of velocities with time of flight methods are dried samples taken from water saturated core samples dried in an oven. This measures the matrix elastic parameters and gives the most realistic results for the hydrological parameter calculations (Song & Suh, 2004). If saturated samples are measured, they will include the elastic moduli of the pore fluid and the matrix. This will give misleading values as to the compressibility of the matrix.

5.3 Modes of travel

There are a number of different ways in which acoustic waves travels in and deform a sample. A few of these distortion modes are shown in Figure 45. These include compressional, shear and torsional modes of vibration.
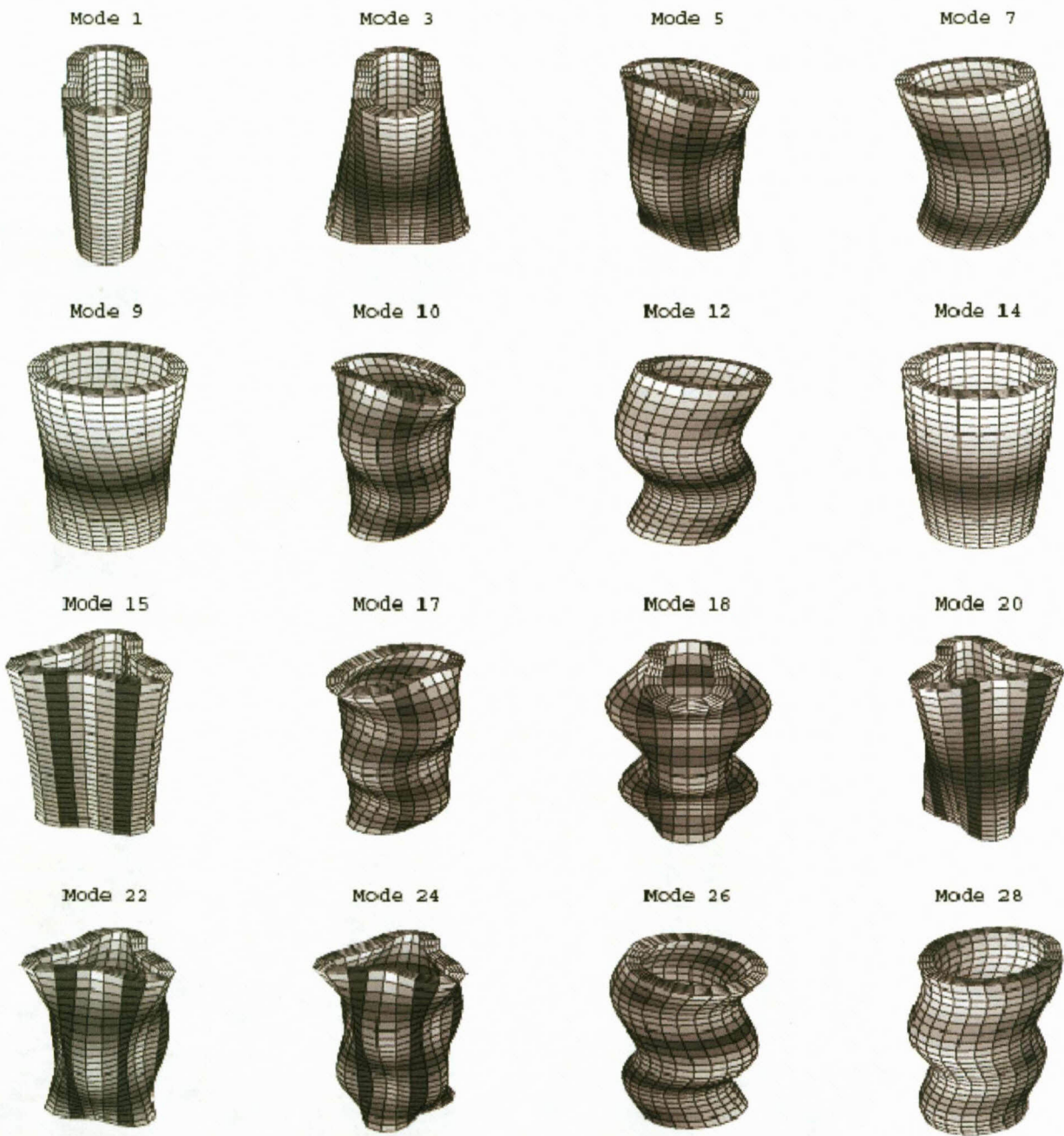
Figure 45 – Modes of vibration (Zadler, Jerome, & Le Rousseau, 2003)

These modes of vibration are controlled by the type of transducer used. Only compressional and shear transducers are used in this study.

The only modes of interest in time of flight testing are the compressional and shear modes. Figure 46 and Figure 47 show these modes.
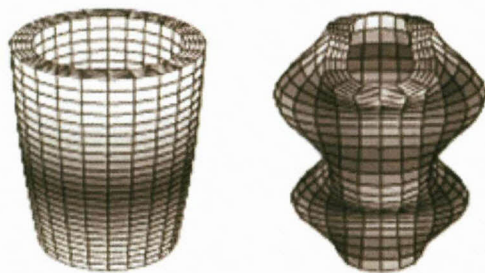
Figure 46 - Compressional vibration modes (Zadler, Jerome, & Le Rousseau, 2003)

Figure 47 - Shear vibration modes (Zadler, Jerome, & Le Rousseau, 2003)

These modes are induced in a sample by using either compressional or shear transducers, as discussed later. The compressional velocity is calculated by measuring the time it takes for an acoustic pulse to travel from a transmitting compressional transducer to a receiving transducer at the opposite end. Equation 34 describes this calculation (Song & Suh, 2004).

$$V_p = \frac{L}{t_p}$$

Equation 34

Where; V_p = Compressional wave velocity

           L   = Length of the sample

           t_p = Compressional wave travel time

The shear velocity is calculated by the measuring the time it takes for an acoustic pulse to travel from a transmitting shear transducer to a receiving transducer at the opposite end. Equation 32 describes this calculation.

$$V_s = \frac{L}{t_s}$$

<div align="right">**Equation 32**</div>

Where; V_s = Compressional wave velocity

   L   = Length of the sample

   t_s = Shear wave travel time

5.4 Calculation of elastic parameters

In time of flight methods, elastic parameters are calculated using the sample velocity measurements for compressional waves and shear waves of a sample. To calculate shear modulus, Equation 29 is used (Song & Suh, 2004).

$$G = V_s^2 \times \rho$$

<div align="right">**Equation 29**</div>

Where;   G   = Shear modulus

   V_s = Shear velocity

   p   = Density of the rock sample

Using the shear modulus G, we can then determine the bulk modulus of the sample using Equation 58 (Song & Suh, 2004):

$$K = V_p^2 \rho - \frac{4G}{3}$$

<div align="right">**Equation 58**</div>

Where;   K   = Bulk modulus

   V_p = Compressional wave velocity

   G   = Shear modulus

   p   = Density of the rock sample

Together, the bulk modulus and the shear modulus describe the elastic parameters of the rock sample.

5.5 Velocity error calculations

An inherent measure of uncertainty is always present in time of flight calculations. This is due to the digital sampling limitations placed on the system by hardware constraints in the rate a voltage can be sampled. In the case of this system, the voltage produced by the receiving piezo transducer is sampled discretely every micro second. This means the system can sample at a rate of one million samples per second. Even though this sounds like an extremely fast sampling rate, there is still a small error or uncertainty in the actual velocity to the measured velocity. The discrete nature of digital sampling produces this error by allowing a small pause between samples. If the pulse arrives at the receiver in between these samples there is an uncertainty as to the exact time the pulse arrived. The error can however be calculated for a given sample length and discrete transit time. If a sample has a length of 1 meter and takes a time of 0.00045106 seconds to travel, using Equation the velocity is calculated to be 2217 m/s. However, the analogue to digital converter used can only sample at a rate 1000000 S/s then the best time resolution available is 1us. This means that the measurable transit time is then 0.000451or 0.000452 seconds and not the actual 0.00045106 seconds. If the velocity is recalculated using Equation and the new time, the velocity works out at 2217.295 m/s which is a bit fast than the actual velocity. If this error is presented as a percentage it works out to be a 1.33% error. This may seem small, however as the velocities increase and/or the sample lengths decrease the error gets larger. Figure 48 shows this velocity error expressed as a percentage of the actual velocity. Series 1 on the graph shows the error over a velocity range of 0m/s to 8000 m/s for a sample length of 1m. Series 2 through 7 are for sample lengths of 0.5m, 0.2m, 0.1m, 0.05m, 0.02m and 0.01m. Figure 48 illustrates that the error increases as velocity increases and sample length decreases. If the error is to be kept at an acceptable value below 5% throughout the velocity range of 0 m/s to 8000 m/s, the sample length must be **no shorter than 0.2 m in length**. However, shorter samples are acceptable if the velocity is low enough to be in the 5% error range. Figure 49 shows the velocity error percentage as a function of sample length over a number of velocities. It can be clearly seen that sample lengths greater than 0.2 m produce errors under 5%. Series 1 through 7 were calculated at velocities from 1000m/s to 7000m/s. In effect this limits the system to use with samples no shorter than 0.2m and velocities lower than 8000m/s in order to remain within 5% error of the true velocity. If equipment with a higher sampling rate is used then shorter and higher velocity samples can be tested.
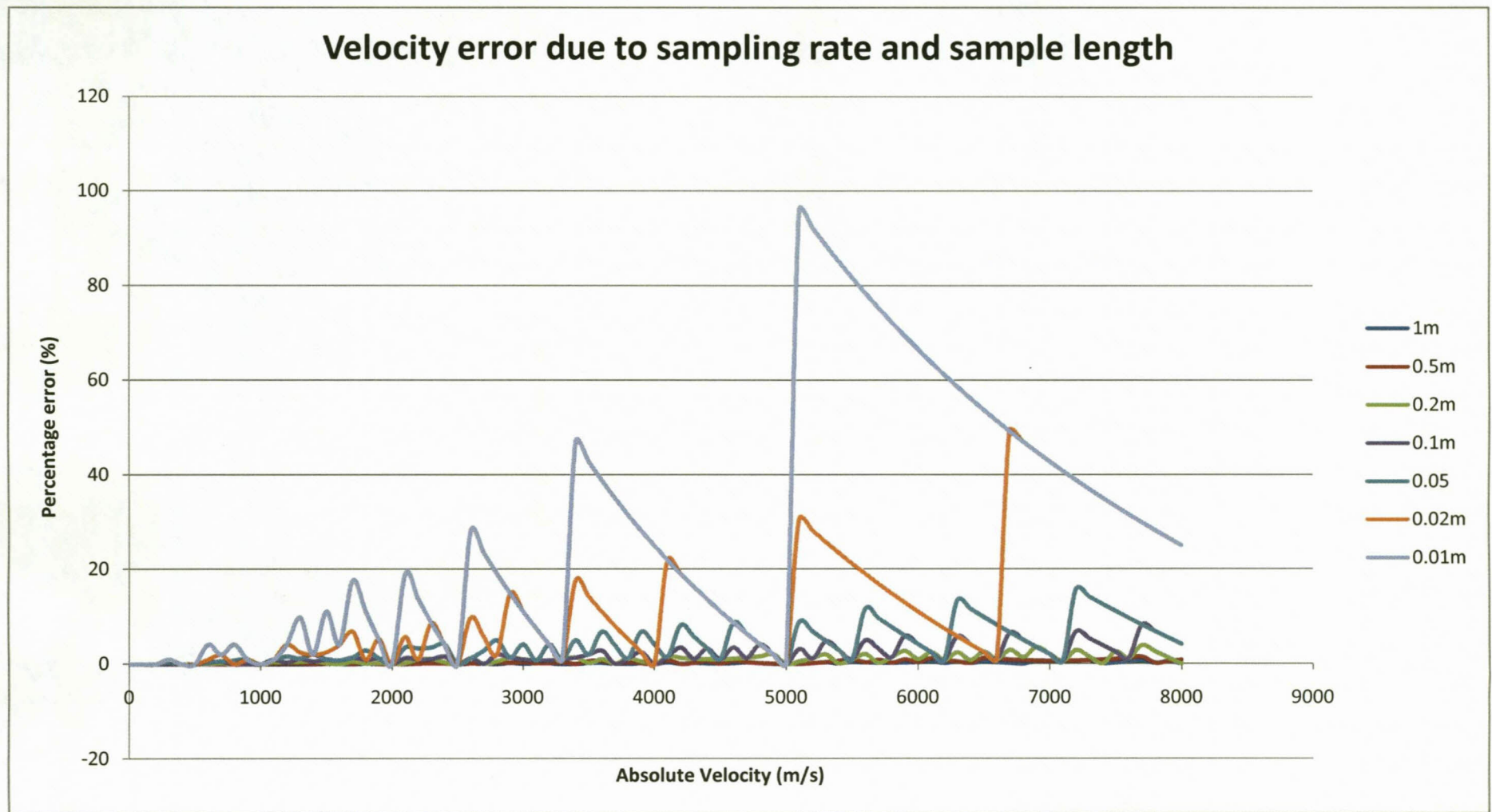
Figure 48 - Velocity error
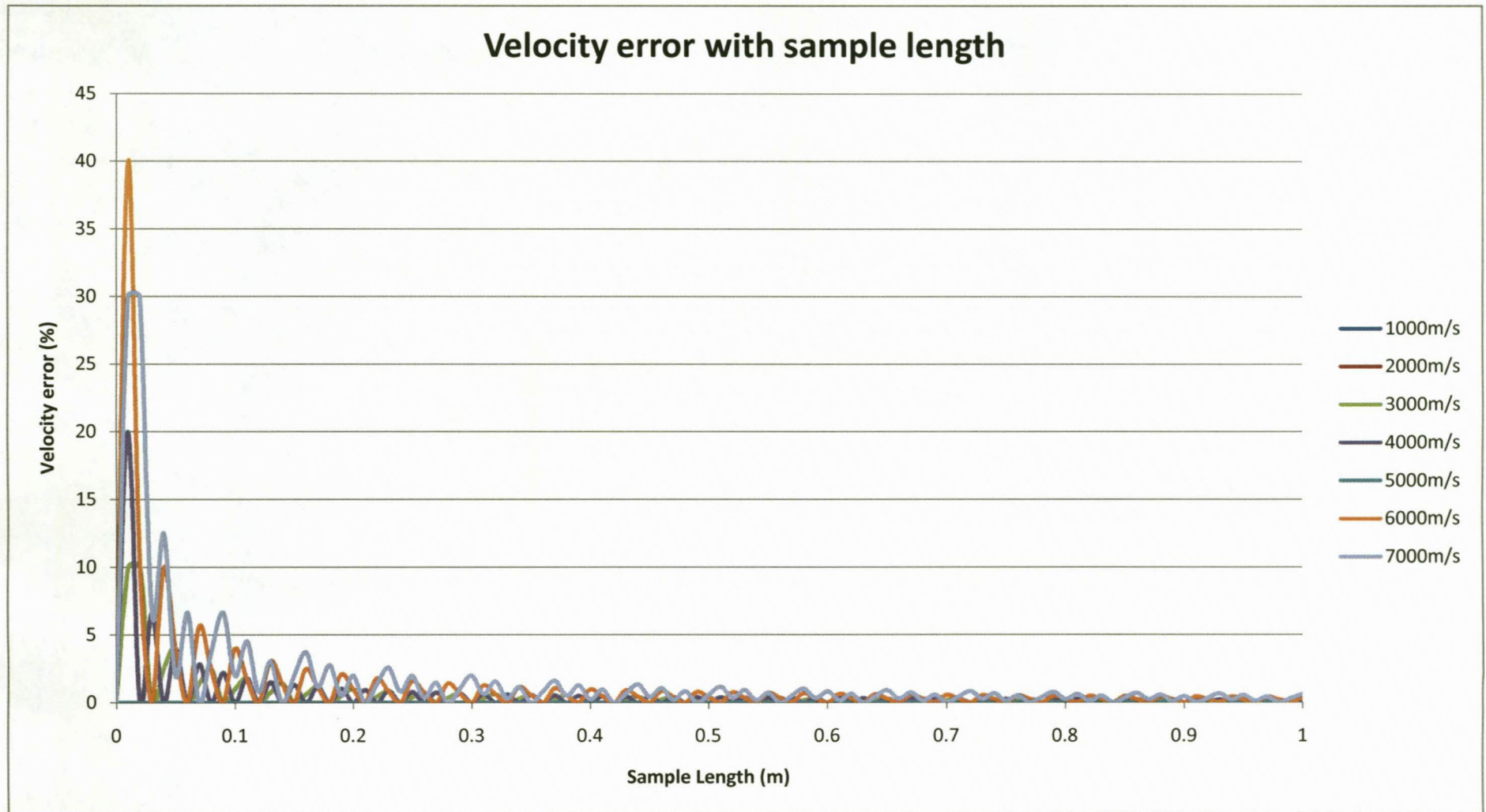
Figure 49 - Velocity error with sample length

Chapter 6 – Resonant ultrasound spectrography

6.1 Introduction
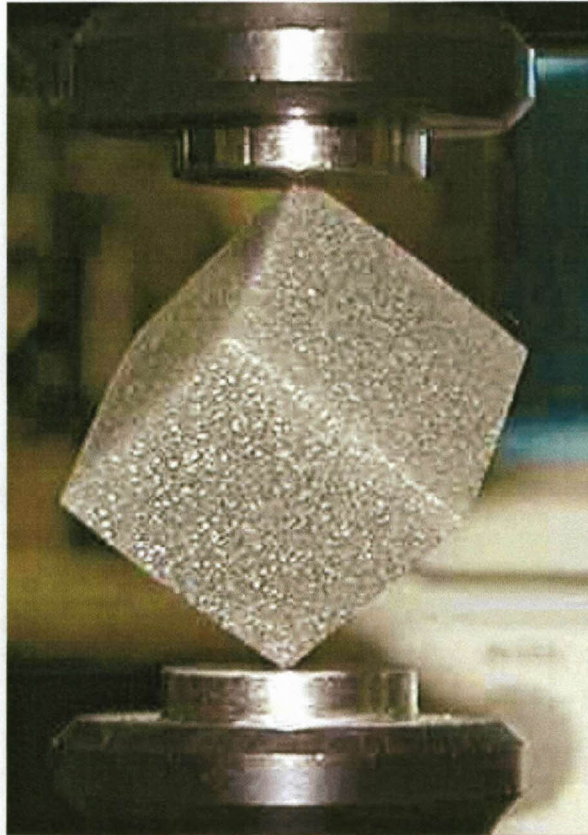
Figure 50 - Resonant ultrasound Spectrography (Viscoelastic Materials, 2007)

Time of flight techniques are very accurate at measuring the elastic parameters in one axis or plane. If three dimentional measurements are required, the sample must be re-orientated to measure velocities in that plane. Resonant ultrasound spectrography is used to measure directional elastic parameters of a sample simultaneously. (Zadler, Jerome, & Le Rousseau, 2003)

Resonant ultrasonic spectrography (RUS) is a method of determining the elastic parameters of a sample of material by inspecting the sample's natural resonant frequencies. These resonant frequencies are determined by the elastic parameters of the material as well as the sample's shape. Acoustic resonance is induced in the sample by "injecting" sound waves into the sample via a piezo-electric transducer. The injected frequency is then gradually increased from a low frequency to a higher

frequency. This swept frequency is then recorded by a second transducer. The amplitudes of the recorded signal are measured against frequency to produce a frequency amplitude plot. The natural resonant frequencies of the sample will appear as peak amplitudes on the plot. These peak frequencies are then used to determine the sample's elastic parameters. Figure 50 shows an example of a cube sample of material clamped between the two transducers of a RUS apparatus. As mentioned before, one is a transmitter and the other a receiver (Viscoelastic Materials, 2007).

RUS techniques make use of regular shaped samples such as cubes, cylinders and spheres to model the elastic parameters to the natural resonant frequencies. Analytical methods are used to calculate the resonant frequencies of a sample of known dimension and estimated elastic properties. This is then compared to the actual measured resonant frequencies. If they are outside a predetermined discrepancy level, the elastic parameters are adjusted and the predicted resonant frequencies are re-calculated. The process is repeated until the predicted frequencies match the recorded frequencies. The predicted frequencies are then representative of the actual elastic parameters. (Zadler, Jerome, & Le Rousseau, 2003)

6.2 Modes of vibration

To better understand RUS methods, a basic understanding of the fundamental modes of distortion of an object must be formed. The natural resonant frequencies distort a sample in a number of ways. These distortions can be divided into three distinct class modes. (Zadler, Jerome, & Le Rousseau, 2003)

- **Flexural class mode**

  Flexural modes are produced by acoustic energy travelling down the sample at an angle other than that of the sensor axis. These are generally caused by the movement of shear wave distortion in the sample. Figure 51 shows a cylindrical shaped sample that has been distorted by a fundamental frequency flexural distortion. The fundamental frequency is the lowest possible frequency for any given mode in a class of distortions.

69
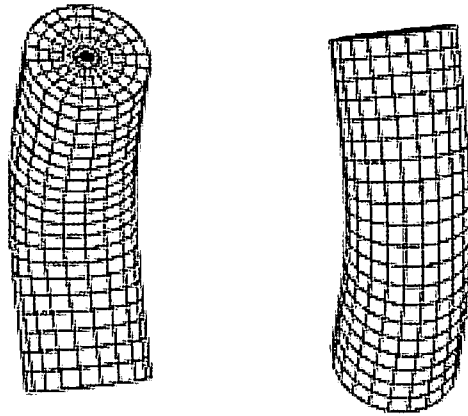
Figure 51 - Flexural class mode (Zadler, Jerome, & Le Rousseau, 2003)

- **Torsional class mode**

  Torsional modes are caused by shear waves passing though the sample and cause a twisting distortion on the sample when resonance of the sample occurs. Figure 52 shows the fundamental torsional frequency distortion. Figure 53 shows the first overture distortion of the fundamental frequency.
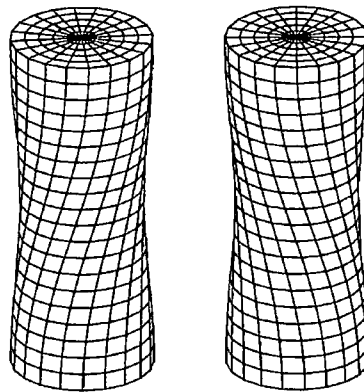
Figure 52 - Torsional class mode fundamental (Zadler, Jerome, & Le Rousseau, 2003)
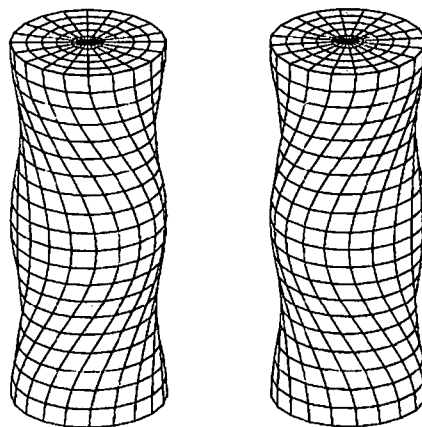
Figure 53 - Torsional class mode first overture (Zadler, Jerome, & Le Rousseau, 2003)

- **Extensional class mode**

  Extensional modes are produced by axis lateral compressions and extensions. These are mostly produced by compressional waves moving along the lateral axis of a sample. Figure 54 shows the fundamental frequency of the extensional distortion mode. Figure 55 illustrates the first overture of the fundamental extensional distortion mode frequency.
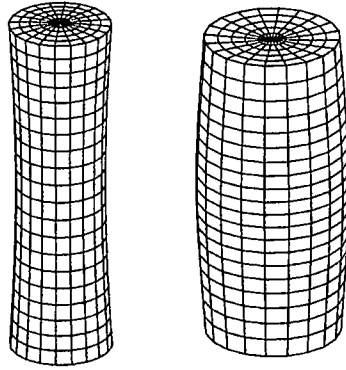
Figure 54 - Extensional class mode fundamental (Zadler, Jerome, & Le Rousseau, 2003)
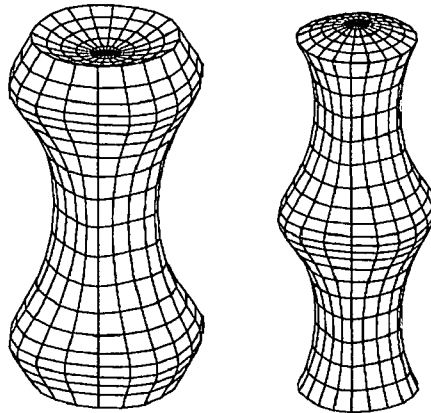
Figure 55 - Extensional class mode first overture (Zadler, Jerome, & Le Rousseau, 2003)

The frequencies at which a sample material resonates at any mode of distortion are unique to each material and sample geometry. Some or all modes can be present in a sample at any time simultaneously, distorting the sample in non-uniform ways. The next section will discuss how the RUS method uses these distortional modes to calculate the elastic parameters.

6.3 Frequency sweep
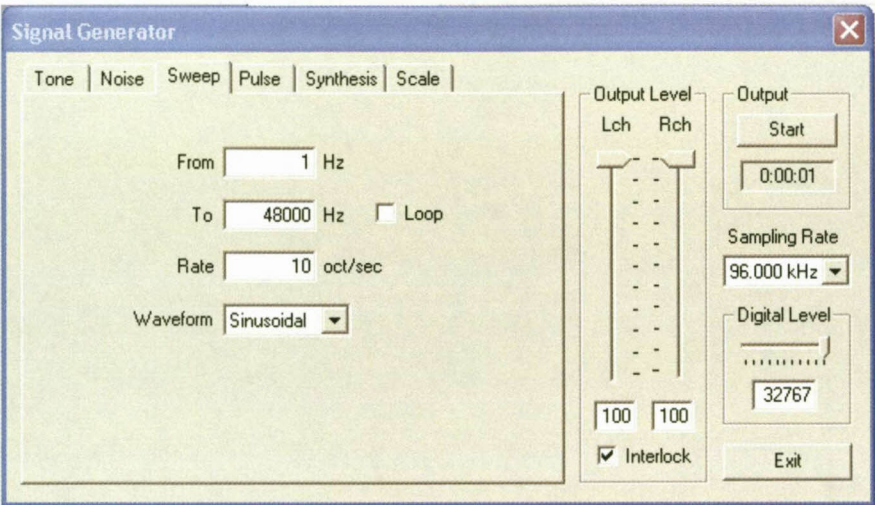
Figure 56 – Audio sweep setup

A frequency sweep is generated by an audio processing program attached to a computer sound card. Figure 56 shows the frequency sweep setup window. The resonant frequency data is then recorded by the computer audio recording device a test frequency sweep recording is shown in Figure 57. This sweep shows distinct amplitude increases at various frequencies.
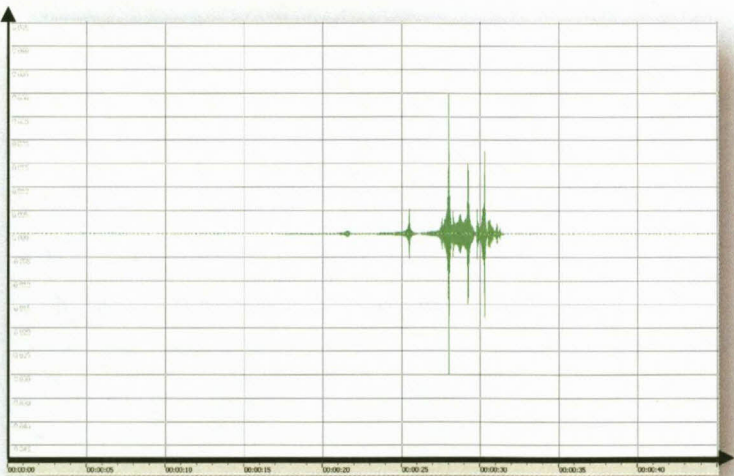
Figure 57 – Recorded waveform

These resonant frequencies are each a fundamental or harmonic of one of the modes of vibration. The resonant frequencies are recorded and stored for further analysis.

6.4 Analytical method

An alternative method can be used to calculate shear modulus by means of an analytical method (Wang & Lakes, 2003). The analytical method makes use of physical constraints on the dimensions of the sample to allow the calculation of the lowest torsional mode of resonance. In the event that a sample with equal diameter and length, is used in RUS, then the lowest or first resonant frequency is the fundamental torsional mode of resonance. This is not a requirement to calculate at which frequency a sample will resonate, it is simply used to define the fundamental torsional frequency. Once this frequency is known, the following equation can be used to calculate the shear modulus of the sample by analytical means. (Wang & Lakes, 2003)

$$f = \frac{n}{2L} \sqrt{\frac{G}{\rho}}$$

Equation 59

Where;   f   = Resonant torsional mode frequency
            n   = 1 for lowest natural frequency
            L   = Length of the sample
            G   = Shear modulus
            ρ   = Density of the rock sample

The use of this method gives the user the ability to apply a far more accurate and simpler method to compare the results of time of flight methods to that of RUS methods. It allows a simple analytical approach and negates the need to use numerical methods to check RUS results. This study uses this approach to determine if the elastic parameters determined for a sample by time of flight methods are correct, by comparing the calculated frequency spectrum using the time of flight data to the actual RUS frequency spectrum recorded from the sample. If the calculated and measured frequency spectrum correlate, then the results are considered

accurate. If not, then the measurements must be taken again with different samples of the same rock type until the results are comparable. (Wang & Lakes, 2003)

The use of this method takes the best advantage of both RUS and time of flight methods and makes efficient use of computer processing power by minimizing the necessary computation time as no complex numerical models are needed to be run.

Chapter 7 – Experimental apparatus

7.1 Introduction

The experimental apparatus had to be developed in order to evaluate the elastic parameter of rock test samples. A basic clamping system was used to fix the samples firmly against the ultrasonic transducers in order to achieve a good acoustic coupling. The clamping system is designed to accommodate up to 40cm long samples, allowing for accurate readings of shear and compressional velocities, but also allowing for a variable sample length for operating flexibility. The software developed for the system allows the user to make use of samples of varied dimensions by making provision for custom dimensions to be input into the calculations for specific storativity. The first task to address when taking velocity measurements in a core sample is to prepare the sample in the correct manner. The next section deals with sample preparation.

7.2 Sample preparation

For this study a total of twenty one samples were used to evaluate the method. These samples were gathered from varying geologies of known hydrological parameters. The samples were of different lengths and diameters as well as shape, i.e. cylindrical or half cylinders. This large variation in size and shape of the samples provided a good platform on which to test the systems performance.

Figure 58 - Test Samples

Figure 58 show the samples used in the evaluation of the method. The most important part in preparing a sample is to make sure the sample core has perpendicular flat edges on either side of the core cylinder. This is achieved by using a cutting disk and core cutter. It is very important that the core sides are cut straight and flat. If this is not done, the acoustic coupling between the core and transducer will be poor and it will attenuate the acoustic wave drastically, making velocity measurements very difficult.

After the sample is cut its mass must be measured by an accurate laboratory mass meter. The sample should then be marked by name and its critical information written on the sample such as mass, length, diameter, and porosity. It is also necessary to try keeping the measurement direction marked on the sample. The compressibility of the sample is a volumetric response so the measurement direction does not matter.

In the case of the compressional wave velocity measurements, glycerin was used between the transmitting and receiving transducers and sample to allow for be acoustic coupling and better signal penetration. Glycerin is used due to the fact that it has an acoustic impedance similar to rock and is easily washed off. Samples should be chosen and cut according to the homogeneity of the sample. If any small fractures or weathering is seen on the sample it must not be used. If there are severe non-

homogeneities in a sample it should not be used as there will be inconsistencies between the time of flight and RUS evaluations of the elastic parameters.

7.3 Experimental hardware

7.3.1 AD Converter
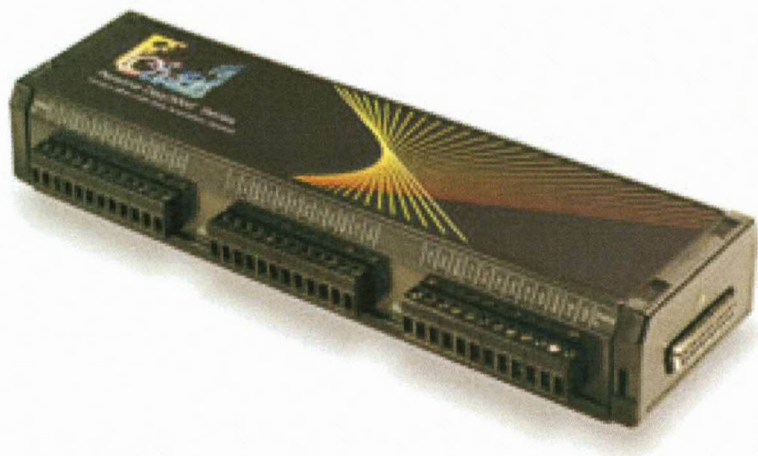
Figure 59- AD Converter (IOTech, 2007)

The analog to digital converter used in this study is the IOTech Personal Daq 3001 series USB converter. It is capable of sample rates of 1 MHz at resolutions of 16 bit over a selectable gain voltage swing of between -100mV to 100mV through to -10V to 10V. Table 2 lists all the selectable gains and accuracies at those levels.

Voltage Range*	Accuracy ±(% of reading + % Range) 23°C ±10°C, 1 year	Temperature Coefficient ±(ppm of reading + ppm Range)/°C -30°C to 13°C and 33°C to 70°C	Noise** (cts RMS)
-10V to 10V	0.031% + 0.008%	14 + 8	2.0
-5V to 5V	0.031% + 0.009%	14 + 9	3.0
-2V to 2V	0.031% + 0.010%	14 + 10	2.0
-1V to 1V	0.031% + 0.02%	14 + 12	3.5
-500 mV to 500 mV	0.031% + 0.04%	14 + 18	5.5
-200 mV to 200 mV	0.036% + 0.05%	14 + 12	8.0
-100 mV to 100 mV	0.042% + 0.10%	14 + 18	14.0

Table 2 - AD converter amplification range (IOTech, 2007)

It is capable of simultaneously reading 8 synchronized differential inputs and has 4 digital to analog converters that can be used in a number of modes. The input and output channels are also capable of synchronous read and write functions. The

system makes use of ultra low noise shielded cable that isolates the input signal from external noise sources such as an AC power line noise which can cause false estimations of velocity measurements if not filtered out of the recorded signal The cables are connected to BNC type plugs which attach to the transducers. This ensures a good contact coupling between the system and the transducers, as well as noise shielding. The Personal 3001 USB system was chosen for this study for a number of reasons. These include:

- The system is capable of sampling at a rate of 1000000 samples per second. This is the most important in the application of time of flight techniques which are reliant on high sampling rates to improve accuracy.

- The system has a high band width due to its high sampling rate. According to the Nyquist criterion (Madeira, Bellis, & Beltran, 1999), an AD converter's bandwidth is half of its sampling rate. This allows the system to define frequencies up to 500 kHz. This is an important factor in RUS techniques that require a large frequency spectrum to define modes of resonance in order to improve its accuracy.

- The system is capable of simultaneously reading data from an AD converter and transmitting a waveform from a DA converter. This is very important in time of flight and RUS techniques. Time of flight data is dependent on knowing exactly when an acoustic pulse was injected into the sample. If the injection time is known and the arrival time at the opposite end of the sample is also known, the acoustic velocity of the sample can be calculated.

- The injected pulse waveform can be programmed into the converter before it is sent. This circumvents the need to have a very fast computer sending the information to the converter.

- The record/transmit cycle can be manually triggered by the user through the supplied user interface software.

- The system has user settable gain settings that allow for a large range of input amplifications. This is useful if the contact between the transducers and

the sample are very bad. The weak signals at the receiver can then be amplified as needed to obtain the time of arrival or RUS data.

- A user programmable number of signals can be recorded before the system stops recording. This helps to keep file sizes imported to the interpretation software down.

- The system uses a USB type connection to a computer. This simplifies the interface to the system and allows the system to be more mobile.

- The system has a Borland builder interface driver that allows the system to be integrated into third party software applications.

7.3.2 Piezo transducers

The piezo transducers used in this study are manufactured by Panametrics. There is a pair of compressional transducers and a pair of shear transducers used to induce compressional waves and shear waves in a sample. These are discussed individually. (Panametrics, 2006)

- **Compressional Transducers**

Figure 60 - Compressional piezo transducer (Panametrics, 2006)

The compressional transducers used are the Panametrics V101 videoscan flat face transducers. They have a center resonance frequency of 500 kHz and are dampened to provide a large frequency bandwidth. This is especially useful in RUS measurements that require a large frequency bandwidth. Figure 60 illustrates the V101 transducer.

Figure 61 - Shear piezo transducer (Panametrics, 2006)

The shear transducers used are the Panametrics V150 videoscan flat face transducers. They have a center resonance frequency of 250 kHz. Figure 61 illustrates the V101 transducer.

7.3.3 Clamp mechanism
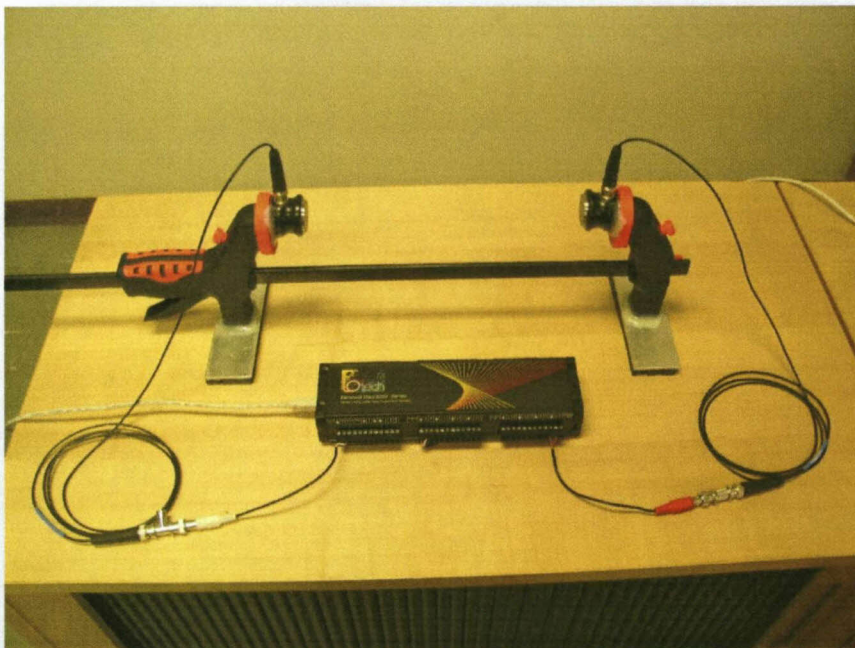
Figure 62 - Clamp mechanism

The clamp mechanism used in this study to attach the samples to the measuring equipment is illustrated in Figure 62. The piezo transducers are connected to the clamp by means of rubber pads that they are glued too. These pads provide acoustic isolation between the transducers and the clamping mechanism. This is important as sound travelling down the clamp mechanism to the opposite transducer can cause

false measurements of velocity. Figure 63 shows the compressional transducer and pad glued together.

Figure 63 - Compressional transducer and pad

There are two configurations that can be used to clamp a sample to the sensor transducers. These are:

- **Time of flight configuration**

  The time of flight clamping configuration makes use of the flat sample faces perpendicular to the center axis. The transducer is placed such that the center axis of the core sample is in line with the center axis of the transducer. The acoustic wave will pass uniformly through the sample. If it is not centered, diffraction effects may cause false readings of velocity. An example of this sample placement can be seen on Figure 64. This configuration must be done with both the compressional as well as the shear transducers in order to measure both compressional and shear velocities.
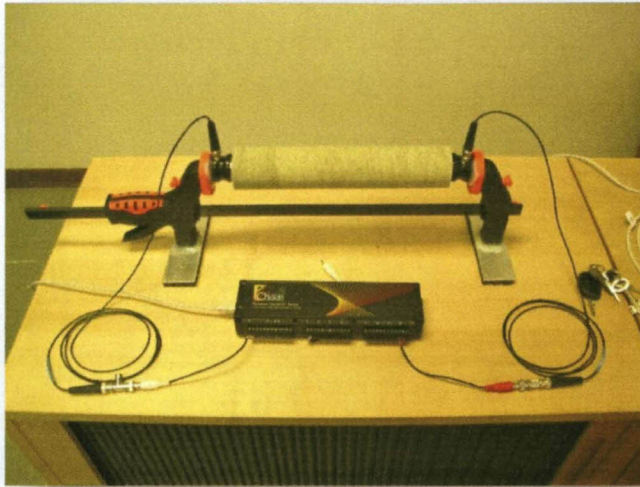
Figure 64 - Time of flight configuration

- **RUS configuration**

The RUS configuration differs from the time of flight configuration in that it is mounted with the sensor axis in line with the diagonal axis of the sample.

Figure 65 - RUS configuration

7.4 Software
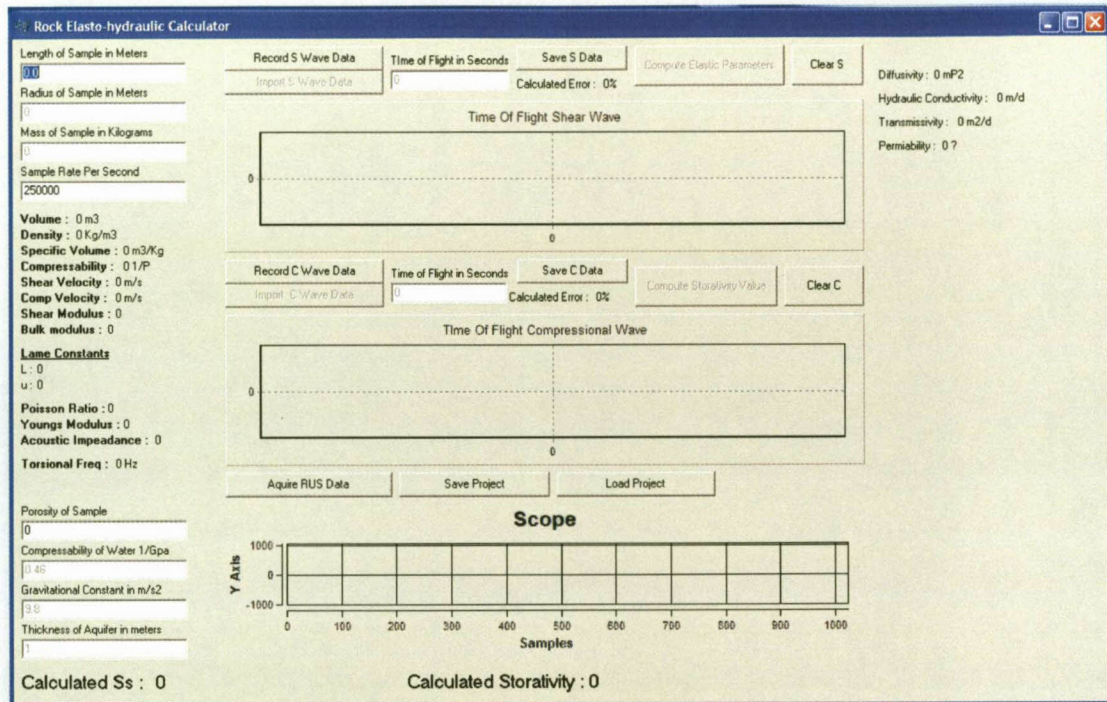
Figure 66 - Analysis software

Figure 66 shows the software developed for the project. This software imports the text file time of flight data captured by the DAQ system and analyses it for velocity values of the sample.

Before an analysis can be done, the user must enter a number of sample parameters such as sample dimensions, density and porosity. There are a few values which are available that are set to default values, such as the compressibility of water and gravitational acceleration. An example of this is the system sample rate and the gravitational constant.

The sample dimensions that the software requires are the length and diameter of the sample. This is necessary for the calculation of the volume of the sample as well as the calculation of the actual compressional and shear velocities of the sample. The mass of the sample is also required to calculate the density of the sample in conjunction with the calculated sample volume. Once these basic parameters are entered into the software, the software will allow the user to import the time of flight

data in text form into the system. The shear wave data is imported first. A line trace is displayed in the shear velocity window. The user must then select the point on the trace where the data shows sine wave oscillations. This indicates the time it took the shear wave to travel along the length of the sample. This time value is displayed in the software and is used to calculate the shear wave velocity for the sample. The software then allows the user to repeat the process for the compressional wave time of flight data. The user selects the time the data starts oscillating and the software uses this time to calculate the compressional wave velocity for the sample.
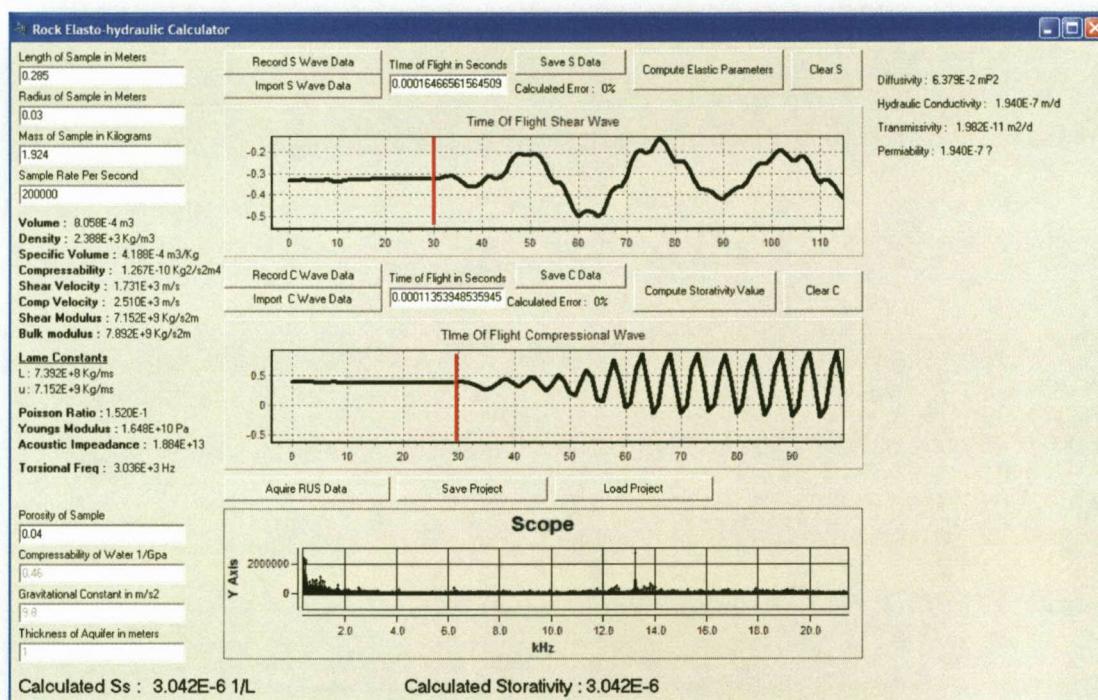
Figure 67 - Imported Data

Figure 67 shows the imported data for the shear and compressional wave velocity calculations. The trace data clearly shows where the ultrasound waves reached the receiving transducers. Once the velocity data for the sample is calculated, the elastic parameters can be calculated. This is done in software by clicking in the "Calculate elastic parameter data" button. A second option of importing the velocity data is to use the software record function. By pressing the "Read S Wave Data" and the "Read C Wave Data" the software automatically sets the hardware setup and reads then displays the data for analysis. Once this is done, the same procedure can be followed to calculate the elastic and hydrological data.

Chapter 8 – Experimental results

8.1 Result summary

A selection of sandstones, gneiss, quartzite, mudstone, shale, dolomite, dolerite, granite and schist were collected and tested in order to determine the systems performance over a variety of South African soft and hard rock types. Samples of different shapes and lengths were used. A description of the samples tested is given in the appendix. These samples were tested using the method described in this study then compared to results derived from independent methods. These comparative results are then discussed in full.

Table 3 and Table 4 summarize the elastic and hydrological parameters measured and calculated by the system as well as the experimentally verified values for porosity, Young's modulus, compressibility, specific storage and hydraulic conductivity by independent testing of the individual samples. The porosity values were independently verified using the boil and bake method. The data of the test are shown in the appendix.

The hydraulic conductivity values were independently verified using a Darcy flow experiment, where the samples were subjected to a hydraulic gradient for a given time period. The drop in hydraulic head was used to calculate the hydraulic conductivity of the sample. The data for the tests are given in the appendix.

The Young's modulus and compressibility values were verified independently through compressive load tests done at the University of the Witwatersrand. These tests put the samples under stress and measure the lateral and axial strain affected on the samples. This is used to calculate the Young's modulus and Poisson's ratio for the sample under different loading conditions. The Young's modulus and Poisson's ratio is then used to calculate the compressibility of the sample.

The specific storage value is verified by using the compressibility values supplied by the stress testing and applying it to specific storage equation. These values are then compared to those measured with the method described in this study. For a complete description of all the values calculated using the acoustic method refer to the appendix tables.

Parameter	Sample1	Sample15	Sample2	Sample7	Sample16	Sample20	Sample3	Sample13	Sample4	Sample14	Unit
Shear Wave Velocity	2.49E+03	2.95E+03	2.37E+03	1.60E+03	1.54E+03	1.73E+03	3.12E+03	2.79E+03	1.94E+03	1.97E+03	m/s
Compressional Wave Velocity	4.26E+03	4.91E+03	3.28E+03	2.47E+03	2.14E+03	2.51E+03	5.14E+03	3.92E+03	2.73E+03	2.96E+03	m/s
Compressibility	3.10E-11	2.36E-11	8.21E-11	1.13E-10	1.91E-10	1.27E-10	2.25E-11	5.06E-11	1.01E-10	7.55E-11	1/Pa
Compressibility Verified	-	-	3.01E-11	2.81E-10	4.60E-11	-	-	-	-	-	1/Pa
Young's Modulus	4.25E+10	6.03E+10	2.92E+10	1.55E+10	1.24E+10	1.65E+10	6.54E+10	4.55E+10	2.26E+10	2.50E+10	Pa
Young's Modulus Verified	-	-	2.84E+10	1.02E+10	4.68E+10	-	-	-	-	-	Pa
Specific Storage	6.15E-07	5.43E-07	1.12E-06	1.35E-06	2.31E-06	1.60E-06	2.31E-07	5.05E-07	1.54E-06	1.29E-06	1/m
Specific Storage Verified	-	-	6.11E-07	3.00E-06	8.87E-07	-	-	-	-	-	1/m
Hydraulic Conductivity	1.07E-04	3.20E-04	1.34E-04	4.75E-05	1.21E-03	8.82E-04	4.02E-05	1.68E-05	1.91E-04	7.64E-04	m/d
Hydraulic Conductivity Verified	1.20E-04	1.20E-04	8.77E-04	5.82E-04	8.77E-04	5.82E-04	7.36E-05	7.36E-05	8.98E-04	8.98E-04	m/d
Sample Type	Basalt	Basalt	Sandstone	TBM Sstone	Sandstone	Sandstone	Quartzite	Quartzite	Kimberlite	Kimberlite	

Table 3 – Parameter results 1

Parameter	Sample5	Sample6	Sample8	Sample11	Sample12	Sample9	Sample10	Sample17	Sample18	Sample19	Unit
Shear Wave Velocity	2.57E+03	1.80E+03	1.28E+03	1.35E+03	1.34E+03	2.05E+03	1.53E+03	3.68E+03	3.02E+03	2.99E+03	m/s
Compressional Wave Velocity	6.19E+03	3.20E+03	2.07E+03	1.97E+03	1.91E+03	3.01E+03	2.20E+03	5.27E+03	4.27E+03	4.09E+03	m/s
Compressibility	1.22E-11	5.39E-11	1.48E-10	1.92E-10	2.08E-10	8.56E-11	1.50E-10	2.46E-11	3.96E-11	4.61E-11	1/Pa
Compressibility Verified	1.26E-11	7.79E-11	-	--	-	9.10E-11	9.54E-11	-	-	-	1/Pa
Young's Modulus	4.78E+10	2.24E+10	1.03E+10	1.06E+10	1.06E+10	2.36E+10	1.41E+10	8.78E+10	5.73E+10	5.41E+10	Pa
Young's Modulus Verified	1.55E+11	3.64E+10	-	-	-	2.94E+10	3.07E+10	-	-	-	Pa
Specific Storage	1.28E-07	6.28E-07	2.24E-06	2.67E-06	2.83E-06	1.26E-06	1.70E-06	2.56E-07	3.90E-07	6.76E-07	1/m
Specific Storage Verified	1.33E-07	8.62E-07	-	-	-	1.31E-06	1.17E-06	-	-	-	1/m
Hydraulic Conductivity	7.02E-06	5.15E-05	6.03E-05	5.48E-05	7.38E-05	4.42E-05	5.67E-05	2.94E-05	5.95E-05	1.03E-04	m/d
Hydraulic Conductivity Verified	6.01E-05	1.83E-04	3.06E-04	3.06E-04	3.06E-04	2.39E-04	2.39E-04	1.82E-04	9.50E-05	7.28E-05	m/d
Sample Type	Gneiss	Schist	Mudstone	Mudstone	Mudstone	Shale	shale	Dolerite	Dolomite	Granite	

Table 4 – Parameter Results 2

Sample No.	Rock Type	Poissons Ratio (Secant)	Test Stress (MPa)	E (Secant) (GPa)	Test Stress (Predicted) (MPa)	Bulk Modulus (Gpa)	Compressibility (1/Pa)	Predicted Compressibility (1/Pa)
2	Sandstone	0.36	3.98	28.40	Atmospheric	33.14	3.02E-11	8.21E-11
16	Sandstone	0.14	3.98	46.78	Atmospheric	21.73	4.60E-11	1.91E-10
6	Shist	0.03	8.23	36.43	Atmospheric	12.82	7.80E-11	5.39E-11
5	Gneiss	0.17	17.04	154.94	Atmospheric	78.90	1.27E-11	1.22E-11
9	Shale	0.05	17.04	29.44	Atmospheric	10.99	9.10E-11	8.56E-11
10	TMG Sstone	0.01	16.47	30.74	Atmospheric	10.48	9.54E-11	1.50E-10
7	Sandstone	0.02	18.75	10.15	Atmospheric	3.55	2.82E-10	1.13E-10

Comparison of results between measured and verified data

Figure 68 - Stress test data
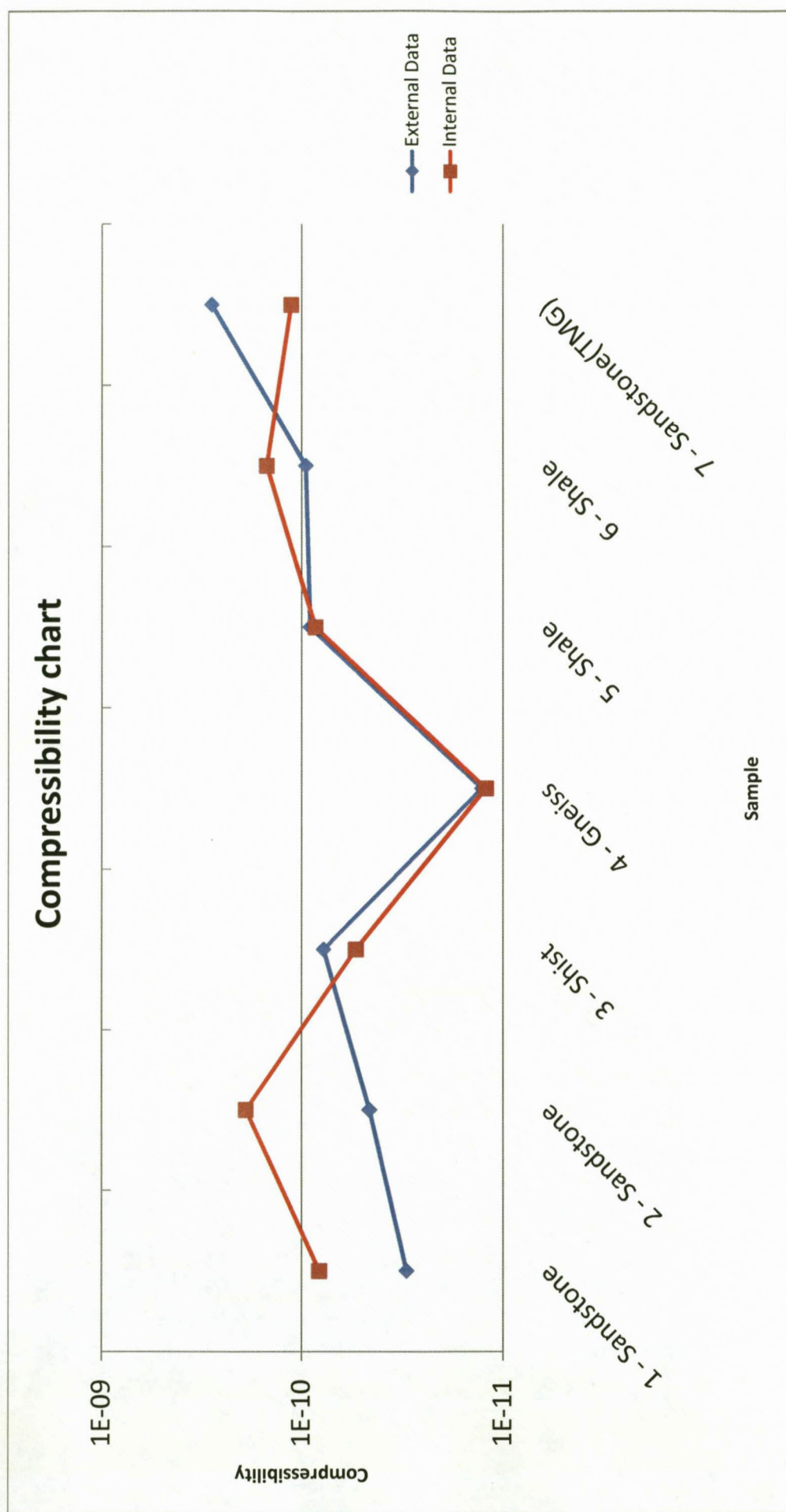
Figure 69 - Compressibility data comparison
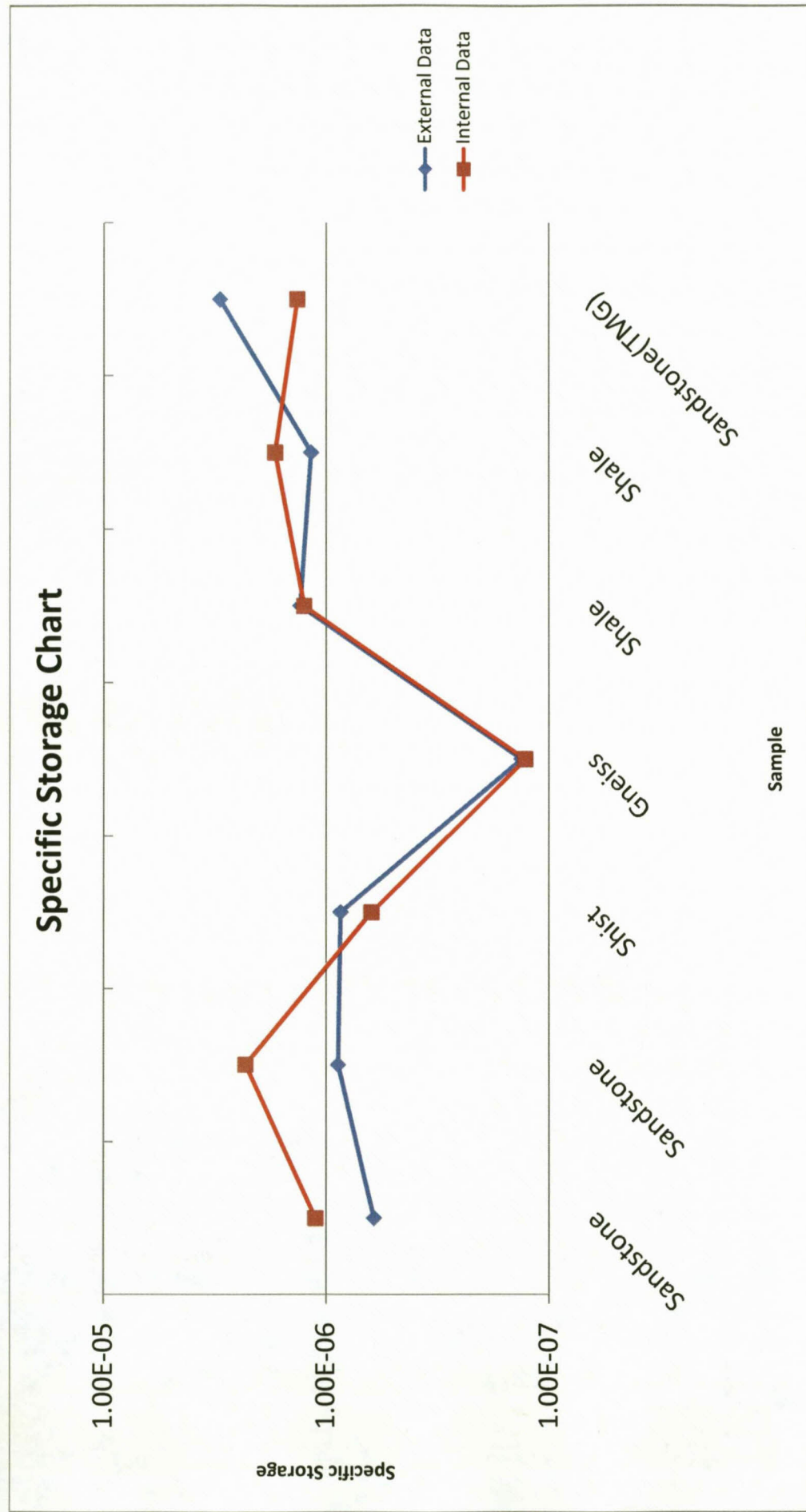
Figure 70 - Specific storage comparison
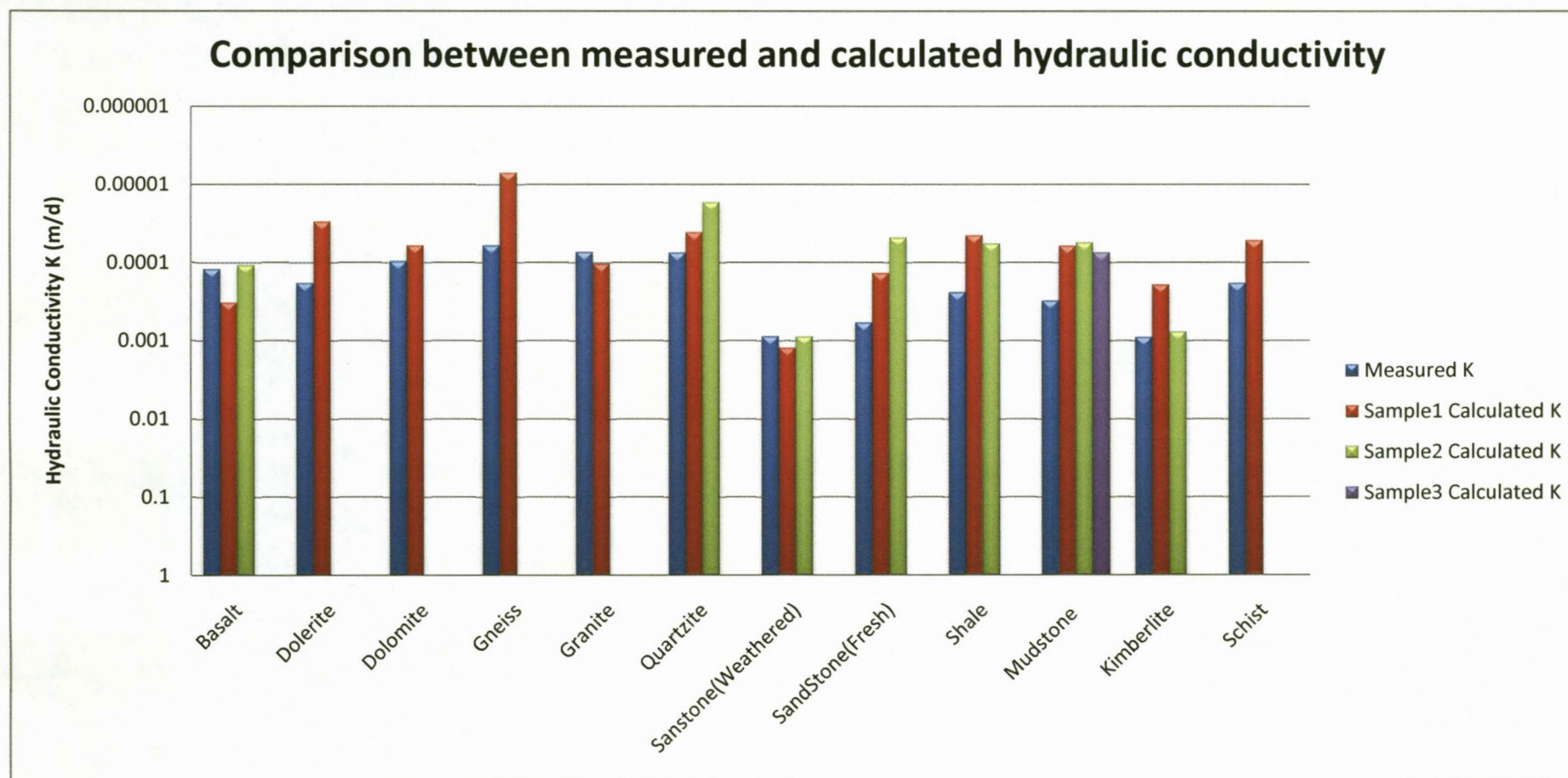
Figure 71 - Hydraulic conductivity comparison

Sample	Calculated(Hz)	Measured(Hz)	Error(%)
1	7.7681E+03	7.7500E+03	0.23
2	8.9105E+03	8.9500E+03	0.44
3	9.7585E+03	9.6500E+03	1.11
4	7.1759E+03	7.1100E+03	0.92
5	1.4272E+04	1.4250E+04	0.16
6	8.1878E+03	8.1500E+03	0.46
7	1.1118E+04	1.1190E+04	0.64
8	1.0157E+04	1.0180E+04	0.22
9	1.4260E+04	1.4230E+04	0.21
10	1.0905E+04	1.0920E+04	0.14
11	1.2237E+04	1.2210E+04	0.22
12	1.0842E+04	No Data	No Data
13	1.9924E+04	1.9900E+04	0.12
14	3.3413E+03	3.3000E+03	1.24
15	4.9914E+03	4.9500E+03	0.83
16	2.7704E+03	2.6000E+03	6.15
17	1.4140E+04	No Data	No Data
18	1.0080E+04	No Data	No Data
19	9.9701E+03	No Data	No Data
20	3.0365E+03	2.9900E+03	1.53
21	8.1651E+03	8.1500E+03	0.18

Table 5 - RUS Results

8.2 Discussion of results

The results tabulated in Table 3 and Table 4 are comparative results between the internal ultrasound method and the data externally obtained through Darcy and stress tests done on the samples. Only 7 of the samples were tested using the stress test for Young's modulus, specific storage and compressibility. These results are shown in Figure 68. All the rock types were tested for hydraulic conductivity. The difference between stress testing for elasticity and using acoustic velocity methods is that stress testing requires that a sample must be placed under stress in order for it to be deformed. These deformations are used to determine its elastic properties. Figure 68 shows the data for the seven samples tested and the conditions under

which they were tested. The test stresses vary between 3 and 19 Mpa which is significantly higher than the atmospheric pressure used in the acoustic method.

The comparative results between the acoustic and stress test compressibility's are shown on Figure 69 This shows an acceptable correlation between the stress test and acoustic test methods. The difference in values could be explained by the difference in test pressure. Even with the large difference in pressure, the two methods yield comparable results. This is especially true for the harder stone types which correlate well. There is a larger error between the compressibility's of the softer sandstone samples. There could be a number of reasons for this disparity which include: micro-fracturing, weathering and test stress differenced. It is apparent from the comparison that the more consolidated a rock sample is, the better the correlation will be between the stress and acoustic test data. However, this needs to be verified. That being stated, the compressibility results derived by the acoustic tests are far more consistent in magnitude than those derived from the stress tests. This could be due to the fact that the stress tests were done at different pressures for each sample under test. This shows an immediate benefit of the acoustic test over stress tests, in that the results are directly comparable. The compressibility results are strengthened by the Young modulus results, which indicate a good correlation between the acoustic and stress test methods. A comparison between referenced Young's modulus data and the data obtained from the acoustic tests are shown in the appendix. All measured data falls into the referenced ranges for Young's modulus. This strengthens the reliability of data obtain though acoustic velocity testing.

The specific storage comparison shown on
Figure 70 indicate a strong correlation between the acoustic and stress test data. This is to be expected as the compressibility values also correlate very well. What is interesting is that the results show that the magnitudes of specific storage are in the order 1 E-6 for the softer sandstones and 1E-7 for the harder gneiss. This is interesting in that pump test data for the campus sandstone indicate a much higher value for specific storage of 1E-5.

The hydraulic conductivity data for the acoustic test and the Darcy flow test are shown in Figure 71. The comparison indicates that there is a good correlation between the measured and calculated values. In general, the measured Darcy flow hydraulic conductivity seems to be higher than the calculated acoustic data. This could be attributed to the small dimensions of the samples used in the Darcy flow

tests as compared to the longer samples used in the acoustic test. The acoustic tests represent a far better average sample hydraulic conductivity as more sample volume is used in the test. That being stated, the acoustic method shows itself to be a good estimate of hydraulic conductivity over a large variation of rock types.

Table 5 shows the results for the RUS experiment. The calculated first torsional frequency derived from the shear modulus calculation of the time of flight method is compared to the measured first torsional frequency response. The relative error is then calculated as a percentage of the measured frequency. The results show that the RUS and time of flight methods produce similar shear modulus results with errors generally smaller than one percent of the measured frequency. This means the calculated compressibility parameter is a good estimate for most of the samples. The frequency error could be due to the in-homogenities in the rock samples. Samples 12, 17, 18 and 19 are not calculated as they are not cylindrical in shape and the torsional frequency cannot be analytically calculated. Sample 16 is very weathered sandstone and this may be the cause of the large error.

Chapter 9 – Conclusions and recommendations

This study has shown that a rock samples hydrological parameters can be determined from its elastic parameters which are measured through the use of acoustic time of flight methods and confirmed by resonant ultrasound spectrography methods. The results obtained show good correlation between data measured using the outlined acoustic methods and independently verified Darcy flow and stress test methods.

The data indicates that the specific storage values lie between 1E-6 and 1E-7 m^{-1} for the range of rock types tested. This differs from the data obtained from pump tests done on the campus site with a sandstone aquifer which is assumed to be confined. The pump test data is in the region of 1E-5 m^{-1} for specific storage. This value is an order of magnitude larger than that shown for the sandstones in this study. This discrepancy could infer that the campus aquifer is not a completely confined aquifer. This is important in that the specific storage values obtained in this study can only be used if the aquifer, it is applied to, is known to be completely confined. More work needs to be done on the application of specific storage values too leaky aquifers.

This being stated, the method outlined in this study is an effective technique of determining realistic estimates for specific storage, and hydraulic conductivity of a rock sample matrix. These estimates can be obtained without the need for extensive laboratory testing and expensive stress testing. The test can be carried out without destroying the samples under test and the results are directly comparable to each other which is not the case for stress test data.

The outlook for this method is to use it as an effective method of determining porosity and the effect porosity will have on specific storage under stress applied to the sample with depth. This can only be achieved if the system is modified to exert pressure on the sample before acoustic velocity measurements are taken. Other improvements that can be made is to include higher power transducers to improve signal to noise ratios and higher sampling rate equipment to improve the methods resolution. A full RUS model should also be included to confirm not only the sample shear modulus, but also its bulk modulus. This may increase the methods ability to detect in-homogenities in a test sample caused by fractures and weathering in the sample.

The effects that micro fracturing have on specific storage and hydraulic conductivity can also be calculated if a sample is placed under stress before it's velocities are measured. This will enable the geo-hydrologist to determine specific storage and hydraulic conductivity at pressures and depths where micro-fracturing may play a role in hydraulic transportation.

References

Akiyoshi, T., Sun, X., & Fuchida, K. (1998). General absorbing boundary conditions for dynamic analysis of fluid-saturated porous media. *Soil Dynamics and Earthquake Engineering Vol. 17* , 397–406.

Argatov, I., & Sabina, F. (2008). Acoustic diffraction by a finite number of small soft bodies. *Wave Motion Vol. 45* , 238–253.

Aster, R. (2006, February 1). Stress, Strain, and Elasticity. New York, New York, USA.

Botha, J. F., & Cloot, A. H. (2004). Deformations and the Karoo aquifers of South Africa. *Advances in Water Resources* , 383 – 398.

Boyd, T. (Author)(cited 2007, March 1). *Introduction to Geophysics Short Course (Internet).* Colorado, USA: Colorado school of mines, 40p. Available from: http://gretchen.geo.rpi.edu/roecker/AppGeo96/lectures/gravity/main.html

Bueche, F. J. (1986). *Introduction to Physics for Scientists and Engineers.* Singapore: McGraw-Hill.

Burbey, T. (2001). Storage coefficient revisted: Is purly vertical strain a good assumption. *Ground water(No.3)* , 459-464.

Cartage (Author)(cited 2007, September 17). *A Little History(Internet).* Cartage, Lebanon: ASA, about 2p , Available from: http://www.cartage.org.lb/en/themes/sciences/physics/Acoustics/history/TheorySound/Littlehistory.htm

Champion, R., & Champion, W. (2007). The extension and oscillation of a non-Hooke's law spring. *European Journal of Mechanics A/Solids Vol. 26* , 286–297.

Crandall, D., & Dahl, L. (1959). *An Introduction to the Mechanics of Solids.* USA: McGraw-Hill.

Dkimages (Author)(cited 2007, October 1). *Discover Science(Internet).* London, UK: Dk Images, about 1 p, Available from: http://www.dkimages.com/discover/Home/Science/Physics-and-Chemistry

Du Preez, M., Dennis, S. R., & van Tonder, G. J. (2007). *Experimental measurement of specific storativity by the determination of rock elastic paramerters.* Pretoria: Water Research Commission, WRC Report No. KV184/07.

DuBose, T., & Baker, A. (2007). Acoustic Doppler shifts in medicine. *Applied Acoustics Vol. 68* , 240–244.

Elmer (Author)(cited 2007, September 26). *The Doppler effect(Internet)*. Espoo,
    Finland: Scientific Computing, 1p, Available from:
    http://www.csc.fi/english/pages/elmer/examples/acoustics/doppler/

Felberbaum, L., Laporte, V., & Mortense, A. (2008). Equilibrium shape of a liquid
    intergranular inclusion in a stressed elastic solid. *Scripta Materialia Vol. 58* ,
    610–613.

Fine, R., & Millero, F. (1973). Compressibility of water as a function of temperature
    and pressure. *Journal of Chemical Physics(59)* , 10.

Gang, H., & Maurice, B. (2003). Description of fluid flow around a wellbore with
    stress-dependent porosity and permeability. *Journal of Petroleum Science
    and Engineering 40 (2003)* , 1 – 16.

GCRP (Author)(cited 2007, October 2). *Gallery of Carbonate Rock Porosity(Internet)*.
    Carolina, USA: University of South Carolina, 2p, Available from:
    http://strata.geol.sc.edu/CarbPorosityGallery/CarbPorosityGallery.html

Gercek, H. (2007). Poisson's ratio values for rocks. *International Journal of Rock
    Mechanics and Mining Sciences, Volume 44, Issue 1*, 1-13.

Gladden, J. R. (2003). *Characterization of thin films and novel materials using
    resonant ultrasound spectroscopy*. Penn State, USA: Pennsylvania State
    University Press.

Hart, D. J., & Hammon, W. S. (2002). *Measurement of hydaulic conductivity and
    specific storage using the shipboard manheim squeezer. in* Proceedings of
    the Ocean Drilling Program: Initial reports, seafloor observatories and the
    Kuroshio Current, covering Leg 195 of the cruises of the drilling vessel
    JOIDES Resolution; Apra Harbor, Guam, to Keelung, Taiwan; sites 1200-
    1202.

Hermance, J. (Author)(cited 2003, January 1). *Brown University Courses(Internet)*.
    Providence, USA: Brown University, 1p, Available from:
    http://www.brown.edu/Courses/GE0158/ge158web/classsupplements/2003/St
    oragePropertiesOfAquifers.ppt

Horseman, S. T., Harrington, J. F., & Noy, D. J. (2006). Swelling and osmotic flow in
    a potential host rock. *Physics and Chemistry of the Earth 32 (2006)* , 408–
    420.

Houdhari, N. K., Kumar, A., Kumar, Y., & Gupta, R. (2002). Evaluation of elastic
    moduli of concrete by ultrasonic velocity. *National Seminar of Isnt* (pp. 1-4).
    India: National Seminar of Isnt.

Hristopulos, D., & Demertzi, M. (2008). A semi-analytical equation for the Young's modulus of isotropic ceramic materials. *Journal of the European Ceramic Society Vol. 28* , 1111–1120.

IOTech (Author)(cited 2007, October 09). *Personal Daq/3000 Series(Internet).* Cleveland, Ohio: IO Tech, 30p, Available from: www.IOTech.com

ISVR (Author)(cited 2007, September 26). *Wave Basics(Internet).* Southampton, UK: University of Southampton, p1, Available from: http://www.isvr.soton.ac.uk

Jennings, D., & Flint, A. (1995). *Introduction to Medical Electronics Applications.* USA: Butterworth-Heinemann.

Kane, J. W., & Sternheim, M. M. (1983). *Physics.* Canada: John Wiley and Sons. Komodromos, P. (2007). Simulation of the earthquake-induced pounding of seismically isolated buildings. *Computers and Structures* , 1-9.

Knudby, C., & Carrera, J. (2006). On the use of apparent hydraulic diffusivity as an indicator of connectivity. *Journal of Hydrology* , 377– 389.

Leisure, R. G., & Willis, F. A. (1997). Resonant Ultrasound spectroscopy. *Journal of Physics Volume 9, Number 28* , 6001 – 6290.

Madeira, M. M., Bellis, S. J., & Beltran, L. A. (1999). High-performance computing for real-time spectral estimation. *Control Engineering Practice* , Volume 7, Number 5, 679-686.

MCEN (Author)(cited 2001, February 02). *Measurement of Elastic Constants Using Ultrasound(Internet).* New York, USA: GE Sensing, 10p, Available from: www.panametrics.com

Migliori, A., & Sarrao, J. L. (1997). *Resonant Ultrasound Spectroscopy: Applications to Physics, Materials Measurements, and Nondestructive Evaluation.* USA: Wiley-Interscience.

Nieves, F., Gascon, F., & Bayon, A. (2007). An analytical, numerical, and experimental study of the axisymmetric vibrations of a short cylinder. *Journal of Sound and Vibration* , Unknown.

Panametrics (Author)(cited 2006, October 01). *Technical notes(Internet).* New York, USA: GE Sensing, 12p, Available from: http://www.gesensing.com/

Petrophysical Studies (Author)(cited 2007, October 2). *PETROPHYSICAL STUDIES(Internet).* Aberdeen, UK: University of Aberdeen, 10p, Available from: http://www.abdn.ac.uk/~wpg010/petrophysics/petrophysics.html

Phani, K., & Sanyal, D. (2008). The Relations between the Shear Modulus, the Bulk Modulus and Young's Modulus for Porous Isotropic Ceramic Materials. *Materials Science and Engineering A* , Unkown.

Physics Curriculum and Instruction (Author)(cited 2007, September 26). *Physics Demonstrations in Sound & Waves(Internet)*. Lakeville, Minnesota: Physics Curriculum & Instruction, 1p, Available from: http://www.physicscurriculum.com/sound_&_waves.htm

Powis, R., & Schwartz, R. (1998). *Practical Doppler ultrasound for the clinician.* USA: Gale Group.

Přikryl, R., Lokajíček, T., Pros, Z., & Klíma, K. (2007). Fabric symmetry of low anisotropic rocks inferred from ultrasonic sounding: Implications for the geomechanical models. *Tectonophysics, Volume 431, Issues 1-4*, 83-96.

Ramos da Silva, M., Schroeder, C., & Verbrugge, J. (2008). Unsaturated rock mechanics applied to a low-porosity shale. *Engineering Geology Vol. 97* , 42–52.

Rock Mechanics Laboratory (Author)(cited 2007, November 16). *Properties of Rock Materials(Internet)*. Lausanne, Switzerland: Rock Mechanics Laboratory, 10p, Available from: http://lmr.epfl.ch/webdav/site/lmr/users/172086/public/RockMechanics/Notes%20-%20Chapter%204.pdf

Sayers, C. M. (2007). Effects of borehole stress concentration on elastic wave velocities in sandstones. *International Journal of Rock Mechanics and Mining Sciences, Volume 44, Issue 7*, 1045-1052.

Seymour, B., & Mortell, M. (2006). A finite-rate theory of resonance in a closed tube: discontinuous solutions of a functional equation. *Journal of fluid Mechanics Digital Archive* , 365-382 .

Song, I., & Suh, M. (2004). Determination of the elastic modulus set of foliated rocks from ultrasonic velocity measurements. *Engineering Geology 72* , 293–308.

Spitz, K., & Moreno, J. (1996). *A practical guide to groundwater and solute transport modeling.* Canada: John Wiley and Sons.

Texas University (Author)(cited 2007, September 26). *Department of Mathematics(Internet)*. Texas, USA: Texas A&M University, 1p, Available from: http://www.math.tamu.edu/~bangerth/pictures.html

Ugural, A., & Fenster, S. (2003). *Advanced Strength and Applied Elasticity.* New Jersey: Prentice Hall.

University of Bradford (Author)(cited 2002, October 11). *University of Bradford(Internet)*. Bradford, UK: University of Bradford, 1p, Available from: http://www.bradford.ac.uk/staff/vtoropov/tmp/week4.pdf

University of Oxford (Author)(cited 2007, September 26). *Vibration ESPI Measurements of CFRP Cylinder(Internet)*. Oxford, UK: University of Oxford, 1p, Available from: http://www.physics.ox.ac.uk/

University of Texas (Author)(cited 2007, November 11). *Geology(Internet)*. Texas, USA: Texas University, 1p, Available from: http://www.geo.utexas.edu/faculty/mosher/RobReed/CLimages/L15-5618C-23.jpg

Viscoelastic Materials (Author)(cited 2007, October 5). *Viscoelasticity(Internet)*. Wisconsin, USA: University of Wisconsin, 2p, Available from: http://silver.neep.wisc.edu/~lakes/VE.html

Wang, Y. C., & Lakes, R. S. (2003). Lakes Resonant ultrasound spectroscopy in shear mode. *Review of scientific instruments,* Volume 74, Issue 3 , 1371-1373.

Wave Express (Author)(cited 2007, September 26). *A history of the study of sound(Internet)*. Unknown location, Unknown publisher, Available from: http://library.thinkquest.org/C005705/English/sound/history.htm

Wayne, R., Hykes, D. L., & Hedrick, W. R. (2005). *Ultrasound physics and instrumentation.* St. Louis: Mosby Year Book.

Weisstein, E. (Author)(cited 2007, March 1). *World of physics(Internet)*. USA: Wolfram Research, 1p, Available from: http://scienceworld.wolfram.com/physics/

Xin, Z. (2000). *The Formula of Sound Absorption Spectrums For Fibrous Materials.* ShangHai: Polytechnic University.

Zadler, B., Jerome, H. L., & Le Rousseau, J. (2004). *Resonant Ultrasound spectroscopy: theory and application.* Geophysical Journal International, Volume 156, Number 1, 154-169.

Appendix A – Elastic and hydraulic results tables

Parameter	Sample1	Sample15	Sample2	Sample7	Sample16	Sample20	Sample3	Sample13	Sample4	Sample14	Unit
Shear Wave Travel Time (s)	6.44E-05	1.00E-04	5.61E-05	4.50E-05	1.81E-04	1.65E-04	5.12E-05	2.51E-05	6.97E-05	1.50E-04	s
Compressional Wave travel Time (s)	3.75E-05	6.01E-05	4.05E-05	2.92E-05	1.30E-04	1.14E-04	3.12E-05	1.79E-05	4.95E-05	9.96E-05	S
Sample Length (m)	1.60E-01	2.95E-01	1.33E-01	7.20E-02	2.78E-01	2.85E-01	1.60E-01	7.00E-02	1.35E-01	2.95E-01	m
Sample Dry Mass (Kg)	7.46E-01	1.35E+00	8.87E-01	4.13E-01	1.87E+00	1.92E+00	5.92E-01	2.54E-01	6.03E-01	1.33E+00	Kg
Sample Radius (m)	2.35E-02	2.30E-02	3.00E-02	2.70E-02	3.00E-02	3.00E-02	2.10E-02	2.10E-02	2.30E-02	2.30E-02	m
Sample Porosity (%)	6.9	6.9	7.0	5.4	9.7	8.0	0.2	0.2	12.3	12.3	%
Aquifer Thickness (m)	1.00E+00	1.00E+00	1.00E+00	1.00E+00	1.00E+00	1.00E+00	1.00E+00	1.00E+00	1.00E+00	1.00E+00	m
Compressibility of Water (1/Pa)	4.60E-10	4.60E-10	4.60E-10	4.60E-10	4.60E-10	4.60E-10	4.60E-10	4.60E-10	4.60E-10	4.60E-10	1/Pa
Gravitational Acceleration (m/s^2)	9.80E+00	9.80E+00	9.80E+00	9.80E+00	9.80E+00	9.80E+00	9.80E+00	9.80E+00	9.80E+00	9.80E+00	m/s^2
Sample Rate (Hz)	2.00E+05	2.00E+05	2.00E+05	2.00E+05	2.00E+05	2.00E+05	2.00E+05	2.00E+05	2.00E+05	2.00E+05	Hz
Shear Wave Velocity (m/s)	2.49E+03	2.95E+03	2.37E+03	1.60E+03	1.54E+03	1.73E+03	3.12E+03	2.79E+03	1.94E+03	1.97E+03	m/s
Compressional Wave Velocity (m/s)	4.26E+03	4.91E+03	3.28E+03	2.47E+03	2.14E+03	2.51E+03	5.14E+03	3.92E+03	2.73E+03	2.96E+03	m/s
Sample Volume (m^3)	2.78E-04	4.90E-04	3.76E-04	1.65E-04	7.86E-04	8.06E-04	2.22E-04	9.70E-05	2.24E-04	4.90E-04	m^3
Sample Density (Kg/m^3)	2.69E+03	2.75E+03	2.36E+03	2.50E+03	2.37E+03	2.39E+03	2.67E+03	2.62E+03	2.69E+03	2.71E+03	Kg/m^3
Specific Volume (m^3/Kg)	3.72E-04	3.63E-04	4.24E-04	3.99E-04	4.21E-04	4.19E-04	3.74E-04	3.82E-04	3.72E-04	3.69E-04	m^3/Kg
Shear Modulus (Pa)	1.66E+10	2.39E+10	1.33E+10	6.42E+09	5.63E+09	7.15E+09	2.60E+10	2.04E+10	1.01E+10	1.05E+10	Pa
Bulk Modulus (Pa)	3.22E+10	4.24E+10	1.22E+10	8.85E+09	5.24E+09	7.89E+09	4.44E+10	1.98E+10	9.89E+09	1.32E+10	Pa
Pore Space Compressibility (1/Pa)	3.10E-11	2.36E-11	8.21E-11	1.13E-10	1.91E-10	1.27E-10	2.25E-11	5.06E-11	1.01E-10	7.55E-11	1/Pa
Lame Constant L (Pa)	1.56E+10	1.85E+10	-1.06E+09	2.43E+09	-3.90E+08	7.39E+08	1.84E+10	-6.21E+08	-1.97E+08	2.71E+09	Pa
Lame Constant u (Pa)	1.66E+10	2.39E+10	1.33E+10	6.42E+09	5.63E+09	7.15E+09	2.60E+10	2.04E+10	1.01E+10	1.05E+10	Pa
Poisson Ratio	2.80E-01	2.63E-01	1.01E-01	2.08E-01	1.04E-01	1.52E-01	2.55E-01	1.16E-01	1.19E-01	1.86E-01	
Young's Modulus (Pa)	4.25E+10	6.03E+10	2.92E+10	1.55E+10	1.24E+10	1.65E+10	6.54E+10	4.55E+10	2.26E+10	2.50E+10	Pa
Acoustic Impedance (Pa s/m^3)	8.66E+13	1.17E+14	2.88E+13	2.22E+13	1.24E+13	1.88E+13	1.19E+14	5.18E+13	2.66E+13	3.59E+13	Pas/m^3
First Torsional Resonance Frequency	7.77E+03	4.99E+03	8.91E+03	1.11E+04	2.77E+03	3.04E+03	9.76E+03	1.99E+04	7.18E+03	3.34E+03	Hz
Specific Storage (1/m)	6.15E-07	5.43E-07	1.12E-06	1.35E-06	2.31E-06	1.60E-06	2.31E-07	5.05E-07	1.54E-06	1.29E-06	1/m
Storativity	6.15E-07	5.43E-07	1.12E-06	1.35E-06	2.31E-06	1.60E-06	2.31E-07	5.05E-07	1.54E-06	1.29E-06	
Hydraulic Diffusivity (m^2/s)	2.01E-03	6.84E-03	1.39E-03	4.07E-04	6.07E-03	6.38E-03	2.01E-03	3.85E-04	1.43E-03	6.84E-03	m^2/s
Hydraulic Conductivity (m/s)	1.24E-09	3.71E-09	1.56E-09	5.50E-10	1.40E-08	1.02E-08	4.65E-10	1.94E-10	2.21E-09	8.84E-09	m/s
Intrinsic Permeability (m^2)	1.26E-13	3.79E-13	1.59E-13	5.62E-14	1.43E-12	1.04E-12	4.75E-14	1.99E-14	2.26E-13	9.03E-13	m^2
Transmissivity (m^2/s)	1.24E-09	3.71E-09	1.56E-09	5.50E-10	1.40E-08	1.02E-08	4.65E-10	1.94E-10	2.21E-09	8.84E-09	m^2/s
Hydraulic Conductivity(m/d)	1.07E-04	3.20E-04	1.34E-04	4.75E-05	1.21E-03	8.82E-04	4.02E-05	1.68E-05	1.91E-04	7.64E-04	m/d
Sample Type	Basalt	Basalt	Sandstone	TBM Sstone	Sandstone	Sandstone	Quartzite	Quartzite	Kimberlite	Kimberlite	

Table 6 - Full parameter table 1

Parameter	Sample5	Sample6	Sample8	Sample11	Sample12	Sample9	Sample10	Sample17	Sample18	Sample19	Unit
Shear Wave Travel Time (s)	3.50E-05	6.11E-05	4.92E-05	4.09E-05	4.61E-05	3.51E-05	4.59E-05	3.54E-05	4.96E-05	5.02E-05	s
Compressional Wave travel Time (s)	1.46E-05	3.44E-05	3.04E-05	2.79E-05	3.24E-05	2.39E-05	3.18E-05	2.47E-05	3.52E-05	3.67E-05	S
Sample Length (m)	9.00E-02	1.10E-01	6.30E-02	5.50E-02	6.20E-02	7.20E-02	7.00E-02	1.30E-01	1.50E-01	1.50E-01	m
Sample Dry Mass (Kg)	3.22E-01	4.05E-01	4.52E-01	3.92E-01	4.54E-01	5.40E-01	4.23E-01	1.31E-01	1.48E-01	1.48E-01	Kg
Sample Radius (m)	2.10E-02	2.10E-02	3.00E-02	3.00E-02	3.00E-02	3.15E-02	2.70E-02	1.50E-02	1.50E-02	1.50E-02	m
Sample Porosity (%)	0.2	2.2	17.6	17.6	17.6	9.3	5.2	0.3	0.1	5.0	%
Aquifer Thickness (m)	1.00E+00	1.00E+00	1.00E+00	1.00E+00	1.00E+00	1.00E+00	1.00E+00	1.00E+00	1.00E+00	1.00E+00	m
Compressibility of Water (1/Pa)	4.60E-10	4.60E-10	4.60E-10	4.60E-10	4.60E-10	4.60E-10	4.60E-10	4.60E-10	4.60E-10	4.60E-10	1/Pa
Gravitational Acceleration (m/s^2)	9.80E+00	9.80E+00	9.80E+00	9.80E+00	9.80E+00	9.80E+00	9.80E+00	9.80E+00	9.80E+00	9.80E+00	m/s^2
Sample Rate (Hz)	2.00E+05	2.00E+05	2.00E+05	2.00E+05	2.00E+05	2.00E+05	2.00E+05	2.00E+05	2.00E+05	2.00E+05	Hz
Shear Wave Velocity (m/s)	2.57E+03	1.80E+03	1.28E+03	1.35E+03	1.34E+03	2.05E+03	1.53E+03	3.68E+03	3.02E+03	2.99E+03	m/s
Compressional Wave Velocity (m/s)	6.19E+03	3.20E+03	2.07E+03	1.97E+03	1.91E+03	3.01E+03	2.20E+03	5.27E+03	4.27E+03	4.09E+03	m/s
Sample Volume (m^3)	1.25E-04	1.52E-04	1.78E-04	1.56E-04	1.75E-04	2.24E-04	1.60E-04	4.59E-05	5.30E-05	5.30E-05	m^3
Sample Density (Kg/m^3)	2.58E+03	2.66E+03	2.54E+03	2.52E+03	2.59E+03	2.41E+03	2.64E+03	2.85E+03	2.79E+03	2.79E+03	Kg/m^3
Specific Volume (m^3/Kg)	3.87E-04	3.76E-04	3.94E-04	3.97E-04	3.86E-04	4.16E-04	3.79E-04	3.51E-04	3.58E-04	3.58E-04	m^3/Kg
Shear Modulus (Pa)	1.70E+10	8.62E+09	4.16E+09	4.57E+09	4.68E+09	1.01E+10	6.15E+09	3.85E+10	2.55E+10	2.50E+10	Pa
Bulk Modulus (Pa)	8.18E+10	1.85E+10	6.76E+09	5.22E+09	4.81E+09	1.17E+10	6.66E+09	4.06E+10	2.53E+10	2.17E+10	Pa
Pore Space Compressibility (1/Pa)	1.22E-11	5.39E-11	1.48E-10	1.92E-10	2.08E-10	8.56E-11	1.50E-10	2.46E-11	3.96E-11	4.61E-11	1/Pa
Lame Constant L (Pa)	6.48E+10	9.92E+09	2.61E+09	6.50E+08	1.25E+08	1.54E+09	5.10E+08	2.07E+09	-2.59E+08	-3.29E+09	Pa
Lame Constant u (Pa)	1.70E+10	8.62E+09	4.16E+09	4.57E+09	4.68E+09	1.01E+10	6.15E+09	3.85E+10	2.55E+10	2.50E+10	Pa
Poisson Ratio	4.03E-01	2.99E-01	2.45E-01	1.61E-01	1.32E-01	1.63E-01	1.47E-01	1.40E-01	1.22E-01	8.40E-02	
Young's Modulus (Pa)	4.78E+10	2.24E+10	1.03E+10	1.06E+10	1.06E+10	2.36E+10	1.41E+10	8.78E+10	5.73E+10	5.41E+10	Pa
Acoustic Impedance (Pa s/m^3)	2.11E+14	4.93E+13	1.72E+13	1.32E+13	1.24E+13	2.81E+13	1.76E+13	1.16E+14	7.06E+13	6.06E+13	Pas/m^3
First Torsional Resonance Frequency	1.43E+04	8.19E+03	1.02E+04	1.22E+04	1.08E+04	1.43E+04	1.09E+04	1.41E+04	1.01E+04	9.97E+03	Hz
Specific Storage (1/m)	1.28E-07	6.28E-07	2.24E-06	2.67E-06	2.83E-06	1.26E-06	1.70E-06	2.56E-07	3.90E-07	6.76E-07	1/m
Storativity	1.28E-07	6.28E-07	2.24E-06	2.67E-06	2.83E-06	1.26E-06	1.70E-06	2.56E-07	3.90E-07	6.76E-07	
Hydraulic Diffusivity (m^2/s)	6.36E-04	9.50E-04	3.12E-04	2.38E-04	3.02E-04	4.07E-04	3.85E-04	1.33E-03	1.77E-03	1.77E-03	m^2/s
Hydraulic Conductivity (m/s)	8.13E-11	5.96E-10	6.98E-10	6.34E-10	8.54E-10	5.12E-10	6.56E-10	3.40E-10	6.89E-10	1.20E-09	m/s
Intrinsic Permeability (m^2)	8.30E-15	6.09E-14	7.13E-14	6.48E-14	8.72E-14	5.23E-14	6.70E-14	3.48E-14	7.04E-14	1.22E-13	m^2
Transmissivity (m^2/s)	8.13E-11	5.96E-10	6.98E-10	6.34E-10	8.54E-10	5.12E-10	6.56E-10	3.40E-10	6.89E-10	1.20E-09	m^2/s
Hydraulic Conductivity(m/d)	7.02E-06	5.15E-05	6.03E-05	5.48E-05	7.38E-05	4.42E-05	5.67E-05	2.94E-05	5.95E-05	1.03E-04	m/d
Sample Type	Gneiss	Schist	Mudstone	Mudstone	Mudstone	Shale	shale	Dolerite	Dolomite	Granite	

Table 7 - Full parameter table 2

Appendix B – Porosity calculations

Sample	Dry Mass (g)	Wet Mass (g)	Pore Fluid Mass (g)	Pore Fluid Volume (m^3)	Radius/ width (m)	Height (m)	Length (m)	Sample Volume (m^3)	Porosity Ratio	Porosity Percentage (%)
1	15.7367	16.1213	0.3846	3.85E-07	0.0235	0.0032		5.55E-06	6.93E-02	6.93E+00
2	22.3575	23.1551	0.7976	7.98E-07	0.03	0.004		1.13E-05	7.05E-02	7.05E+00
3	12.9988	13.0092	0.0104	1.04E-08	0.021	0.003		4.16E-06	2.50E-03	2.50E-01
4	38.6782	40.4596	1.7814	1.78E-06	0.024	0.008		1.45E-05	1.23E-01	1.23E+01
5	9.2002	9.2054	0.0052	5.20E-09	0.021	0.002		2.77E-06	1.88E-03	1.88E-01
6	21.1038	21.2588	0.155	1.55E-07	0.021	0.005		6.93E-06	2.24E-02	2.24E+00
7	21.8699	22.3227	0.4528	4.53E-07	0.0275	0.0035		8.32E-06	5.45E-02	5.45E+00
8	94.8661	103.318	8.4519	8.45E-06	0.03	0.017		4.81E-05	1.76E-01	1.76E+01
9	31.7376	32.9015	1.1639	1.16E-06	0.0315	0.004		1.25E-05	9.34E-02	9.34E+00
10	21.2485	21.6811	0.4326	4.33E-07	0.0275	0.0035		8.32E-06	5.20E-02	5.20E+00
11	94.8661	103.318	8.4519	8.45E-06	0.03	0.017		4.81E-05	1.76E-01	1.76E+01
12	94.8661	103.318	8.4519	8.45E-06	0.03	0.017		4.81E-05	1.76E-01	1.76E+01
13	13.2194	13.2317	0.0123	1.23E-08	0.021	0.0038		5.26E-06	2.34E-03	2.34E-01
14	38.6782	40.4596	1.7814	1.78E-06	0.024	0.008		1.45E-05	1.23E-01	1.23E+01
15	15.7367	16.1213	0.3846	3.85E-07	0.0235	0.0032		5.55E-06	6.93E-02	6.93E+00
16	22.3846	23.212	0.8274	8.27E-07	0.03	0.003		8.48E-06	9.75E-02	9.75E+00
17	17.7085	17.7175	0.009	9.00E-09	0.043	0.031	0.004	5.33E-06	1.69E-03	1.69E-01
18	11.4342	11.4358	0.0016	1.60E-09	0.044	0.031	0.0035	4.77E-06	3.35E-04	3.35E-02
19	11.3933	11.5017	0.1084	1.08E-07	0.045	0.031	0.003	4.19E-06	2.59E-02	2.59E+00
20	23.3091	24.2313	0.9222	9.22E-07	0.03	0.004		1.13E-05	8.15E-02	8.15E+00
21	21.1038	21.2588	0.155	1.55E-07	0.021	0.005		6.93E-06	2.24E-02	2.24E+00

Table 8 - Porosity calculations
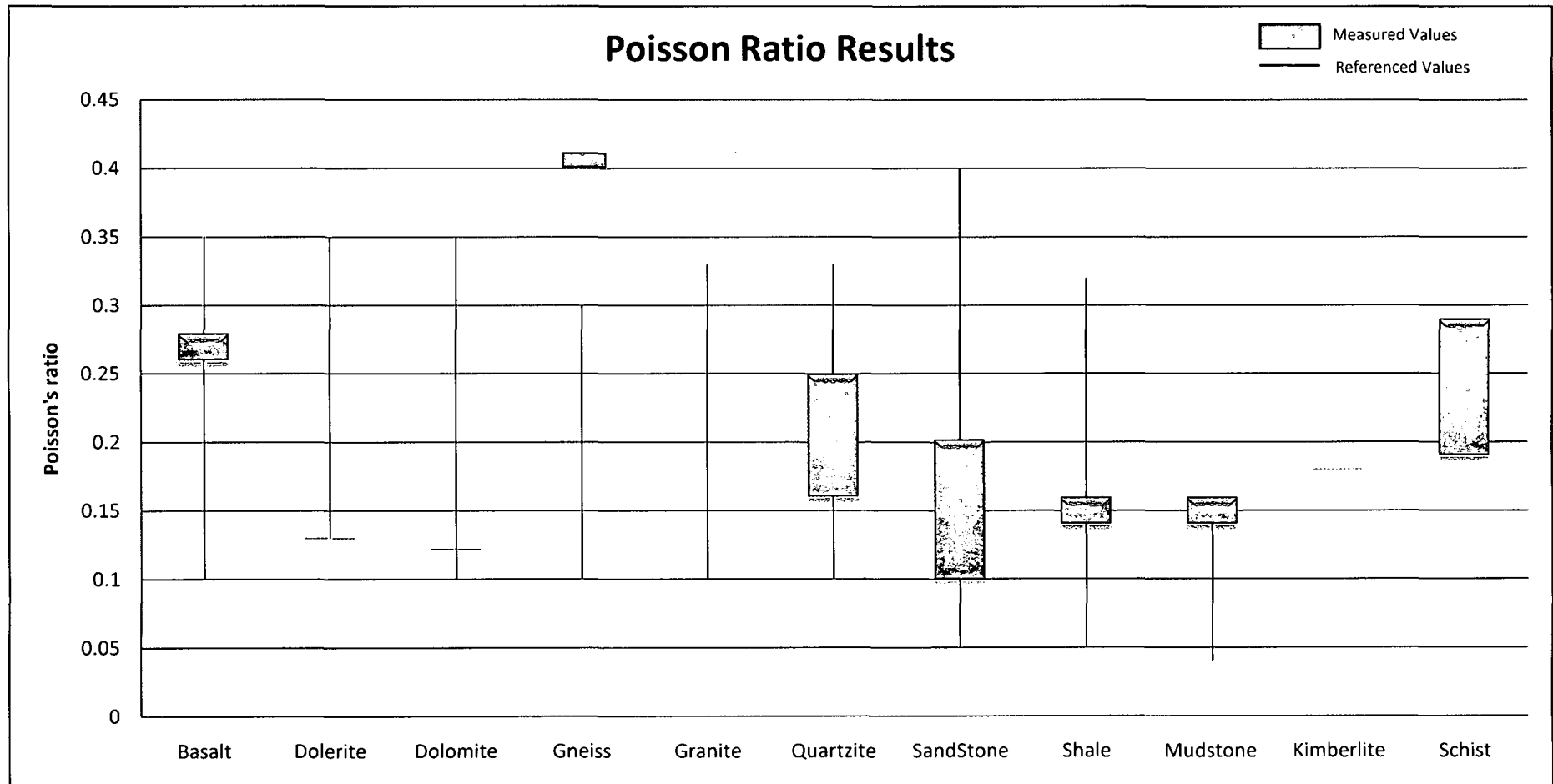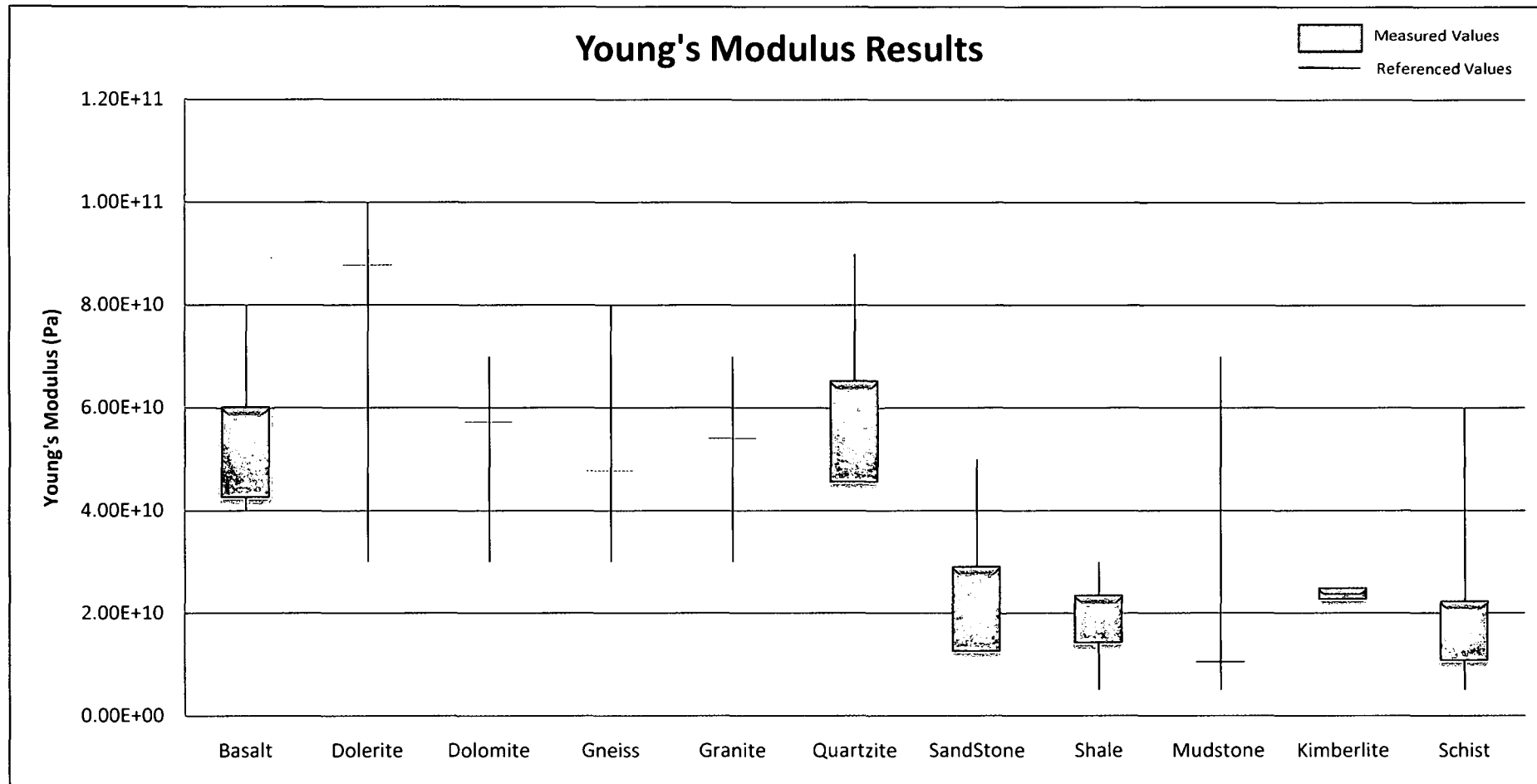
Appendix C – Referenced value comparisons

**Figure 72 – Poisson's ratio comparison (Rock Mechanics Laboratory, 2007)**

Figure 73 - Young's modulus comparison (Rock Mechanics Laboratory, 2007)

Young's Modulus Results

Appendix D – Hydraulic conductivity calculations

Table 9 - Hydraulic conductivity calculations

Parameter	Sample16	Sample2	Sample17	Sample13	Sample5	Sample6	Sample21	Sample19	Sample11	Sample9	Sample1	Sample4
Type	Sstone	Sstone	Dolorite	Quartzite	Gneiss	Schist	Dolomite	Granite	Mudstone	Shale	Basalt	Kimberlite
Tube radius(m)	6.50E-03	6.50E-03	6.50E-03	6.50E-03	6.50E-03	6.50E-03	6.50E-03	6.50E-03	6.50E-03	6.50E-03	6.50E-03	6.50E-03
Initial head(m)	1.88E+00	1.95E+00	1.91E+00	1.89E+00	1.93E+00	1.90E+00	1.83E+00	1.91E+00	1.82E+00	1.94E+00	1.93E+00	1.81E+00
Delayed head(m)	1.87E+00	1.94E+00	1.91E+00	1.89E+00	1.93E+00	1.90E+00	1.83E+00	1.91E+00	1.82E+00	1.94E+00	1.93E+00	1.80E+00
Tube Area(m²)	2.65E-04	2.65E-04	2.65E-04	2.65E-04	2.65E-04	2.65E-04	2.65E-04	2.65E-04	2.65E-04	2.65E-04	2.65E-04	2.65E-04
Measurement time(s)	3.30E+03	2.58E+03	1.20E+03	3.00E+03	3.60E+03	2.40E+03	2.40E+03	3.00E+03	3.00E+03	1.80E+03	1.80E+03	1.80E+03
Sample thickness(m)	4.00E-03	4.00E-03	4.00E-03	4.00E-03	4.00E-03	4.00E-03	4.00E-03	4.00E-03	4.00E-03	4.00E-03	4.00E-03	4.00E-03
Sample area(m²)	2.20E-04	2.20E-04	2.20E-04	2.20E-04	2.20E-04	2.20E-04	2.20E-04	2.20E-04	2.20E-04	2.20E-04	2.20E-04	2.20E-04
K(m/s)	1.02E-08	6.73E-09	2.11E-09	8.52E-10	6.95E-10	2.12E-09	1.10E-09	8.43E-10	3.54E-09	2.77E-09	1.39E-09	1.04E-08
K(m/d)	8.77E-04	5.82E-04	1.82E-04	7.36E-05	6.01E-05	1.83E-04	9.50E-05	7.28E-05	3.06E-04	2.39E-04	1.20E-04	8.98E-04
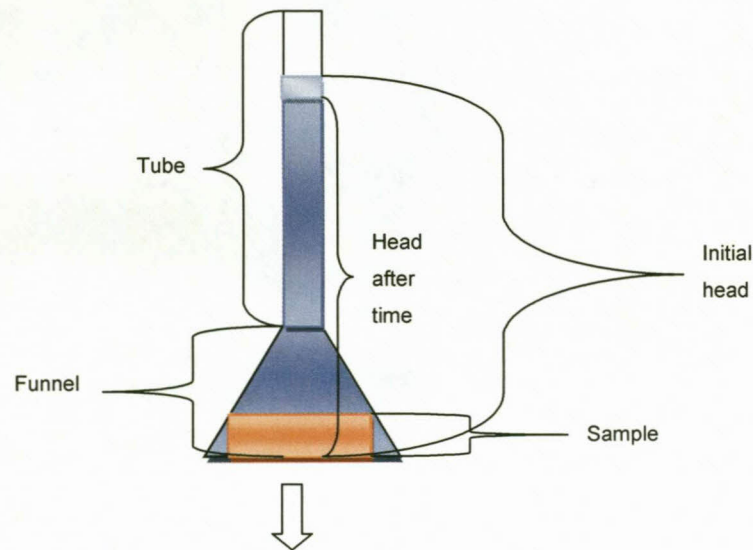
The Darcy hydraulic conductivity test apparatus is shown to the left. It consists of a transparent tube, a funnel and the sample under test. The sample is glued to the funnel and silicon is applied to the corners of the sample to prevent water passing through the sides of the sample. The tube is attached to the funnel and filled with water. The bubbles of air in the funnel and tube are then removed by shaking the tube. A timer is then started to measure the elapsed time between maesuements of head. An initial head is then measured and after a suitable time has passed the head is measured again. The hydraulic conductivity is then calculated using the equation:

$$K = \frac{Tube\ Volume}{Sample\ Area \times Elapsed\ time} \times \ln\left(\frac{Initial\ Head}{Head\ after\ elapsed\ time}\right)$$

Summary

As groundwater becomes increasingly vital as a viable source of fresh water in arid or remote areas, where surface water supplies are insufficient to sustain life, agriculture and industry, it has become important to accurately estimate, manage and monitor this valuable resource. Much has been done to improve the management of this precious resource by the development of numerical models that give a realistic estimate on how groundwater reserves will react to changing circumstances in groundwater conditions. The accuracy of these predictions is however limited to the effective accuracy of the predictive model, which in turn relies on accurate data for all the variables which will affect the flow of groundwater. This thesis presents a method to determine hydrological parameters of a rock sample by measuring its elastic parameters, using non-destructive ultrasound methods.

This is done in two ways;
- The first of these is call the time of flight method. This method measures the compressive and shear wave velocities of the rock, by inducing an ultrasonic pulse into one side of the sample and measuring the time it takes the pulse to travel through the sample. The travel times are then converted into compressive and shear wave velocities, which in turn are used to determine the bulk modulus and shear modulus of the sample.
- The second method is to use resonant ultrasound spectrography, which measures the natural resonance frequencies of a rock sample induced by an ultrasonic frequency sweep. These resonance frequencies are then analytically verified against the bulk modulus and shear modulus of the rock sample determined by the time of flight method.

Both of these methods use apparatus which clamp a cylindrical rock core sample between two sets of ultrasonic transducers. One set of transducers produce compressive ultrasonic waves and the other produce shear ultrasonic waves. An analogue to digital converter is used to read the changing voltage levels in the transducers, induced by the ultrasonic pulse travelling through the sample or the resonant vibrations induced by the ultrasonic frequency sweep in the sample. Once the rock samples elastic parameters are known they are applied to equations which related hydrological parameters to the samples elastic parameters. The resultant hydrological parameter values can then be determined.

Opsomming

Soos grondwater toenemend noodsaaklik word as 'n varswaterbron in droë of afgeleë gebiede, waar oppervlakwaterbronne ontoereikend is vir lewensonderhoud, sowel as landbou en die industrie, het dit belangrik geword om hierdie waardevolle bron akkuraat te bepaal, bestuur en moniteer. Daar is reeds baie gedoen om die bestuur van grondwater te verbeter deur die ontwikkeling van numeriese modelle wat 'n realistiese bepaling gee van hoe grondwaterreserwes op veranderende omstandigehede in grondwatertoestande sal reageer. Die akkuraatheid van hierdie voorspellings word derhalwe ingekort deur die doeltreffende akkuraatheid van die voorspellingsmodelle, wat weer afhanklik is van akkurate data vir al die veranderlikes wat grondwatervloei beïnvloed. Die tesis bied 'n metode om die hidrologiese parameters van 'n klipmonster te bepaal deur sy elastiese parameters te meet deur nie-vernietigende ultrasoniese metodes te gebruik.

Die word gedoen op twee wyses:

- Die eerste metode word die vlugtydmetode genoem. Hierdie metode meet die saamdrukkende en suiwer golfsnelhede in die klip deur 'n ultrasoniese puls deur die monster te stuur, en die tyd te meet wat dit neem om daardeur te gaan. Die tyd wat verkry is, word dan na saamdrukkende en suiwer golfsnelhede omgeskakel, wat op hulle beurt weer gebruik word om die massa en suiwer modulus van die monster te bepaal.
- Die tweede metode is die gebruik van resonante ultrsoniese spektrografie, wat die natuurlike resonansie frekwensies van 'n klipmonster meet. Dit word veroorsaak deur 'n ultrasoniese frekwensiestryk. Hierdie resonante frekwensies word dan analities bevestig teenoor die massa en suiwer modulus van die klipmonster, soos bepaal deur die vlugtyd metode.

Albei hierdie metodes maak gebruik van apparaat wat 'n silindriese klipkernmonster tussen twee stelle ultrasoniese transduktors vasheg. Een stel transduktors produseer saamdrukkende ultrasoniese golwe en die ander suiwer ultrasoniese golwe. 'n Analoog tot digitale omsetter word gebruik om die veranderende voltvlakke in die transduktors te lees, veroorsaak deur ultrasoniese pulse wat deur die monster gaan, of deur die resonante vibrasies as gevolg van die ultrasoniese frekwensiestryk in die monster. Wanneer die elastiese parameters van die klipmonsters bekend is, word hulle toegepas op vergelykings. Dit bring dan 'n verwantskap mee tussen die

hidrologiese en elastiese parameters van die monsters. Die gevolglike hidrologiese parameterwaardes kan dan bepaal word.